Interfacing Liposomes with Metal Ions and Metal Oxides:

Coordination Chemistry, Surface Forces and Membrane Integrity

by

Yibo Liu

A thesis

presented to the University of Waterloo

in fulfilment of the

thesis requirement for the degree of

Doctor of Philosophy

in

Chemistry

Waterloo, Ontario, Canada, 2020

Examining Committee Membership

The following served on the Examining Committee for this thesis. The decision of the Examining Committee is by majority vote.

External Examiner	**Dr. Gang Zheng** Professor, Department of Medical Biophysics, University of Toronto, Toronto, Canada
Supervisor	**Dr. Juewen Liu** Professor, Department of Chemistry, University of Waterloo, Waterloo, Canada
Internal Member	**Dr. Michael Tam** Professor, Department of Chemical Engineering, University of Waterloo, Waterloo, Canada
Internal Member	**Dr. Mario Gauthier** Professor, Department of Chemistry, University of Waterloo, Waterloo, Canada
Internal Member	**Dr. Shirley Tang** Professor, Department of Chemistry, University of Waterloo, Waterloo, Canada

Author's Declaration

This thesis consists of material all of which I authored or co-authored: see Statement of Contributions included in the thesis. This is a true copy of the thesis, including any required final revisions, as accepted by my examiners.

I understand that my thesis may be made electronically available to the public.

Statement of Contributions

The work presented in the thesis was performed by the author and collaborators. The resulting publications and contributions of each collaborator are listed below in details.

The work in Chapter 2 has been published as: Yibo Liu and Juewen Liu. Zn^{2+} Induced Irreversible Aggregation, Stacking, and Leakage of Choline Phosphate Liposomes, *Langmuir*, **2017**, 33, 14472-14479. All the experiments were performed by the first author. The manuscript was written by both authors.

The work in Chapter 3 has been published as: Yibo Liu and Juewen Liu, Cu^{2+}-Directed Liposome Membrane Fusion, Positive-Stain Electron Microscopy, and Oxidation, *Langmuir*, **2018**, 34, 7545-7553. All the experiments were performed by the first author. The manuscript was written by both authors.

The work in Chapter 4 has been published as: Yibo Liu and Juewen Liu, Growing a Nucleotide/Lanthanide Coordination Polymer Shell on Liposomes, *Langmuir*, **2019**, 35, 11217-11224. All the experiments were performed by the first author. The manuscript was written by both authors.

The work in Chapter 5 has been published as: Yibo Liu and Juewen Liu, Adsorption of Nanoceria by Phosphocholine Liposomes, *Langmuir*, **2016**, 32, 13276-13283. All the experiments were performed by the first author. The manuscript was written by both authors.

The work in Chapter 6 has been published as: Yibo Liu and Juewen Liu, Leakage and Rupture of Lipid Membranes by Charged Polymers and Nanoparticles, *Langmuir*, **2020**, 36, 810-818. All the experiments were performed by the first author. The manuscript was written by both authors.

Abstract

Liposomes are self-closed vesicles composed of lipid bilayer walls that have been widely used as models for cell membranes and drug delivery vehicles. One interesting research direction is to study the interactions of membranes with various ions, molecules and materials. Among them, metal ions and metal oxides are attractive because of their biological/technological significance and their unique coordination interactions with lipid headgroups. Previous studies reported in the literature focused mainly on electrostatic interactions, while more specific chemical interactions were overlooked. The primary focus of this thesis was to study the liposome interactions with metal ions and metal oxide nanoparticles (NPs) to provide insights into contributions of lipid headgroup chemistry. In my study, the main types of surface forces were probed, the effects of these interactions on liposome stability and membrane integrity were investigated, and general interaction models were proposed for each system.

In Chapter 1, the relevant background knowledge on lipids and liposomes is introduced. The research progress in the literature of the interactions between lipid membranes and various metal ions/metal-containing NPs is reviewed. Most previous work focused on group 1A and 2A metal ions, such as Na^+ and Ca^{2+}, while the work on transition metal ions and lanthanide ions was much less frequent. In addition, SiO_2 or glass surfaces were most widely used for interfacing with liposomes, while transition metal oxides were less explored. With this context, the motivation and goals of my research are described at the end of this chapter along with the outline of the thesis, and my research focused on transition metals, lanthanides and metal oxides.

In Chapter 2, the binding of Zn^{2+} to headgroup-inversed choline phosphate (CP) liposomes was systematically studied and compared to standard phosphocholine (PC) liposomes. The CP lipid has an exposed terminal phosphate, which has a stronger metal binding affinity compared to the bridging phosphate in a PC lipid. Zn^{2+} caused significant aggregation, stacking, fusion, and transient leakage of the CP liposomes, while it had little effect on the PC liposomes. Isothermal titration calorimetry (ITC) showed that the binding between Zn^{2+} and CP liposomes was endothermic and, in contrast, no heat was

detected by titrating Zn^{2+} to the PC liposomes. Negative stain transmission electron microscopy (TEM) revealed multilamellar CP lipid structures attributable to Zn^{2+} sandwiched between lipid bilayers. A reaction mechanism was proposed and the stronger adsorption of Zn^{2+} with CP liposomes was attributed to the stronger metal binding affinity of the terminal phosphate.

In Chapter 3, I studied the binding between Cu^{2+} and four types of liposomes: PC, phosphoglycerol (PG), phosphoserine (PS), and CP. Using a fluorescence quenching assay, I demonstrated that Cu^{2+} strongly bound to the CP and PS liposomes, while the binding with the PC and PG liposomes was much weaker. The membrane integrity of the PC liposomes was not affected by Cu^{2+}, whereas liposome fusion and leakage occurred for the other three liposomes. Under TEM, Cu^{2+} stained all four types of liposomes with a short incubation time (< 1 min). In addition, the oxidative catalytic property of Cu^{2+} was inhibited by the tight binding of the PS liposomes. Finally, a model interaction for each liposome was proposed, with each liposome having a different metal binding mechanism. In combination with Chapter 2, I demonstrated that different metal ions interact with each lipid differently.

In Chapter 4, liposome-directed growth of gadolinium/adenosine monophosphate (Gd^{3+}/AMP) coordination polymer shells was demonstrated. First, the binding of a lanthanide ion (Gd^{3+}) to the CP and PS liposomes was studied. Gd^{3+} binding did not cause significant liposome fusion, and no leakage for the PS liposomes was observed. Taking advantage of this observation, adenosine monophosphate (AMP) was added to crosslink Gd^{3+} on the liposome surfaces forming a Gd^{3+}/AMP coordination polymer shell with the contents remaining inside the liposomes. The shell protected the liposomes against leakage induced by ZnO NPs but not against a surfactant molecule Triton X-100, suggesting a porous structure of the Gd^{3+}/AMP shell. This work not only provides a simple method to coat liposomes, but also offers a fundamental understanding of liposome adsorption of lanthanide ions.

In Chapter 5, the adsorption of nanoceria (CeO_2 NPs, ~5 nm in size) onto PC liposomes was studied. CeO_2 NPs possess different surface charges at pH 4 and pH 7.6. The CeO_2 NPs were adsorbed by the PC liposomes at both pH's, but different adsorption isotherms were observed. At pH 7.6, the

CeO_2 NPs were nearly charge neutral and induced aggregation of the PC liposomes at all CeO_2 concentrations. At pH 4, CeO_2 NPs were positively charged, and a restabilization in the presence of a relatively high amount of the CeO_2 NPs was observed. The phosphate group in the PC lipid was mainly responsible for the adsorption, and the adsorbed CeO_2 NPs could be displaced by free inorganic phosphate ions. The CeO_2 NP-induced liposome leakage was attributable to a transient lipid phase transition, and the overall integrity of the liposome was retained. This study provides a fundamental understanding of the interaction between lipid bilayers and CeO_2 NPs at a molecular level, which may offer insights into the interaction of CeO_2 with cell membranes.

In Chapter 6, to investigate a perception in the literature that cationic nanomaterials are more membrane disruptive, the leakage and rupture of lipid membranes by a few charged NPs were systematically studied. In this work, instead of solely using different materials for testing the effect of charge, we used the same materials and obtained different surface charges by adjusting the solution pH. A total of three types of liposomes, PC liposomes with saturated and unsaturated tails and PS liposomes, were tested with three types of metal oxide NPs, namely ZnO, TiO_2 and Fe_3O_4. The adsorption and membrane leakage were carefully studied by varying NP surface charges, surface-capping ligands and solution ionic strength. Overall, this study suggests that charge alone is not the determining factor for membrane damage, but rather a strong interaction strength is key for membrane leakage.

Finally, the conclusions of the thesis are summarized, and future research opportunities are given in Chapter 7.

Acknowledgements

I would like to express my sincere gratitude to my supervisor Prof. Juewen Liu for his constant guidance and support for my PhD study. His immense knowledge, motivation and enthusiasm about research inspired me throughout my study. I would like to extend my gratitude to my PhD committee: Prof. Michael Tam, Prof. Mario Gauthier, and Prof. Shirley Tang for their consistent support and help during my studies. I would also like to thank my external examiner, Prof. Gang Zheng, for attending my examination. I also want to thank Dr. Sue Stathopulos, Dr. Laura Marrone, Dr. Guy Guillemette, Dr. Eric Prouzet and Dr. Leanne Racicot for their guidance in my TA terms. I would also like to thank Cathy van Esch and Kim Rawson for administrative support.

I would like to thank all lab membranes: Dr. Feng Wang, Dr. Jimmy Huang, Dr. Biwu Liu, Dr. Runjhun Saran, Dr. Zijie Zhang, Dr. Jinyi Zhang, Anand Lopez, Zhicheng Huang, Lingzi Ma, Yuqing Li, Mohamad Zandieh, Tianmeng Yu, Woohyun J. Moon, Yichen Zhao and other members and visiting scholars. My gratitude also goes to Dr. Robert Harris at the University of Guelph, for his assistance with cryo-TEM experiments. I would also like to thank Karla Maria Castro Bravo for proofreading part of my thesis. I also want to take this opportunity to thank Dr. Xiaosong Wang, without him I would never meet the great place, which is the University of Waterloo.

I would like to express my greatest gratitude to my families. Your support, love, encourage, and give make me to pursue, to dream, to love and to be loved. I also want to thank my little son, you are the most amazing project I have achieved.

Finally, I am thankful for the PhD experience I have had, it is not about how much knowledge I have gained, but the ability to learn and the ability to accept myself.

Dedication

I would like to dedicate this thesis to my family for their love and support.

Table of Contents

List of Figures

List of Abbreviations

2,4-DP	2,4-dichlorophenol
4-AP	4-aminoantipyrine
AMF	atomic force microscopy
AMP	adenosine monophosphate
AuNPs	gold nanoparticles
CP	choline phosphate
Cryo-TEM	cryogenic-TEM
DLPC	1,2-dilauroyl-*sn*-glycero-3-phosphocholine
DLS	dynamic light scattering
DLVO theory	Derjaguin-Landau-Verwey-Overbeek theory
DMPC	1,2-dimyristoyl-*sn*-glycero-3-phosphocholine
DOCP	2-((2,3-bis(oleoyloxy)propyl)dimethylammonio)ethyl hydrogen phosphate
DOCPe	2-((2,3-bis(oleoyloxy)propyl)dimethylammonio)ethyl ethyl phosphate
DOPA	1,2-dioleoyl-*sn*-glycero-3-phosphate
DOPC	1,2-dioleoyl-*sn*-glycero-3-phosphocholine
DOPG	1,2- dioleoyl-*sn*-glycero-3-phospho-(1'-*rac*-glycerol)
DOPS	1,2-dioleoyl-*sn*-glycero-3-phospho-L-serine
DOTAP	1,2-dioleoyl-3-trimethylammonium-propane
DPPC	1,2-dipalmitoyl-*sn*-glycero-3-phosphocholine
DSC	differential scanning calorimetry
EDTA	ethylenediaminetetraacetic acid
FTIR	Fourier-transform infrared spectroscopy

Gd^{3+}/AMP	gadolinium/adenosine monophosphate
GUVs	giant unilamellar vesicles
HEPES	4-(2-hydroxyetyl)-1-piperazineethanesulfonic acid
HRTEM	high-resolution TEM
ITC	isothermal titration calorimetry
K_d	dissociation constant
L_o/L_d	liquid-ordered/liquid-disordered
LUV	large unilamellar vesicle
L_α	liquid-crystalline phase
L_β	gel phase
MES	2-(N-morpholino)ethanesulfonic acid
MLVs	multilamellar vesicles
MOFs	metal-organic frameworks
MRI	magnetic resonance imaging
NMR	nuclear magnetic resonance spectroscopy
NPs	nanoparticles
PC	phosphocholine
PE	phosphatidylethanolamine
PG	phosphoglycerol
PS	phosphoserine
PZC	point of zero charge
Rh	rhodamine
Rh-PE	1,2-dioleoyl-*sn*-glycero-3-phosphoethanolamine-N-(lissamine rhodamine B sulfonyl)
ROS	reactive oxygen species

SAXS	small-angle X-ray scattering
SLBs	supported lipid bilayers
SPR	surface plasmon resonance
SUVs	small unilamellar vesicles
T_c	gel to liquid-crystalline transition temperature
TEM	transmission electron microscopy
UV-Vis	ultraviolet-visible
VSFG	vibrational sum frequency generation spectroscopy

Chapter 1 Introduction

1.1 Lipids, Cell Membranes and Model Membranes

Cell membranes are of critical importance to both compartmentalize the interior of cells from the extracellular environment and to perform essential biological functions.[1,2] Cell membranes are remarkably diverse in lipid composition; and the membrane surfaces associate with a large number of proteins; as well, the lipid molecules are fluidic thus continuously reorganize in lateral dimensions.[3-5] Due to the structure and dynamic complexity of cell membranes, model membrane systems, with precisely-controlled composition and properties, are desired to investigate fundamental interactions under well-defined conditions.[6-8] Liposomes, which are closed vesicles with lipid bilayer walls, offer a powerful model system to study cell membrane properties. They have been widely used to study protein binding,[9,10] lipid oxidation,[11,12] membrane fusion,[6,13,14] and lipid lateral organization.[8,15] A full understanding of lipid membrane biological and physicochemical properties requires fundamental knowledge of lipid structure and dynamics.

1.1.1 Structure of lipids

A typical lipid molecule contains a hydrophilic headgroup and two hydrophobic tails. Biological membranes contain an astonishing diversity of lipids, with glycerol-based phospholipids being the predominant species in mammalian cell membranes. In these lipids, the glycerol hydroxyl groups are esterified with one phosphate headgroup and two fatty acid tails (Figure 1.1a). The charge of lipids and their chemical properties can be varied by changing the headgroup, while the hydrophobic tails mainly govern the lipid packing.

Since the molecular cross-sectional area of the lipid headgroup is similar to that of the acyl tail, the lipid molecules can be modeled as cylinders with zero curvature. Such lipids can self-assemble into lipid bilayers in aqueous solution, with an approximate thickness of 5 nm (Figure 1.1b). The lipids can also assemble into other structures (lipid polymorphism), depending on the shape of the lipids.[16] If the

cross-sectional area of the lipid headgroup is larger than that of the acyl tail, structures with positive curvature will form, e.g., micelles (Figure 1.1c). In contrast, if the cross-sectional area of the lipid headgroup is smaller, the formation of assemblies with negative curvature is favored, e.g., the inverted hexagonal phase (H_{II}) (Figure 1.1d).

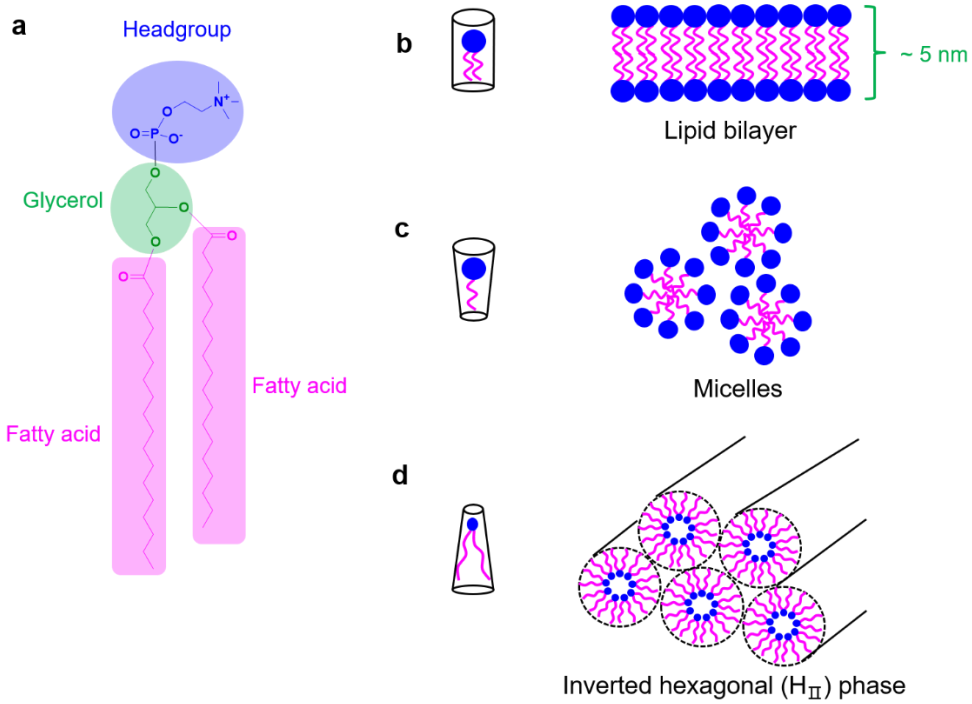

Figure 1.1 (a) Chemical structure of a typical phospholipid molecule. Lipid molecules with different shapes self-assemble into (b) lipid bilayer, (c) micelles and (d) the inverted hexagonal (H_{II}) phase. Figure (b), (c) and (d) reproduced with permission from ref ([16]). Copyright © 2004 Elsevier B.V.

1.1.2 Lipid phase behavior

1.1.2.1 Gel to liquid-crystalline phase transition

The gel to liquid-crystalline transition temperature (T_c) is an important property of lipids and profoundly influences their packing and mobility (Figure 1.2).[8,15,17] When maintained below T_c, the lipids exist in a gel state (L_β), in which the hydrocarbon chains are fully extended in an all *trans* conformation, and the packing is highly ordered with a small diffusion coefficient. At temperatures

above T_c, the lipids change to the liquid-crystalline phase (L_α). In this phase, acyl chains adopt a gauche conformation with increased lipid lateral diffusion (Figure 1.2a). Generally, T_c increases with increasing carbon numbers in the acyl chains. For example, 1,2-dilauroyl-*sn*-glycero-3-phosphocholine (DLPC), which contains 12 carbons, has a T_c of -2 °C. Adding two carbons to the tail, as in 1,2-dimyristoyl-*sn*-glycero-3-phosphocholine (DMPC), increases the T_c to 24 °C. In contrast, T_c notably decreases by including double bonds in the tails. For instance, 1,2-dipalmitoyl-*sn*-glycero-3-phosphocholine (DPPC), with two saturated acyl chains, has a T_c of 41°C, while the T_c drops to -17 °C for 1,2-dioleoyl-*sn*-glycero-3-phosphocholine (DOPC), which contains *cis* double bonds.

Permeability of the bilayer membrane is greatest at the T_c of the lipid (Figure 1.2).[18,19] At T_c, a gel to liquid-crystalline transition takes place, creating boundaries between the two phases where the permeability is enhanced. Below or above T_c, liposomes can retain their contents well since the gel/liquid interfaces have been eliminated.

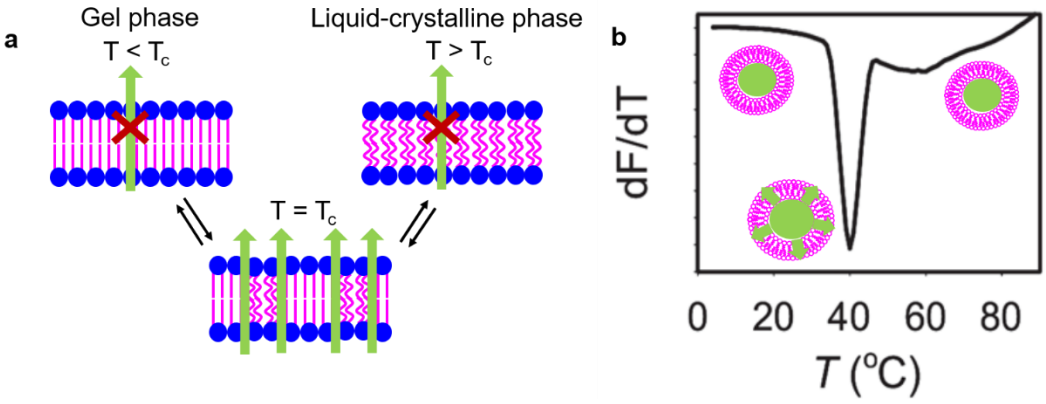

Figure 1.2 (a) Schematic illustration of the lipid phase transition. (b) A calcein release curve of DPPC liposomes (T_c: 41 °C) as a function of temperature. Figure (b) adapted with permission from ref ([19]).

1.1.2.2 Lipid phase separation

Liquid-liquid (liquid-ordered/liquid-disordered, L_o/L_d) phase separations have been widely demonstrated over a wide range of lipid compositions. Usually, the presence of cholesterol is the key.[2,8,15,17,20] On one hand, cholesterol exerts a fluidizing effect that imposes the lateral mobility of gel phase lipids. On the other hand, it exerts a condensing effect on liquid-crystalline phase lipids that increases the lipid packing and reduces the lateral mobility (Figure 1.3a).[20] When a sufficient amount of cholesterol is added, both the gel and liquid-crystalline phase convert to a new phase, termed liquid-ordered phase (L_o phase), which has an intermediate conformational order of liquid-crystalline phase and gel phase.[2,8,17,20] When added to lipid mixtures, cholesterol has a favorable interaction with unsaturated acyl chains, facilitating the formation of "lipid rafts" with cholesterol-rich high-phase transition lipids (L_o phase) that float in cholesterol-poor low melting lipid bilayers (liquid disordered phase, L_d phase). By incorporating fluorescent dyes that selectively partition in L_o or L_d phase, the L_o/L_d phase separation can be directly visualized in giant unilamellar vesicles (GUVs) using confocal fluorescence microscopy (Figure 1.3b).[21] The liquid-liquid (L_o/L_d) phase diagrams are well-established in model membranes of ternary lipid systems.[22-24] In addition, the lipid raft hypothesis is highly relevant to protein sorting and cellular signaling in biological systems.[2,25,26]

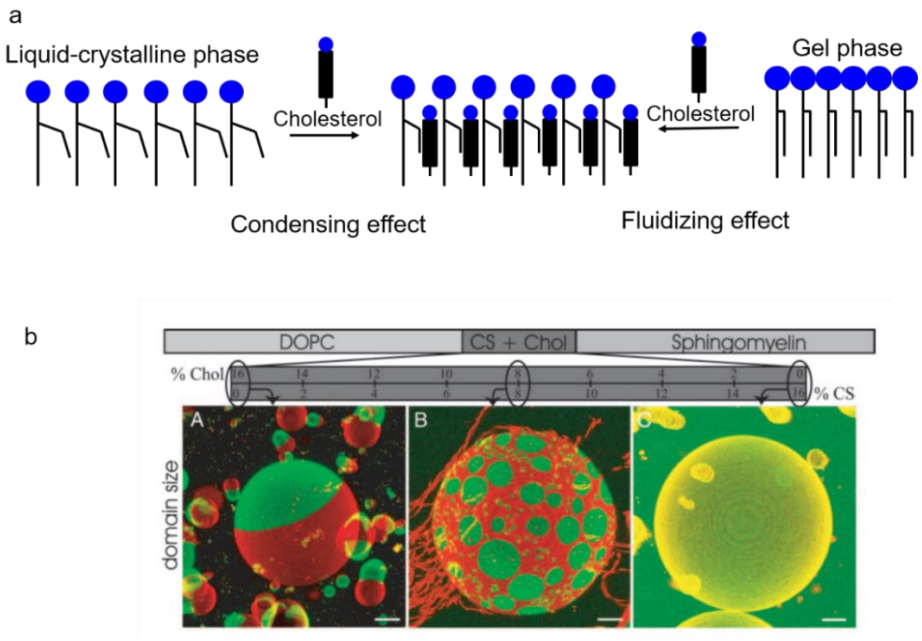

Figure 1.3 (a) Schematic illustration of the incorporation of cholesterol into liquid-crystalline phase lipids and gel phase lipids. (b) Confocal microscopy images of L_d/L_o phase separation in GUVs with different cholesterol contents. Dil-C18 fluorophore stains the L_d phase (red) and cholera toxin fluorophore stains the L_o phase (green). Scale bar: 10 μM. Figure (a) adapted with permission from ref ([20]). Copyright © 2014 American Chemical Society. Figure (b) adapted with permission from ref ([21]). Copyright © 2005 by The National Academy of Sciences of the USA.

1.1.3 Different types of lipids

A vast number of lipids have been identified in nature, and more are available through chemical synthesis. Figure 1.4 lists some common lipids. Phosphocholine (PC) lipids (Figure 1.4a and b) are the main constituents of the outer membrane of eukaryotic cells. They are highly biocompatible and are the most widely-used lipids in model cell membranes. The headgroup of PC lipids contains a phosphate and a choline group. Choline is a quaternary ammonium cation, and phosphate has a pK_a lower than two showing a negative charge over a wide range of pH's.[27,28] Therefore, PC lipids are zwitterionic and overall charge neutral. Although PC headgroups are highly hydrated and possess strong antifouling

properties (e.g., resistant to protein adsorption),[29,30] they can readily adsorb with many kinds of organic and inorganic materials via different interaction mechanisms.[31,32] The phase behavior can easily be modified by changing the structure of the tails. As shown in Figure 1.4a, DOPC lipid, containing two carbon double bonds in the tails, has a low T_c of -17 °C, while DPPC lipid with two saturated acyl chains possesses a T_c of 41 °C (Figure 1.4 b).

Phosphatidylethanolamine (PE) lipids (Figure 1.4c) are the second-most abundant lipids in mammalian cell membranes (~25% of total lipids). They are especially rich, in brain membranes, with an abundance of approximately 45%.[33] PE lipids are also zwitterionic at biological pH. Compared to PC lipids that tend to form flat bilayers, PE lipids tend to form non-lamellar structures because of their negative curvature. As a result, formation of stable PE lipid bilayers requires the assistance of other lipids.[34,35]

Phosphatidylserine (PS) lipids are found in a variety of cell types with only moderate abundance (5-10 mol % of total lipids); however, they are involved in important biological functions.[33,36] PS lipids are asymmetrically distributed across the membrane bilayers with the inner leaflet is enriched with PS lipids. The flipping of PS lipids to the outer leaflet initiates blood clotting and cell apoptosis. A number of proteins interact particularly with PS lipids.[37-39] The PS headgroup is negatively charged at physiological pH and contains several metal-binding ligands, such as amine and carboxyl groups. PS lipids are known to complex with many kinds of metal ions and metal oxides.[40-42]

Although the majority of natural-occurring lipids are negative or neutral, positively-charged lipids can be obtained synthetically. 1,2-Dioleoyl-3-trimethylammonium-propane (DOTAP) (Figure 1.4e) is a positively-charged synthetic lipid containing trimethylammonium in the headgroup. On one hand, the cationic liposomes can interact with negatively-charged cell membranes, which significantly improves endocytosis.[43,44] On the other hand, cationic liposomes affect immune responses and cell signaling pathways, which can be toxic to cells.[45]

Headgroup-inversed lipids were first obtained via chemical synthesis by Szoka's group in 2012.[46] Such lipids have an inverse headgroup charge orientation relatively to traditional PC lipids;

they are termed choline phosphate (CP) lipids (Figure 1.4f and g). DOCP (2-((2,3-bis(oleoyloxy)propyl)-dimethylammonio)ethyl hydrogen phosphate) shows a negative charge at physiological pH. Because it contains a terminal phosphate group, strong coordination can happen with metal and metal oxides.[47-50] By adding an ethane group at the terminal phosphate, a zwitterionic headgroup-inversed lipid, DOCPe (2-((2,3-bis(oleoyloxy)propyl)dimethylammonio)ethyl ethyl phosphate) (Figure 1.4g), is generated. Their blood circulation property is different from traditional zwitterionic PC lipids.[51]

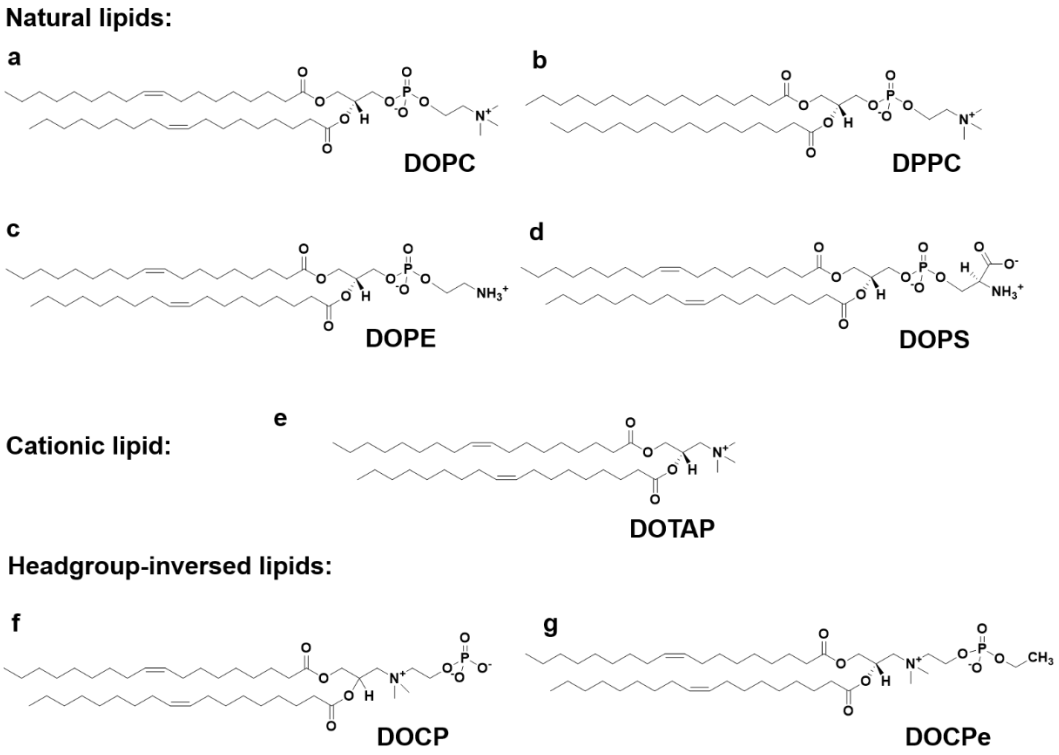

Figure 1.4 Chemical structures of typical phospholipids. (a) DOPC, (b) DPPC, (c) DOPE, (d) DOPS, (e) DOTAP, (f) DOCP and (g) DOCPe.

1.1.4 Model lipid membranes

The complexity of biological membranes has motivated the development of simple model systems with precisely-tailored geometry and composition.[7,8,52] The most widely-used model membrane

systems are solid supported lipid bilayers (SLBs) and liposomes. The SLBs are lipid bilayers that sit on the solid support (Figure 1.5a). They are typically prepared by fusion of lipid vesicles from an aqueous suspension or by Langmuir-Blodgett transfer. Silica and mica are commonly used substrates, as they are hydrophilic, smooth and clean to support membranes with few defects. The lateral diffusion of the lipids is maintained by a layer of water trapped between the substrate and lipid bilayers.[53] SLBs are robust, and allow a wide variety of surface-specific analytical techniques for characterization, including atomic force microscopy (AMF), surface plasmon resonance (SPR), and vibrational sum frequency generation spectroscopy (VSFG). One major disadvantage of SLBs is that targets might have unfavorable interactions with the underlying substrates.

Liposomes are lipid vesicles made of lipid bilayers that disperse in aqueous solution (Figure 1.5b). Soon after their description in the 1960s,[54-56] liposomes received ever-increasing interest for both fundamental research and practical applications. They have been widely used in drug delivery because of their excellent biocompatibility, facile size and charge manipulation, and their effective encapsulation of both hydrophobic and hydrophilic molecules.[57,58] Liposomes are also widely used in nanotechnology for templated synthesis and biosensors.[59,60] Apart from these, liposomes, as closed-volume containers, represent the simplest cell model systems to study membrane biology and biophysics.[60] Understanding the interactions that occur at the lipid bilayer interface not only is of importance to understand cellular processes, but also benefits material science. In my work, I will use liposomes as a cell model to study the membrane interactions with incoming materials, since liposomes allow studies to take place in solution phase and avoid undesirable interactions with underlying substrates. The following section also includes previous studies carried out on SLBs.

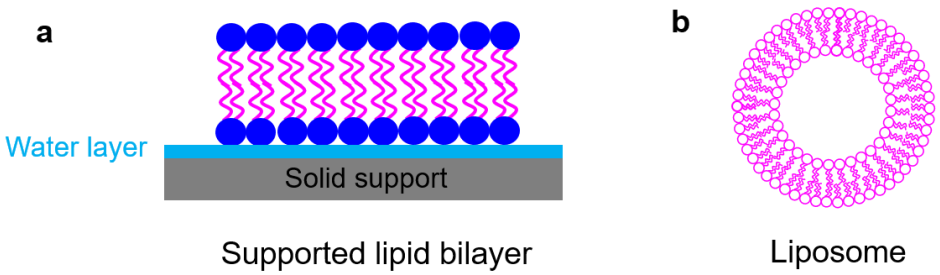

Figure 1.5 Schematic illustration of structures of (a) SLB and (b) liposome.

1.2 Liposomes

1.2.1 Liposome classification and preparation

Liposomes are generally classified based on their size and number of bilayers.[57,61] Small unilamellar vesicles (SUVs) have a size between 20 nm and 100 nm, large unilamellar vesicles (LUVs) possess a size up to 1000 nm, and GUVs typically have a size in the micrometer range which can be visually resolved using optical microscopy. Liposomes with more than one lipid bilayer are termed multilamellar vesicles (MLVs).

The first described method for liposome preparation is the Bangham method.[56] This method involves forming a lipid film by dissolving lipids in organic solvents, followed by completely removing the solvent. The films are then rehydrated with aqueous solvents. After rehydration, MLVs with a heterogeneous size distribution are formed (Figure 1.6a). Additional size reduction techniques are needed to generate homogeneous liposomes with controlled sizes. The extrusion method is commonly used to produce SUVs with defined sizes and distribution. This method involves multiple extrusions through a polycarbonate membrane (Figure 1.6b). The degree of size reduction depends on the number of extrusions and the pore size of the polycarbonate membrane. It is noteworthy that the extrusion processes need to be carried out above the T_c of lipids.[57,62] Such a method allows uniform liposomes with a size of 50 nm to 200 nm to be prepared. Sonication is an alternative method to reduce the size of liposomes, but the drawbacks may include high temperatures and metal contamination. In addition

to the Bangham method, other methods have been also used to prepare liposome with homogeneous sizes, including reverse phase evaporation techniques, solvent injection techniques, and detergent dialysis.[57] However, these methods may have remaining trace amounts of organic solvent, which can interact with lipids.

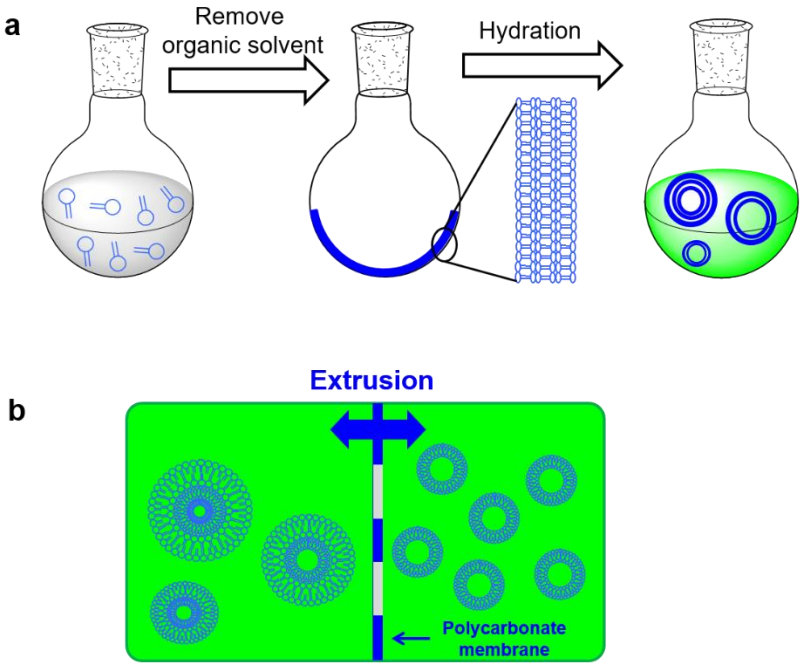

Figure 1.6 Schematic illustration of (a) liposome preparation by the Bangham method and (b) liposome size reduction by extrusion.

1.2.2 Liposome interfaces

Liposomes can interact with a wide range of materials, including proteins, organic polymers, metal ions, and inorganic/organic NPs.[9,31,63-65] Depending on the composition and surface properties of both liposomes and incoming materials, various interactions are possible. Some materials can simply adsorb on the liposome surface and stabilize the liposome structure (Figure 1.7a), while others may induce membrane disruption and content release (Figure 1.7b). With stronger interactions, lipid membranes can rupture and rearrange on the material surfaces to form SLBs (Figure 1.7c). In other

cases, liposome aggregation (Figure 1.7d) or fusion (Figure 1.7e) can be promoted upon interaction. Among a wide variety of materials, we have an interest in liposome interactions with metal ions and metal-containing materials.

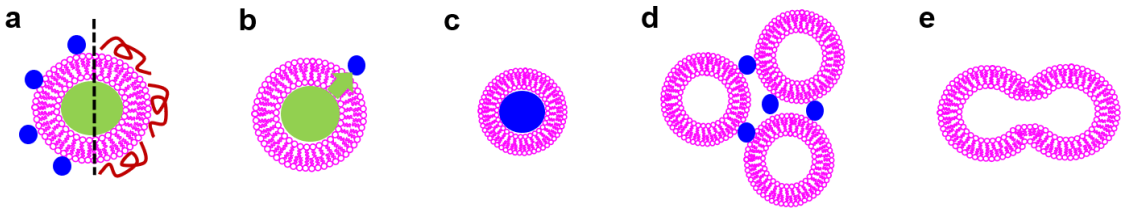

Figure 1.7 Schematic illustration of different interactions with liposomes: (a) adsorption and stabilization, (b) adsorption and membrane leakage, (c) the formation of SLBs, (d) liposome aggregation, and (e) liposome fusion.

1.3 Interfacing Phospholipids with Metal Ions/Metal-Containing Materials

The study of the interactions between lipid membranes and metal ions/metal-containing materials is important. First, naturally-occurring lipids contain many metal-binding ligands. Their interaction with metal ions in biological systems is ubiquitous. In fact, many essential cellular processes are regulated by binding of metal ions with membrane lipids, such as cellular signalling, membrane fusion and protein regulation.[66,67] Second, interactions can happen through coordination forces, which is a unique ability for materials containing metal elements. Together with the diversity of metal centers, many distinct features are observed compared to materials without metals.[68-70] Lastly, although many metals do not exist in biological systems, they have exceptional properties that are useful for drug delivery and bioimaging.[71] Studying their interactions with lipid membranes is particularly important to predict their cytotoxicity.[72] In addition, engineering these materials with lipids is an effective way to improve their biocompatibility and stability.[73]

Herein, we confine our work to the direct interactions between lipid membranes and metal-containing materials. In other words, the lipids used have no further functional group modification, and the metal-containing materials are "naked" without surface-ligand capping. In the following section, we first briefly discuss the surface forces commonly encountered in the interactions with lipid bilayers. The interactions of lipid bilayers with metal ions and metal oxides are then reviewed. Finally, interactions with gold nanoparticles (AuNPs) are introduced to illustrate adsorption-induced local gelation and its effect on membrane integrity.

1.3.1 Interaction forces

1.3.1.1 Van der Waals forces

Van der Waals forces are the most ubiquitous nanoscale interactions that originate from dipole interactions between atoms or molecules.[74] Three components contribute to van der Waals forces: 1) Keesom interactions, the interactions between two permanent dipoles, 2) Debye interactions, the dipole-induced dipole interactions, and 3) London dispersion interactions, the interactions between two instantaneous dipoles. The van der Waals interactions between atoms/molecules may be expressed by the well-known formula

$$W_{vdw}(r) = -C_{vdw}/r^6$$

where r is the distance between atoms/molecules and, $C_{vdw} = C_{Keesom} + C_{Debye} + C_{London}$, which accounts for the three above-mentioned van der Waals components. Between molecules, the van der Waals energy decreases steeply with $1/r^6$. The van der Waals forces between similar materials are always attractive, and larger van der Waals forces are characterized by a larger Hamaker constant. For the interactions with lipid bilayers, such force is responsible for AuNPs and SiO_2 adsorption with DOPC liposomes.[31]

1.3.1.2 Electrostatic forces

Liposomes can easily interact via electrostatic interactions since the lipid headgroup can be positive, negative and zwitterionic. Zwitterionic liposomes are always used to minimize electrostatic interactions. Attractive forces are generated when oppositely-charged liposomes and materials are mixed. A well-known example is the adsorption of negative nucleic acids by cationic liposomes, which is widely used in gene therapy.[44]

Electrostatic repulsion arises when liposomes are mixed with NPs bearing the same surface charge. Such repulsion is the result of electrostatic double layer forces (Figure 1.8a). When charged surfaces are dispersed in aqueous solution, the charged electrolyte forms an electrostatic double layer with a compact Helmholtz layer and a loosely packed diffusion layer.[75] When approaching each other, electrostatic double layers overlap, resulting in a repulsive force. The Derjaguin-Landau-Verwey-Overbeek (DLVO) theory, which describes the sum of the attractive van der Waals forces and repulsive electrostatic double layer forces, has been established to quantitatively predict the interactions between dispersed particles (Figure 1.8b).[75,76] The overall repulsion force is important for colloidal stability. However, it sometimes prevents two particles from getting close, which hinders adsorption. Strong electrostatic attraction or repulsion can be screened by increasing the ionic strength of the solution.[76,77]

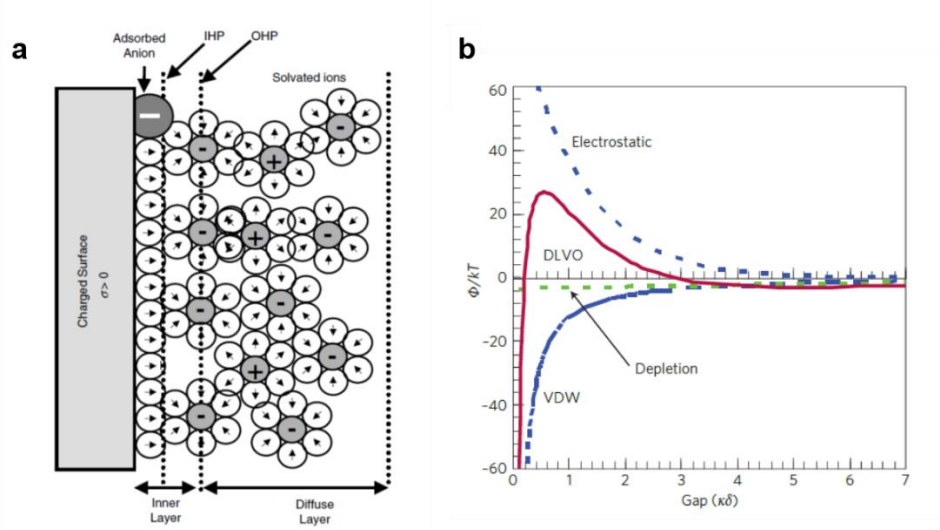

Figure 1.8 (a) Schematic representation of the double layer structure according to the Stern-Gouy-Chapman (SGC) model. (b) DLVO theory. Figure (a) reprinted with permission from ref ([75]). Copyright © 2010 John Wiley and Sons. Figure (b) reprinted with permission from ref ([76]). Copyright © 2009 Macmillan Publishers Limited.

1.3.1.3 Metal coordination

Transition metals and lanthanide metals have the ability to accept electron pairs from ligands to form coordination bonds. Lipid headgroups contain many ligands that are ready to coordinate with metal ions. For example, PS and PE lipids are good ligands for metal ions (see Section 1.3.2.2 for detail).

1.3.1.4 Hydration forces

When two hydrophilic surfaces are brought into contact, repulsive forces of approximately 1 nm have been measured in aqueous electrolytes between a variety of surfaces, including mica, silica, alumina and lipids.[78] Although the origin of hydration force is not well understood, such repulsive force has been attributed to the energy required to remove the water molecules from the surface.[6,13] It has been reported that the repulsive hydration force must be overcome to induce liposome fusion.[79,80] In

addition, the binding of several metal ions alters the hydration of the lipid molecules.[81,82] Moreover, the surface hydration forces strongly influence lipid adsorption on metal oxide surfaces.[83,84]

1.3.2 Metal ion binding to lipid bilayers

The binding of metal ions with lipid membranes has been long studied. Extensive studies have been carried out on the calcium ion because of its biological relevance. Recently, the importance of transition metal binding with lipids has also been realized. Although they are present in a much lower concentration in the body, they may bind to lipids with higher affinity due to their coordination ability.

1.3.2.1 Binding of Ca^{2+} with lipid bilayers

The binding of Ca^{2+} with lipids is stronger compared to alkali metal ions (e.g., Na^+, Li^+ and K^+) and other alkaline earth metal ions (e.g., Mg^{2+} and Sr^{2+}).[85-87] Ca^{2+}-induced lipid membrane fusion is well documented.[13,88-90] It is generally accepted that the presence of Ca^{2+} enhances lipid packing, induces lipid orientation and conformation changes, and causes dehydration of lipid headgroups.[82,87,91-94] It can also neutralize and cluster negatively-charged lipids.[81,93,95] In addition to electrostatic interactions, Ca^{2+} binds to specific sites in the lipids. For instance, the binding of Ca^{2+} with phosphate, carboxyl and carbonyl groups has been reported.[87,92-94,96,97] The binding affinity (characterised by K_d) of Ca^{2+} with lipids is usually in the millimolar range. Recently, with the successful synthesis of headgroup-inversed lipids, the effect of lipid headgroup dipole on lipid binding with Ca^{2+} has been studied.[46,98] The effect of Ca^{2+} binding on headgroup-inversed liposomes of DOCPe and DOCP is different compared to traditional zwitterionic DOPC and negatively-charged DOPS and DOPA. Ca^{2+} causes a slower DOCP aggregation compared to DOPS and DOPA. In addition, a plateau effect at higher Ca^{2+} concentrations was observed for DOCP, which was absent with DOPS and DOPA (Figure 1.9a). For zwitterionic liposomes, the binding of Ca^{2+} increased the DOPC surface potential to positive. In contrast, the overall potential remained negative for DOCPe (Figure 1.9b).[46]

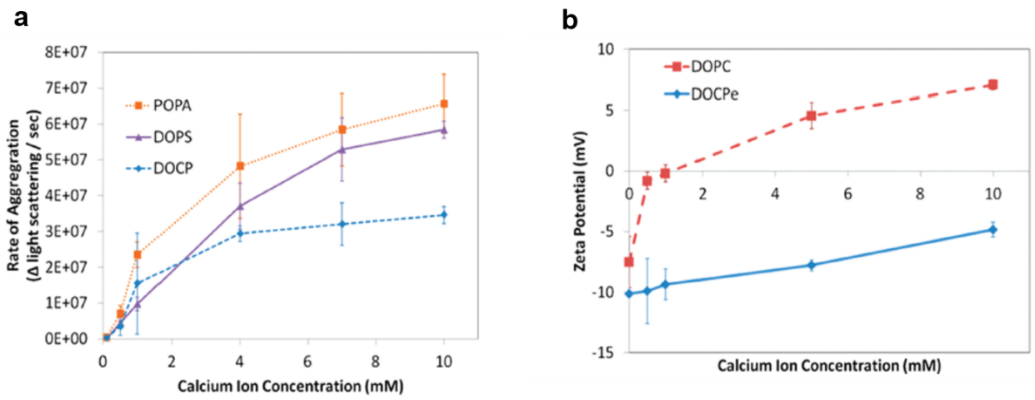

Figure 1.9 (a) The aggregation rates of anionic liposomes induced by Ca^{2+}. (b) ξ-potential of zwitterionic liposomes in the presence of Ca^{2+}. Figures reprinted with permission from ref ([46]). Copyright © 2012 American Chemical Society.

1.3.2.2 Binding of transition metal ions with lipid bilayers

Transition metal ions usually bind to lipids stronger than Ca^{2+}. While electrostatic interactions exist, coordination interactions play an additional important role. Cremer's group studied the binding of Cu^{2+} with PS and PE lipids supported on a silica surface (Figure 1.10).[40,41,99] Using a fluorescence quenching method, they demonstrated that the Cu^{2+} tightly bound to PE lipids.[99] At physiological pH, the apparent equilibrium dissociation constant, K_{DAPP}, was approximately 2 μM, and it was insensitive to the PE content in the membrane. The K_{DAPP} significantly decreased when the pH was increased to 10 (Figure 1.10a) and also changed as a function of PE content (Figure 1.10b), with 10 μM for SLBs containing 1 mol % DOPE and 150 nM for SLBs containing 70 mol % DOPE. The tightening at pH 10 was because PE has an intrinsic pK_a of 9.6; thus, PE lipids bear a negative charge at pH 10. As such, the interfacial charge increased with PE content, resulting in an increase in Cu^{2+} concentration at the membrane surface. The binding was believed to happen between the Cu^{2+} and the amine group in PE (Figure 1.10c). Once bound, Cu^{2+} participated in Fenton-like chemistry to produce hydroxyl radicals/superoxide, which enhanced the oxidation of double bonds in the lipid tails (Figure 1.10d). The

oxidation rate was 8.2 times faster for bilayers containing 70 mol % PE than pure PC bilayers upon exposure to 70 μM Cu^{2+} and 10 mM hydrogen peroxide.

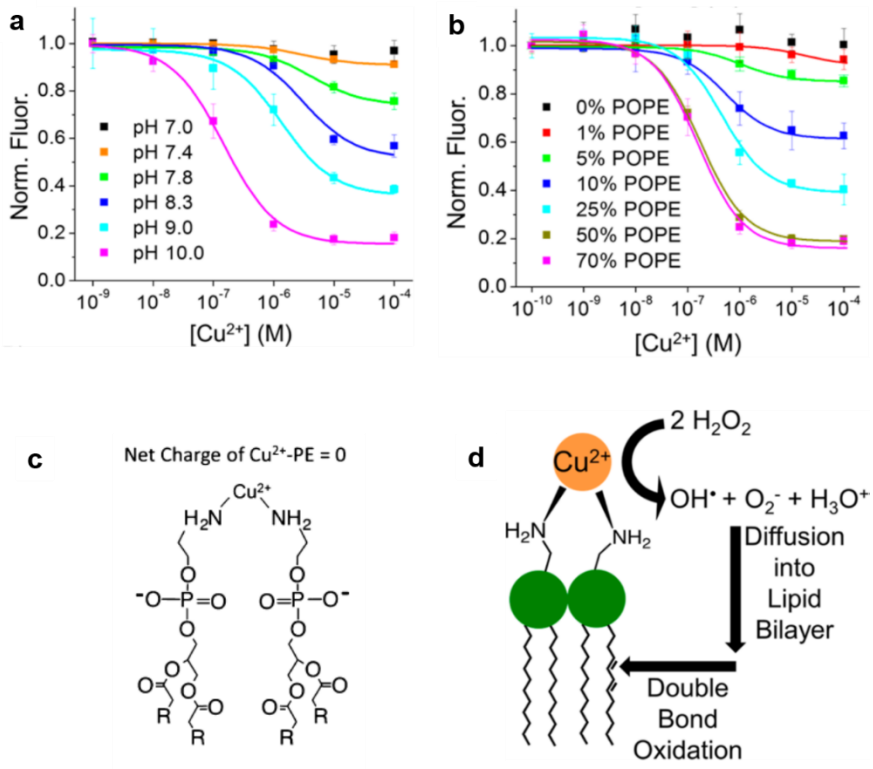

Figure 1.10 (a) Normalized fluorescence of SLBs in the presence of Cu^{2+} from pH 7.0 to 10.0. (b) Normalized fluorescence of SLBs containing 0 to 70 mol % DOPE at pH 10.0. (c) Cu^{2+} binds to the amine on two PE lipids, forming a bivalent complex with a net-neutral charge. (d) Schematic illustration of lipid oxidation enhanced by Cu^{2+} binding. Figures adapted with permission from ref ([99]). Copyright © 2016 American Chemical Society.

Compared to the binding to PE lipids, Cu^{2+} binds to PS lipids even stronger.[40,41] The K_{DAPP} is down to the pM region, which is nearly 5 orders of magnitude tighter than that of Cu^{2+}-PE under the same conditions. This tighter binding was attributed to the unquenchable surface potential of PS-containing surfaces.[41] This was because the binding of Cu^{2+} with the amine group releases two protons, making them still negatively charged after binding (Figure 1.11b). Such unquenchable surface potential

increases the Cu^{2+} concentration in the double layer (Figure 1.11a). In contrast, when bound to the above-mentioned PE lipids, the net charge of Cu^{2+}-PE is zero (Figure 1.10c). In addition, Cu^{2+} binds to PS lipids in a pH-dependent manner, whereas the Cu^{2+} is strongly bound to PS lipids at basic pH, and while dissociation occurs when the pH is lowered.[40] These studies provide molecular information of Cu^{2+} binding to lipids. However, they were carried out using SLBs; the effects of metal binding on membrane aggregation and integrity were not studied. In our study, we used liposomes to investigate these effects.

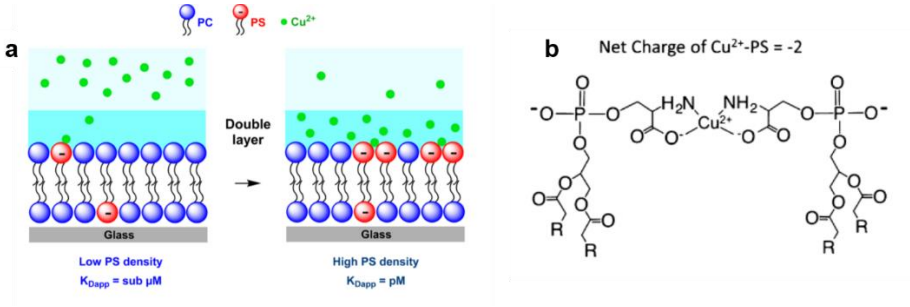

Figure 1.11 (a) Schematic representation of the change of K_{Dapp} with PS density in SLBs. (b) Cu^{2+} binds to the amine and carboxylate of two PS lipids to form a bivalent complex with a net charge of -2. Figure (a) adapted with permission from ref ([41]). Copyright © 2015 American Chemical Society. Figure (b) adapted with permission from ref ([99]). Copyright © 2016 American Chemical Society.

1.3.3 Interfacing liposomes with metal oxides

1.3.3.1 Metal oxides

Metal oxides are important materials that display exceptional electrical, optical, and magnetic properties, making them promising candidates for a wide variety of applications.[100] Their controllable surface structures make them ready to interact with other components. Once dispersed in an aqueous medium, the oxides become charged as a result of the ionisation of surface groups, with the charge related to solution pH. Using TiO_2 as an example, it has a point of zero charge (PZC) of pH 5.8. At pH 5.8, the charge of TiO_2 is zero. Below pH 5.8, the TiO_2 is positively charged:

$$Ti\text{-}OH + H^+ \longrightarrow Ti\text{-}OH_2^+$$

At a pH higher than 5.8, it is negatively charged:

$$Ti\text{-}OH + OH^- \longrightarrow Ti\text{-}O^- + H_2O$$

Since each metal oxide has unique surface chemical properties, they interact with lipid molecules in various ways. Early studies in the field focused on the interaction of liposomes with planar SiO_2 surfaces. Inspired by this, studies have been carried out on planar TiO_2 surfaces. Most recently, the interactions of liposomes with nanosized TiO_2 have been investigated.

1.3.3.2 Interfacing liposomes with planar oxide surfaces

The initial work centered on the interactions of PC liposomes with SiO_2 surfaces.[53,101] Strictly speaking, SiO_2 is not a metal oxide, but the study of it provides an important fundamental understanding of and comparison to metal oxides. The general agreement is that PC liposomes can adsorb and fuse with SiO_2 surfaces forming SLBs. The interactions between PC lipids and SiO_2 surfaces are considered to involve van der Waals forces.[31] In this process, the balance between the adhesion energy and the curvature energy determines the liposome deformation and fusion. The importance of cooperative effects of neighboring vesicles has been demonstrated, whereas the liposomes need critical coverage to form SLBs, below which the liposomes are adsorbed intact.[102,103] Electrostatic forces, which can be modulated by ionic strength, solution pH, and divalent metals, provide an extra contribution on top of the attractive van der Waals forces to facilitate PC liposomes fusion on SiO_2.[104,105] The PC headgroup and SiO_2 surfaces are not directly attached; instead, they are separated by a thin water layer (~ 1 nm). Thus, the fluidity of SLBs is largely maintained.

Later research interests changed to TiO_2 surfaces because of their excellent biocompatibility. In comparison to SiO_2, liposome fusion with TiO_2 is generally considered difficult. Early work reported that PC liposomes adsorbed intact on TiO_2 surfaces without rupture, even in the presence of Ca^{2+}.[106,107] While later research demonstrated that with a high liposome concentration and a long incubation time, PC liposomes could form bilayers on TiO_2 that were similar to those on SiO_2, and the interaction energy

was 20-fold higher than on SiO_2. In other methods, PC liposome fusion could occur below pH 4.[108,109] It was proposed that van der Waals forces were not strong enough to rupture liposomes on the TiO_2 surface, and additional electrostatic interactions were needed, which could be generated at pH below the pK_a of TiO_2.[109] Besides the zwitterionic PC liposomes, the fusion of negatively-charged liposomes with TiO_2 could occur in the presence of Ca^{2+}.[101,110]

1.3.3.3 Interfacing liposomes with metal oxide NPs

1.3.3.3.1 PC liposomes adsorb intact on TiO_2 NPs via chemical interactions

The adsorption of DOPC liposomes on TiO_2 NPs has been studied by Liu's group.[111] Instead of van der Waals force-driven SiO_2/DOPC adsorption, a strong chemisorption mechanism was proposed based on several different observations for DOPC adsorption on TiO_2 compared to SiO_2.[111] First, the amount of adsorbed DOPC on TiO_2 is insensitive to ionic strength, but the adsorption by SiO_2 is promoted by NaCl. Second, TiO_2 adsorption is pH-dependent, in which the adsorption is significantly weakened at a pH higher than the PZC (pH 6.8), but SiO_2 retained adsorption capacity even at pH 11. The high pH only provided a kinetic barrier for TiO_2 adsorption, because once adsorbed, the stability of the hybrid materials was not affected by raising the pH. Lastly, phosphate inhibited DOPC adsorption on TiO_2 but not on SiO_2. Based on these observations, the formation of a covalent bond between lipid phosphates and Ti centers via nucleophilic attack was proposed (Figure 1.12e). Cryogenic-TEM (Cryo-TEM) showed DOPC adsorbed on TiO_2 NPs as intact liposomes (Figure 1.12f), while the adsorption on SiO_2 resulted in SLBs (Figure 1.12c). The lack of SLB formation was attributed to the strong steric effect of choline that impedes the DOPC liposome rupture.

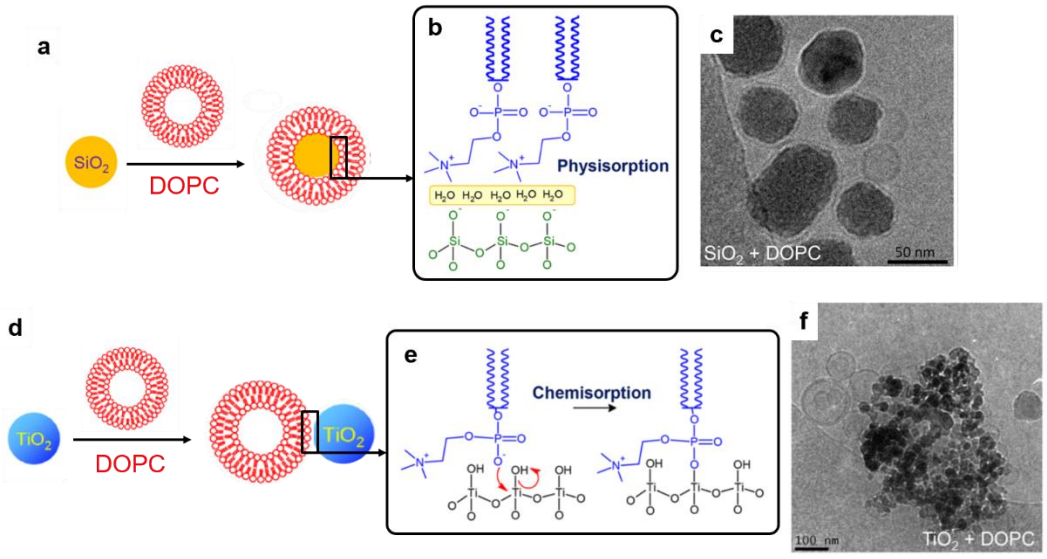

Figure 1.12 (a) Schematic illustration, (b) proposed interaction mechanism, and (c) cryo-TEM micrograph of DOPC liposomes interacting with SiO_2 NPs. (d) Schematic illustration, (e) proposed interaction mechanism, and (f) cryo-TEM micrograph of DOPC liposomes interacting with TiO_2 NPs. Figures adapted with permission from ref ([111]). Copyright © 2014 Wiley-VCH Verlag GmbH & Co. KGaA, Weinheim.

1.3.3.3.2 CP and PS liposomes form SLBs on TiO_2 NPs

Inspired by the hypothesis that the lack of DOPC fusion on TiO_2 at neutral pH is due to the steric effect of the choline group, the interaction of TiO_2 with headgroup-inversed DOCP liposomes was studied (Figure 1.13).[47,49] DOCP has a directly exposed phosphate; thus, in this way, the steric effect is eliminated. The difference between DOPC and DOCP was first observed in a calcein leakage test. When using calcein loaded DOPC liposomes, adding TiO_2 did not cause leakage from the liposomes (Figure 1.13f). In comparison, TiO_2 leaked DOCP liposomes upon mixing (Figure 1.13g), suggesting that liposome rupture might take place. Indeed, the presence of supported DOCP bilayers surrounding the TiO_2 surfaces was confirmed using cryo-TEM (Figure 1.13d). The generation of such features was attributed to the stronger interactions of TiO_2 with the terminal phosphate and the absence

of steric effects from the choline group (Figure 1.13b). The formation of DOCP SLBs on TiO_2 could occur between pH 3 and pH 10.[42] In addition to DOCP liposomes, the negatively-charged DOPS liposomes can also form SLBs on TiO_2 in the same pH range (Figure 1.13e).[42] This was attributed to the coordinating ability of serine groups. The carboxyl group was believed to be involved in bonding with TiO_2 NPs (Figure 1.13c).

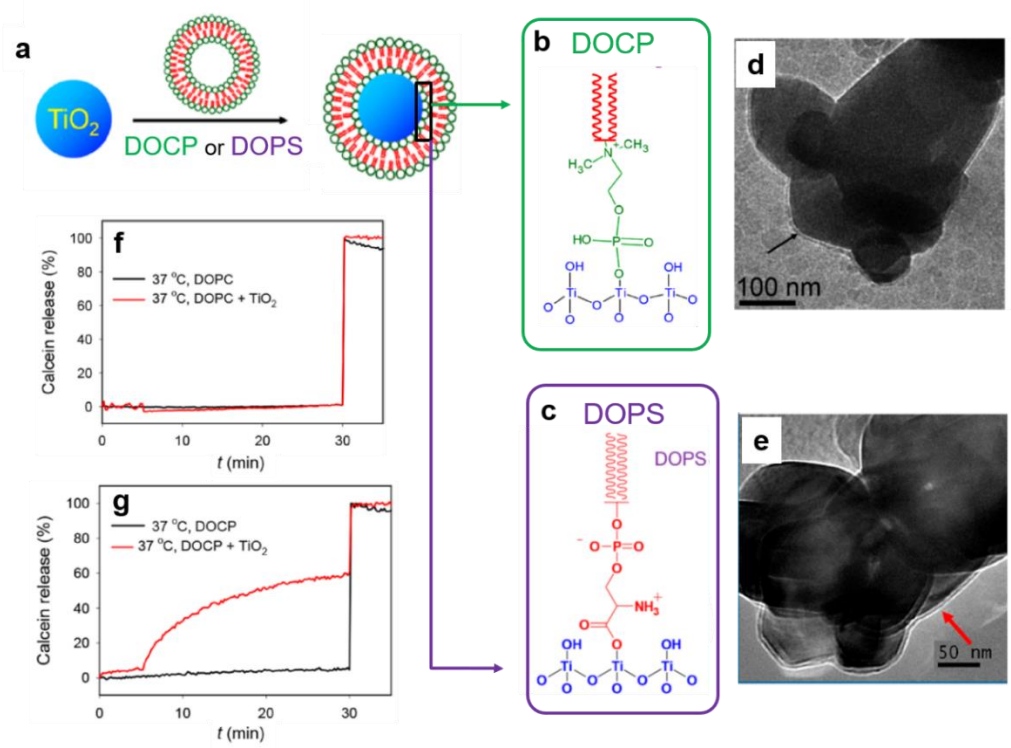

Figure 1.13 (a) Schematic illustration of (b) DOCP and (c) DOPS liposomes forming SLBs on TiO_2 NPs. Cryo-TEM micrographs of TiO_2 NPs interacting with (d) DOCP liposomes and (e) DOPS liposomes. Calcein-loaded liposome fusion tests when TiO_2 NPs mixed with (f) DOPC liposomes and (g) DOCP liposomes. Figures adapted with permission from ref ([47]), Copyright © 2015 American Chemical Society, and ref ([42]), Copyright © 2018 American Chemical Society.

1.3.4 Interfacing liposomes with AuNPs

AuNPs are particularly attractive for nanotechnology because of their unique distance-dependent color, tunable surface chemistry and high biocompatibility.[112,113] AuNPs are featured with high inter-particle van der Waals forces (i.e., larger Hamaker constants), yielding low colloidal stability. Interfacing lipid bilayers with AuNPs has been extensively studied for both fundamental understanding and practical applications. Most studies used AuNPs capped by surface ligands.[114,115] Although surface capping improves colloidal stability, the native AuNP surface is masked, which hinders interactions emerging directly from the Au core. Most AuNPs prepared in aqueous solution are capped by citrate, which is a weak ligand and can be readily displaced. Therefore, citrate-capped AuNPs are generally considered to be naked and are used to study the direct interactions between AuNP cores and lipid bilayers.

1.3.4.1 Adsorption-induced local lipid gelation and gel/fluid interface merging

The interactions of citrate-capped AuNPs with DOPC liposomes have been studied.[116,117] Citrate-capped AuNPs could be adsorbed and aggregated on the liposome surface. The adsorption did not rupture the overall liposome structure; however, it caused membrane leakage. Since the leakage also happened when AuNPs were removed or more AuNPs were added, local transient leakage was suggested.

Together with the fact that liposomes leak their contents most rapidly at T_c and local lipid surface reconstruction reported by Granick's group,[32] a citrate-AuNPs adsorption-induced local fluid-to-gel phase transition was proposed. In this model, the PC group is roughly parallel to the liposome surface. In the presence of negatively-charged NPs, the headgroup is tilted to favor interactions with the positively-charged choline, which reduces the headgroup area and induces gelation (Figure 1.14a). As such, DOPC lipids undergo a fluid-to-gel phase transition at the sites of citrate-Au adsorption, and leakage occurs during this transition; once the gel state is reached, leakage stops. Upon removing the AuNPs, the sites undergo a reverse transition, also resulting in transient leakage. This hypothesis was

further supported by the fact that no leakage was induced by AuNPs adsorption on DPPC liposomes, since they were already in gel phase and no phase transition occurred. Indeed, an increased T_c was observed, demonstrating the strengthening of DPPC lipid packing upon citrate-AuNP adsorption.

Varying the PC liposome fluidity by using PC lipids with different T_c, Liu's group also demonstrated a model of AuNPs merged on the surface of DOPC liposomes attributable to the local gelation of the fluid DOPC liposomes (Figure 1.14b, top). [117] Since the local gelation created fluid/gel lipid interfaces associated with a high interfacial energy, there was a thermodynamic driving force to merge the AuNPs to eliminate the interfaces or fluid/gel phase boundaries. In contrast, such merging was unfavorable in the gel phase DPPC liposomes since no fluid/gel lipid interfaces existed (Figure 1.14b bottom).

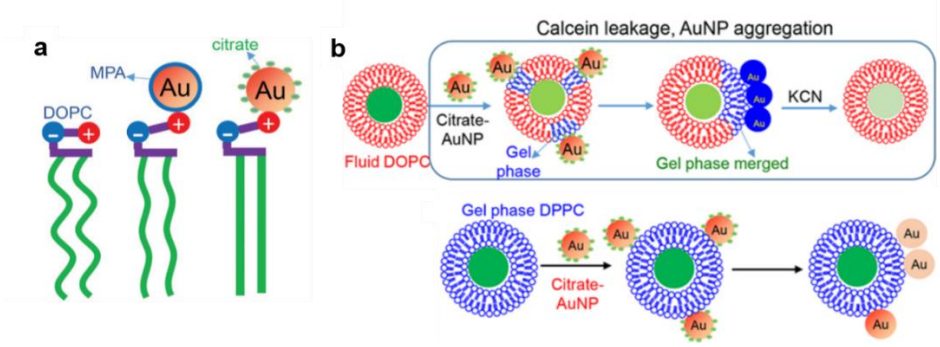

Figure 1.14 Schematic illustration of (a) AuNP-induced PC liposome leakage via a phase transition and (b) citrate-AuNP adsorption by DOPC inducing local gelation and emerging of gelled areas (top) and citrate-AuNP adsorbed by DPPC (bottom). Figure (a) adapted with permission from ref ([116]). Copyright © The Royal Society of Chemistry 2015. Figure (b) adapted with permission from ref ([117]). Copyright © 2015 American Chemical Society.

1.3.4.2 Manipulating surface forces by capping the AuNP surface with various ligands

The strong surface forces between PC lipids and AuNPs was proposed to be van der Waals forces.[116,117] Such very short-ranged forces can be precisely tailored by surface capping of AuNPs with various halide ions, including Cl^-, Br^- and I^- (Figure 1.15a).[118] These halide ions have sizes of 3.34 Å, 3.64 Å, and 4.12 Å, respectively. When mixed with DOPC liposomes, the color of AuNPs turned to purple, indicating aggregation. The aggregation was most extensive for citrate- and Cl^--capped samples, followed by Br^-, whereas the sample capped with I^- aggregated the least (Figure 1.15b). This indicates that Cl^--capped AuNPs had a similar effect to citrate-AuNPs. When the ligand size increased, the interactions decreased. I^--capped AuNPs had the weakest interactions with PC liposome, which was also demonstrated by only moderate leakage and a T_c increase (Figure 1.15c and d). Furthermore, the interactions between AuNPs and PC were totally blocked by coating the AuNPs with larger molecules greater than 10 Å. This work demonstrates that surface ligand capping has a strong influence on interactions with lipid bilayers.

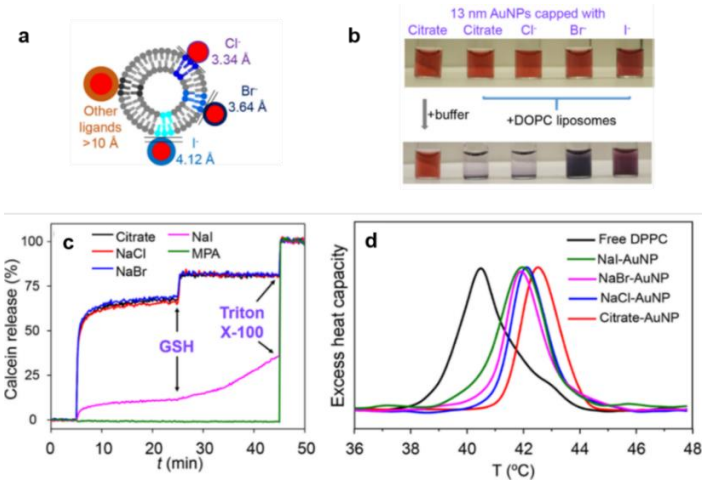

Figure 1.15 (a) Schematic of DOPC liposomes adsorbing AuNPs coated with various halides. (b) Photographs of AuNPs capped by various ligands before and after adding DOPC liposomes. (c) Calcein leakage tests of DOPC liposomes after adding various AuNPs. (d) Differential scanning calorimetry (DSC) traces of DPPC liposomes after mixing with various AuNPs. Figures adapted with permission from ref ([118]). Copyright © 2018 American Chemical Society.

1.4 Research Goals and Thesis Outline

Previous studies have shown that the association of metal ions/metal-containing materials with lipid bilayers significantly alters lipid bilayer constructions and their physicochemical properties. The majority of previous studies have focused on electrostatic interactions, while chemical interactions were overlooked. Because lipid molecules have versatile headgroup chemistry and metals possess unique coordination interactions, chemical interactions between them are inevitable. Focusing on their chemical structure may provide a molecular-level understanding of their interactions. Therefore, the primary focus of this thesis is to study the interactions between lipid bilayers and metal ions/metal oxides, with particular attention to chemical interactions. The metal ions studied mainly include transition metal ions and lanthanide metal ions due to their strong coordination ability. The metal oxides studied include TiO_2, ZnO, CeO_2 and Fe_3O_4 NPs, which were chosen for their biotechnological relevance. The goals of this thesis include: 1) studying the adsorption mechanisms, 2) identifying the surface forces, 3) investigating the membrane integrity, and 4) proposing general interaction models. The thesis consists of seven chapters.

Chapters 2 and 3 focus on the interactions of liposomes with transition metal ions. In Chapter 2, Zn^{2+} binding with headgroup-inversed CP liposomes is studied and compared to PC liposomes. The irreversible aggregation, stacking, and leakage of CP liposomes induced by Zn^{2+} was demonstrated, while no such behavior was observed with DOPC liposomes. The binding of Zn^{2+} to CP liposomes and PC liposomes was also studied using isothermal titration calorimetry (ITC). This work highlights the function of the terminal phosphate group in metal binding in liposomes. Chapter 3 describes Cu^{2+} binding to liposomes with four types of headgroups, PC, phosphoglycerol (PG), PS and CP. The binding was studied using a fluorescence quenching method. Membrane integrity was studied using dynamic light scattering (DLS), transmission electron microscopy (TEM) and calcein leakage assays. In addition, we demonstrated that Cu^{2+} stained individual liposomes with a short incubation time under TEM. It was found that the oxidative catalytic property of Cu^{2+} was inhibited by the tight binding of PS

liposomes. Finally, we proposed a model for the interactions of Cu^{2+} with each liposome. In combination with Chapter 2, we demonstrated that different metal ions interact with each lipid differently, so it is worthwhile to consider each case individually.

In Chapter 4, the growth of a nucleotide lanthanide coordination polymer shell on liposomes is demonstrated. First, the interactions of Gd^{3+} with CP and PS liposomes were studied systematically, including the surface potential and membrane integrity. With the conclusion that Gd^{3+} binding has no disruption on the PS membrane, a Gd^{3+}/AMP coordination polymer shell was coated on DOPS liposomes. The improved stability toward larger ZnO NPs but not the small surfactant molecule Triton X-100 was demonstrated. This work not only provides a simple method to coat liposomes, but also offers a fundamental understanding of liposome adsorption with lanthanide ions.

In Chapter 5, the interactions of nanoceria (CeO_2 NPs) with PC liposomes are studied. The nanoceria adsorption isotherms were determined at various pH's and ionic strengths using a fluorescence quenching assay. Calcein leakage, TEM and differential scanning calorimetry (DSC) studies indicated that nanoceria induced liposome leakage because of a transient local lipid phase transition. This study provided biointerfacial information at a molecular level regarding the interactions of nanoceria and model cell membranes.

In Chapter 6, the leakage and rupture of lipid membranes by charged metal oxide NPs are investigated. The perception in the field is that cationic nanomaterials can damage lipid membranes, while some reports suggest the opposite. To investigate this, instead of using different materials for testing the effect of charge, we used the same material to obtain different charges by varying the pH of the solution. By using calcein leakage assays to probe membrane leakage, we demonstrated that the charge alone is unimportant for membrane leakage; rather, the key is the interaction strength.

Chapter 7 describes the conclusions from each chapter, the original contributions of this research, and recommendations for further studies.

Chapter 2 Zn^{2+}-Induced Irreversible Aggregation, Stacking, and Leakage of Choline Phosphate Liposomes

The results presented in this chapter have been published as:

Yibo Liu and Juewen Liu, Zn^{2+} Induced Irreversible Aggregation, Stacking, and Leakage of Choline Phosphate Liposomes, *Langmuir*, **2017**, 33, 14472-14479.

2.1 Introduction

Cell membranes respond to ligand binding to allow cell signaling, endocytosis, membrane fusion and other biological processes.[76,119,120] Most phospholipids can self-assemble to form liposomes, which provide an excellent model system for biological membranes.[121,122] After loading drugs and fluorophores, stimuli-responsive liposomes are useful as drug delivery vehicles and biosensors.[123-127] While proteins and small molecules have been the most popular ligands to trigger reactions on lipid membranes, metal ions also attracted more and more attention recently.[40,41,94,99,128,129] For example, the role of Ca^{2+} in promoting liposome fusion has long been documented,[13,88] where Ca^{2+} brings liposomes closer and rearranges local lipids required for fusion.[88] Ca^{2+} binding to lipid by electrostatic interactions, dehydration, and specific site binding.[81,82,94] Such binding may rigidify lipid bilayers, reorient the headgroup, and cluster negative charged lipids.[81,82,94]

Cu^{2+} was reported to damage lipids by generating reactive oxygen species (ROS).[130-132] Cremer and coworkers studied metal binding to PS and PE lipids.[40,41,99,133] They reported extremely strong binding between Cu^{2+} and PS lipids.[40] The binding with PE lipids enhanced the oxidation of a lipid associated dye.[99] Sasaki and coworkers synthesized lipids modified with a pyrene in the tail and an iminodiacetic acid in the headgroup. Metal binding affected the packing of pyrene for highly sensitive detection of Cu^{2+} and Hg^{2+}.[134,135] They further demonstrated self-assembly of column structures of stacked lipid bilayers by adding Cu^{2+}.[128] Metal ions may also induce liposome leakage. For example, Hg^{2+} strongly binds to PE lipids resulting in the leakage of PE-containing liposomes as demonstrated

by Lu and coworkers.[129] Na^+ binding to lipid membranes was studied by DLS and ITC.[136,137] Finally, fluorescent ligands were also inserted in liposomes for metal detection.[138,139]

Most of the above studies focused on serine, amine and carboxyl groups for metal binding. The phosphate group is ubiquitous in phospholipids, however it has been overlooked in most studies involving transition metals. A general perception is that phosphate is chemically inert, and only certain high valent metals can bind.[140-142] The Liu lab recently emphasized the role of lipid phosphate in the adsorption of various metal oxides. For example, the phosphate in PC lipids can bind to TiO_2, Fe_3O_4 and ZnO surfaces.[31,47,49,111] The phosphate affinity to these oxides was significantly enhanced by inversing the headgroup to make CP lipids,[47,49] where the phosphate is fully exposed.[46,143] This indicates that CP might be a stronger metal ligand than PC. In addition, the inversed headgroup enhanced the phosphate interaction with metal ions since terminal phosphate has stronger metal binding affinity than bridging phosphate.[144] As such, we are interested in further studying its metal binding.

Zn^{2+} is abundant in biology for cellular communication and the development of skeletal systems.[145] Being a strong Lewis acid, Zn^{2+} is a common metal cofactor in many metalloproteins. Previous studies showed that Zn^{2+} could bind to negatively-charged PS liposomes, preventing lipid oxidation due to Fe^{2+} and Cu^{2+}.[146] In contrast, no such protection was observed with neutral PC lipids alone. Zn^{2+} might bind to lipid membranes via both electrostatic interactions and also Lewis acid/base interactions.[147,148] Herein, we study the binding of Zn^{2+} to PC and CP liposomes, highlighting the importance of the phosphate groups. This work revealed CP to be a high affinity ligand for Zn^{2+}, and various interesting nanoscale lipid structures were produced from such interactions.

2.2 Materials and Methods

2.2.1 Chemicals

All the phospholipids were purchased from Avanti Polar Lipids (Alabaster, AL). Zinc chloride, disodium calcein, Triton X-100, and phosphotungstic acid were purchased from Sigma-Aldrich. Sodium acetate, magnesium chloride, calcium chloride, sodium chloride, ethylenediaminetetraacetic

acid disodium salt (EDTA), 2-(N-morpholino)ethanesulfonic acid (MES), and 4-(2-hydroxyetyl)-1-piperazineethanesulfonic acid (HEPES) were from Mandel Scientific (Guelph, ON, Canada). Milli-Q water was used to prepare all the buffers, solutions, and suspensions.

2.2.2 Preparation of liposomes

Liposomes were prepared using the standard extrusion method.[47,49] DOPC or DOCP (2.5 mg) was dissolved in chloroform. After evaporating chloroform by blowing N_2, the samples were dried in a vacuum oven at room temperature overnight to fully remove chloroform. The dried lipid films were stored at -20 °C in a N_2 atmosphere prior to use. To prepare liposomes, the lipid films were hydrated with 0.5 mL of buffer A (10 mM HEPES, pH 7.6 with 100 mM NaCl), yielding a lipid concentration of 5 mg mL^{-1}. The resulting cloudy suspension was extruded 21 times through two stacked polycarbonate membrane with a pore size of 100 or 50 nm. To encapsulate calcein, the lipid films were hydrated with 100 mM calcein overnight followed by extrusion. Free calcein was removed by passing 35 µL of the sample through a PD-10 column using buffer A for elution. The first 600 µL of the fluorescent fraction were collected.

2.2.3 DLS and ζ-potential measurements

$ZnCl_2$ solution was gradually titrated to a DOPC or DOCP liposome suspension (100 µg mL^{-1}) in different buffers all containing 100 mM NaCl (50 mM acetate for pH 5; 50 mM MES for pH 6; and 10 mM HEPES for pH 7.6). The hydrodynamic diameter and ζ-potential were determined on a Malvern Zetasizer Nano ZS 90 with a He-Ne laser (633 nm) at 90° and 25 °C. The data were analyzed by Malvern Dispersion Technology Software 4.20. The ζ-potential was determined from the measured electrophoretic mobility using the Smoluchowski approximation. The hydrodynamic diameter was determined from the measured diffusion of particles using the Stokes-Einstein relationship.

2.2.4 Liposome leakage tests

To monitor the leakage of liposomes, 3 µL of purified calcein-loaded liposomes were added to 597 µL of MES buffer (50 mM MES 100 mM NaCl, pH 6) in a quartz cuvette at room temperature. The background fluorescence was monitored for 5 min before adding metal ions (typically 10 µL of 10 mM metal ions). The fluorescence was monitored for another 25 min. At 30 min, 10 µL of 5% Triton X-100 was added to fully rupture the liposomes. Calcein was excited at 485 nm, and the emission was monitored at 525 nm using a Varian Eclipse fluorescence spectrophotometer.

2.2.5 ITC

ITC experiments were performed on a VP-ITC Microcalorimeter instrument (MicroCal). The samples were degassed to remove air bubbles prior to injection. DOPC or DOCP (100 or 50 µg mL^{-1}) in 50 mM MES (pH 6) with 100 mM NaCl were loaded in a 1.45 mL ITC cell at 25 °C. $ZnCl_2$ (280 µL, 5 mM) or $CaCl_2$ (280 µL, 10 mM) in the same buffer was titrated into the cell through a syringe (10 µL for each injection, except for the first injection of 2 µL).

2.2.6 TEM

TEM measurements were performed on a Philips CM10 transmission electron microscope. A 10 µL DOCP (100 µg mL^{-1}) and $ZnCl_2$ (2 mM) mixture was spotted on a 230 mesh holey carbon copper grid, extra solution on the grid was removed by filter paper, and the sample was dried in air. To visualize the lipid bilayers under normal TEM, negative staining was performed. A 10 µL drop of phosphotungstic acid (2%, 6.9 mM) was spotted on the grid. After 60 s the extra solution was removed by filter paper, and the sample was dried in air before imaging.

2.3 Results and Discussion

2.3.1 PC and CP lipids

In this study, two lipids with opposite headgroup dipole directions are used. The structure of a DOPC lipid is shown in Figure 2.1a. Its headgroup contains a negatively-charged phosphate and a

cationic choline, rendering an overall neutral charge. By flipping the headgroup, the resulting lipid is named DOCP (Figure 2.1b). Since its phosphate group is fully exposed, a DOCP can accept two protons with both p*K*a's below ~3.[46] Therefore, at neutral pH, DOCP carries two negative charges and one positive charge, resulting in a net negative charge. It has been reported that headgroup-switched lipids show very different interactions with metal oxide NPs and circulation properties.[47,49,51] The main goal of this work is to study the interaction between Zn^{2+} and these lipids, and a few other metal ions were also studied for comparison.

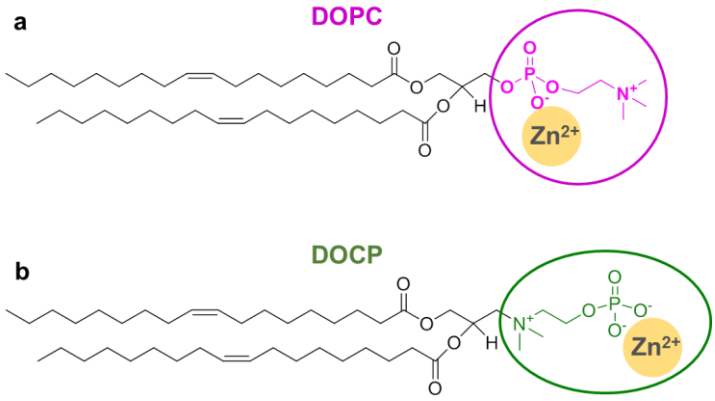

Figure 2.1 Chemical structures of the (a) DOPC and (b) DOCP lipids, and their phosphate group binding to Zn^{2+}.

2.3.2 Metal-induced aggregation of liposomes

The two types of liposomes were prepared by extrusion, resulting an average hydrodynamic diameter of ~100 nm from DLS (Figure 2.2a). We first followed their sizes by titrating Zn^{2+}. When the DOPC liposomes were mixed with Zn^{2+}, no size increase was observed at pH 5 (Figure 2.2d), pH 6 (Figure 2.2e), or pH 7.6 (Figure 2.2f), indicating the lack of aggregation of DOPC liposomes. The above experiment used up to 1 mM Zn^{2+} (Figure 2.2b). Even with 50 mM Zn^{2+}, the DOPC liposomes still did not aggregate (Figure 2.2c). In contrast, when Zn^{2+} was mixed with the DOCP liposomes, the average size gradually increased from 100 to ~300 nm at pH 5 (Figure 2.3a), to ~700 nm at pH 6.0 (Figure

2.3b), and to over 1 μm at pH 7.6 (Figure 2.3c). This suggests that Zn^{2+} may bridge DOCP liposomes to form large aggregates, or it might lead to liposome fusion, or both. The same phenomenon was also observed when DOCP liposomes of 50 nm were used (Figure 2.3e), indicating the interaction was independent of the size of liposomes.

Zn^{2+} has a relatively low solubility at high pH, and it might hydrolyze to form ZnO or $Zn(OH)_2$.[149] Since ZnO NPs can adsorb DOPC liposomes,[49] the lack of size change for the DOPC liposome mixed with Zn^{2+} at pH 7.6 (Figure 2.2f) suggests the effect of ZnO precipitation should be minimal under our experimental conditions. As a control, we also measured the DLS size distributions of Zn^{2+} in buffers at different pH values (e.g., no liposomes, Figure 2.3f), and no signal was observed. Therefore, the observed size change should be due to Zn^{2+}-mediated DOCP aggregation.

We reason that protons may better compete with Zn^{2+} for binding to the phosphate at lower pH, and thus weaken Zn^{2+} binding, which may explain the smaller size change of DOCP liposomes at more acidic pH. The relatively narrow DLS peaks suggested that the bridging effect of Zn^{2+} was balanced by repulsive forces, and the system did not undergo extensive aggregation, which might be explained by the surface charge (*vide infra*).

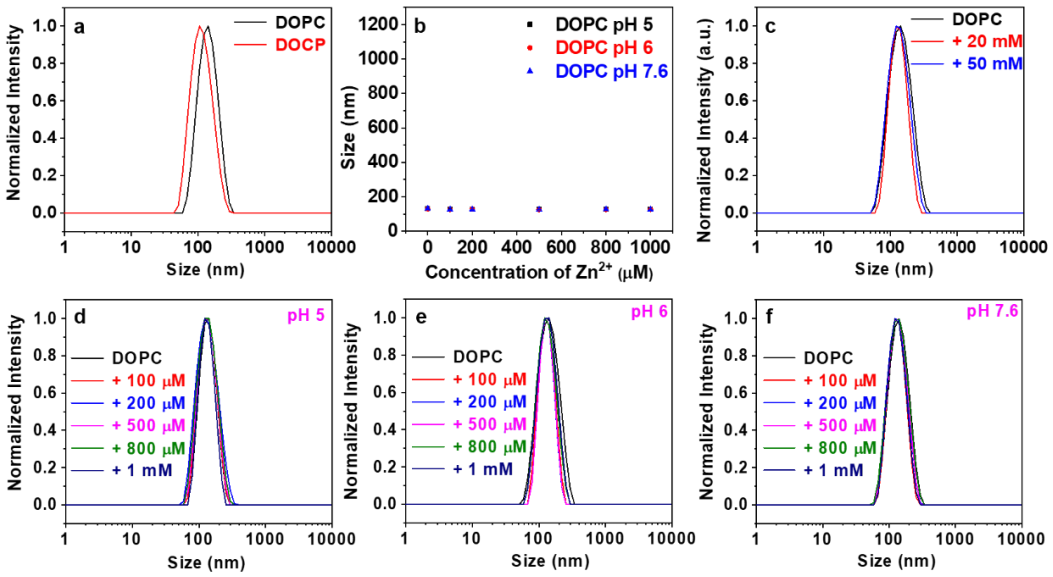

Figure 2.2 (a) Normalized DLS size distributions of DOPC and DOCP liposomes at pH 7.6. (b) Average hydrodynamic diameter of DOPC as a function of Zn^{2+} concentration at pH 5, pH 6, and pH 7.6. (c) DLS size distributions of DOPC liposomes with 20 mM and 50 mM Zn^{2+}. Normalized DLS size distributions of DOPC liposomes with different amounts of Zn^{2+} at (d) pH 5, (e) pH 6, and (f) pH 7.6. The liposome concentration is 100 μg mL^{-1}. The buffer used are 50 mM acetate, 100 mM NaCl for pH 5, 50 mM MES, 100 mM NaCl for pH 6, and 10 mM HEPES, 100 mM NaCl for pH 7.6.

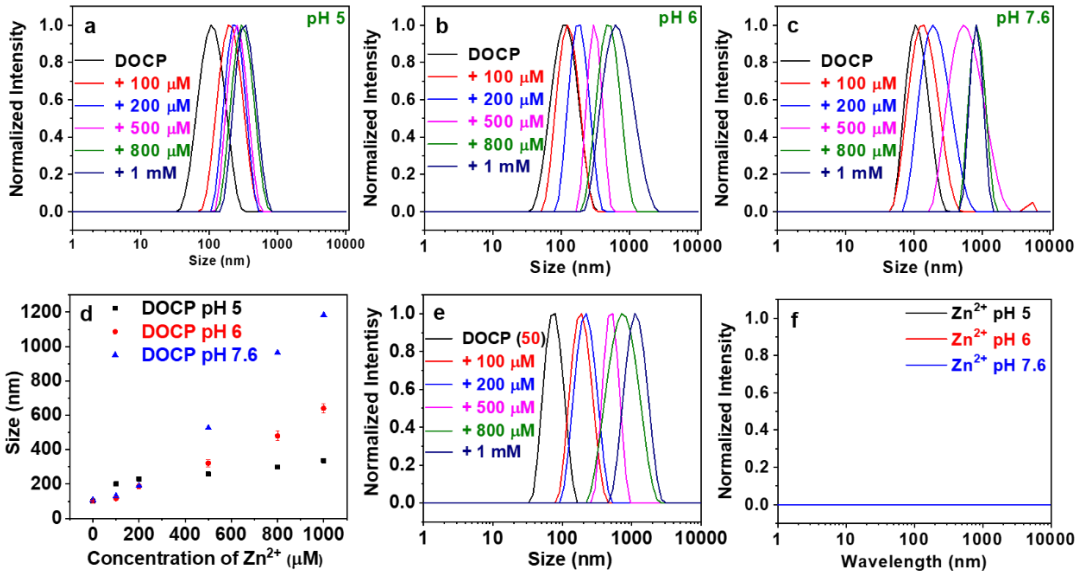

Figure 2.3 Normalized DLS size distributions of DOCP with different amount of Zn^{2+} at (a) pH 5, (b) pH 6, and (c) pH 7.6. (d) Average hydrodynamic diameter of DOCP as a function of Zn^{2+} concentration at pH 5, pH 6, and pH 7.6. (e) Normalized DLS size distributions of DOCP liposomes extruded through 50 nm pore-sized membranes with different concentrations of Zn^{2+} at pH 6. (f) DLS size distributions of 1 mM Zn^{2+} in pH 5, pH 6 and pH 7.6 buffer. The liposome concentration is 100 μL mL^{-1}. The buffer used are 50 mM acetate, 100 mM NaCl for pH 5, 50 mM MES, 100 mM NaCl for pH 6, and 10 mM HEPES, 100 mM NaCl for pH 7.6.

The above studies used each pure lipid. We also prepared liposomes using DOPC and DOCP mixtures. As shown in Figure 2.4, 20% DOCP behaved like pure DOPC and no aggregation was observed with Zn^{2+}, while 50% DOCP aggregated by Zn^{2+}. It appears that the density of the DOCP lipid needs to reach a certain level to have a synergistic effect. Otherwise, sparse individual binding could not support a collective behavior to trigger aggregation.

This simple size measurement already has nontrivial implications. It suggests a specific binding between the phosphate group in DOCP and Zn^{2+}, and Zn^{2+} can bridge different liposomes. On the other

hand, the phosphate in DOPC has a much weaker affinity for Zn^{2+}. However, we cannot fully rule out the binding between DOPC and Zn^{2+} at this moment.

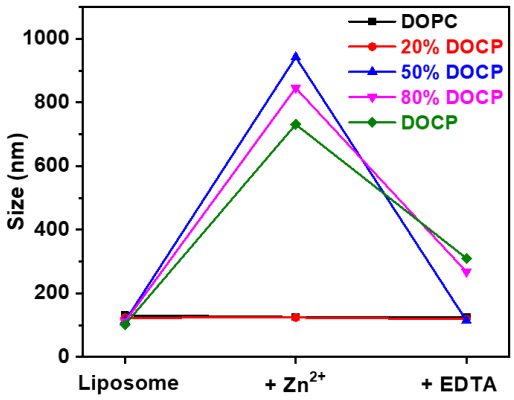

Figure 2.4 Hydrodynamic diameter of DOPC and DOCP mixtures after adding Zn^{2+} and then adding EDTA in buffer (50 mM MES, pH 6, with 100 mM NaCl).

2.3.3 Zn^{2+} binding followed by ζ-potential

To further follow Zn^{2+} binding, we monitored the ζ-potential of the liposomes (Figure 2.5). With the extra charge on the phosphate group, free DOCP liposomes at pH 6 had a ζ-potential of about -20 mV, which increased to ca. -10 mV by adding 200 μM Zn^{2+}, and little further increase was observed beyond that. This may explain the limited aggregation of DOCP liposomes in the presence of Zn^{2+} since the liposome remained negatively charged and repel each other even with saturated Zn^{2+}. This is different from the PC or PC/PS binds to Ca^{2+} ions, in which their ζ-potential turned positive with excess amount of Ca^{2+}.[94] This might be due to a difference in the hydrolysis of these ions. Zn^{2+} bound water is more easily hydrolyzed to produce OH^- groups to make the surface still negatively charged, while Ca^{2+} bound water is adsorbed as neutral water and thus keeping its positive charge. In comparison, the ζ-potential of DOPC was not affected by Zn^{2+}, which further proves the weak binding between DOPC and Zn^{2+}.

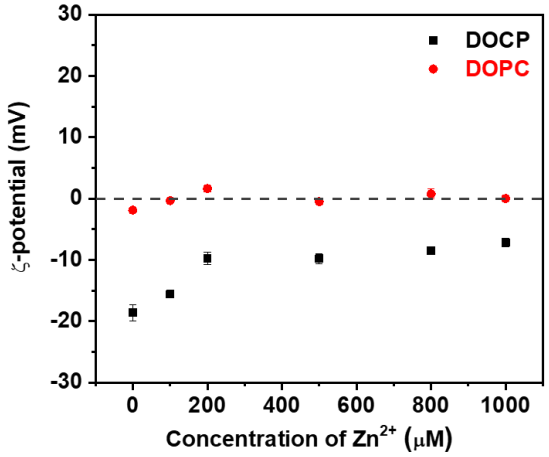

Figure 2.5 ξ-potential of DOPC and DOCP liposomes (100 μg mL^{-1} each) as a function of Zn^{2+} concentration in 50 mM MES, pH 6, with 100 mM NaCl.

2.3.4 ITC

The above studies have established a strong interaction between Zn^{2+} and DOCP liposomes. We then quantitatively measured their binding using ITC. ITC is a biophysical technique for measuring the heat produced during binding reactions. Zn^{2+} was gradually titrated into DOCP liposomes (0.129 mM total lipid) at pH 6. Zn^{2+} titration in buffer produced a small endothermic signal, which was subtracted as background. Heat absorption was observed when Zn^{2+} was titrated to DOCP liposomes (Figure 2.6a). The integrated heat was fitted to a one-site binding model (Figure 2.6b) with a K_d of 110 μM Zn^{2+}. This affinity is much stronger than Ca^{2+} or Mg^{2+} binding to PS lipids (K_d = ~ 1 mM),[41] while much weaker than Cu^{2+} binding to PE and PS lipids.[99]

Since the binding is endothermic, it has to be an entropy-driven reaction. We reason that hydrated Zn^{2+} and the phosphate headgroup have to release some water molecules to bind.[82,94] This process needs energy but increases entropy. The endothermic binding process was also observed when Ca^{2+} binds to PC/PS lipids, and alkali metals bind to PC liposomes in buffer.[81,137] The binding stoichiometry is ~1.2, suggesting that each CP headgroup can bind one Zn^{2+}. In comparison, no heat

was observed when titrating Zn^{2+} into DOPC liposomes (Figure 2.6c), also consistent with their weak interaction. A previous Fourier-transform infrared spectroscopy (FTIR) study indicated that Zn^{2+} can still bind to PC lipids, reducing the hydrophilicity of the PC headgroup and affecting lipid phase transition. It needs to be noted that the FTIR was carried out in a dried state.[82]

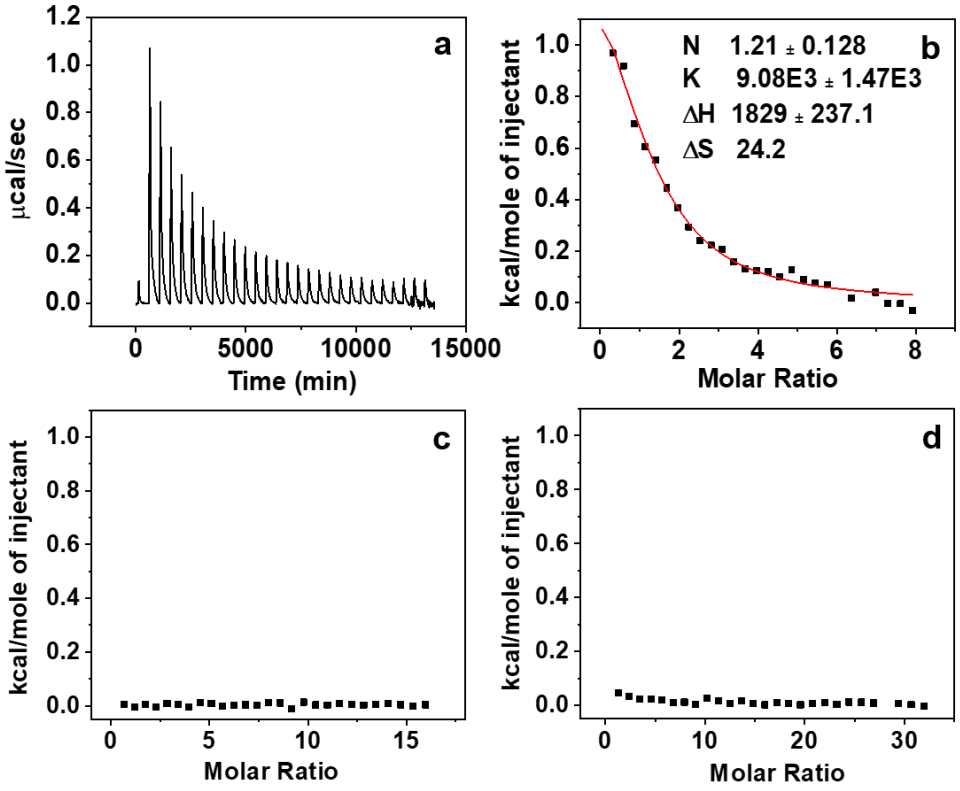

Figure 2.6 (a) An ITC trace of titrating 5 mM Zn^{2+} to DOCP liposomes (100 µg mL^{-1}, 0.129 mM). (b) Integrated heat showing the binding profile and the fitted one-site binding curve. In the figure legend, *N* denotes the number of binding sites, *K* denotes binding consistent (M^{-1}), *ΔH* denotes the enthalpy (kcal mol^{-1}), and *ΔS* denotes the entropy (cal K^{-1} mol^{-1}) of the reaction. Integrated heat of (c) titrating 5 mM $ZnCl_2$ to DOPC liposomes (100 µg mL^{-1}, 0.129 mM) and (d) 10 mM Ca^{2+} to DOCP liposomes (50 µg mL^{-1}, 0.065 mM). All experiments were carried out in 50 mM MES buffer, pH 6, with 100 mM NaCl.

We previously studied the adsorption of DOPC and DOCP liposomes by ZnO NPs.[49,111] In both cases, strong interactions were observed. ZnO leaked both liposomes, which might be related to its cationic surface charge. For the Zn^{2+} ion studied here, its binding by DOCP is much stronger, while binding to DOPC can hardly be measured. For further comparison, we also titrated Ca^{2+} to DOCP, and a very moderate amount of heat was detected (Figure 2.6d), suggesting much weaker binding of Ca^{2+} compared to Zn^{2+}.

2.3.5 Zn^{2+} leaks DOCP liposomes

An important aspect of liposome property is its membrane integrity. The above experiments have clearly established a strong interaction between DOCP liposomes and Zn^{2+}. To understand the integrity of liposomes after Zn^{2+} binding, a leakage assay was designed by encapsulating 100 mM calcein in the liposomes leading to self-quenched fluorescence. If the liposome is disrupted, calcein releases to the whole solution leading to fluorescence enhancement.

We first studied the DOCP liposomes with Zn^{2+} at pH 6 (Figure 2.7a). The background fluorescence was followed at 525 nm for 5 min, and no change was observed, indicating that the liposomes were stable. At 5 min, a final of 167 μM Zn^{2+} was added, and an immediate fluorescence enhancement was observed, indicating compromised membrane integrity. On the other hand, Mg^{2+} and Ca^{2+} failed to induce any leakage of the DOCP liposome (Figure 2.7b). In contrast, Zn^{2+} also failed to leak DOPC liposomes (Figure 2.7c), consistent with its lack of strong Zn^{2+} binding.

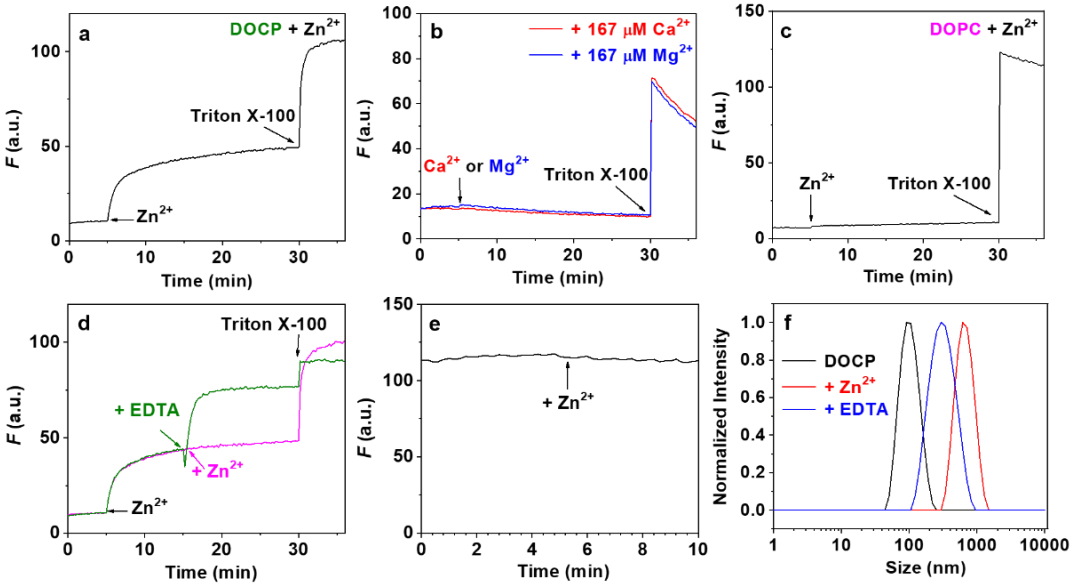

Figure 2.7 Leakage tests of calcein-loaded DOCP liposomes with (a) Zn^{2+}, (b) Ca^{2+}, and Mg^{2+} (final concentration: 167 μM) at pH 6. (c) Leakage test of calcein-loaded DOPC with Zn^{2+} at pH 6. (d) Leakage test of DOCP liposomes by Zn^{2+} added in two steps, and no further leakage occurred at the second dose of Zn^{2+}. Adding EDTA to the DOCP/Zn^{2+} complex induced further leakage. (e) Fluorescence of adding Zn^{2+} to free calcein at pH 6. (f) Normalized DLS size distributions of adding EDTA to DOCP/Zn^{2+} at pH 6. These experiments were performed in 50 mM MES, pH 6, with 100 mM NaCl.

We notice that the 167 μM Zn^{2+} did not fully leak all the calcein since Triton X-100 still induced a significant fluorescence enhancement. Therefore, on top of the first dose of 167 μM Zn^{2+}, we added an additional 167 μM Zn^{2+}, which however did not induce further leakage (Figure 2.7d, pink trace). This suggests that the first dose has already reached saturated binding structure, and further adding Zn^{2+} had no effect. If small pores are formed by Zn^{2+}, we expect a full leakage, which is clearly not the case here.

Since adding more Zn^{2+} did not induce further leakage and some calcein remained encapsulated, we next tested removing Zn^{2+} by adding EDTA (Figure 2.7d, green trace). Interestingly, further leakage

was observed. Note that the fluorescence reached almost the same level after adding Triton X-100 with or without EDTA, so the fluorescence increase after the addition of EDTA was not because of dequenching of Zn^{2+}. In addition, no fluorescence quenching was observed when Zn^{2+} added to free calcein (Figure 2.7e), which also supported that the fluorescence increase after adding EDTA was due to the further leakage of DOCP. This also implies that the liposomes were not fully disrupted by Zn^{2+}.

We previously observed a similar phenomenon upon adding citrate-coated AuNPs or nanoceria to DOPC liposomes.[116,117,150] Leakage was observed upon addition of AuNPs, and the liposome leaked again upon removing the AuNPs either by adding a thiol-containing compound or by adding KCN to dissolve the AuNPs.[116] A liposome leaks the fastest at the T_c. DOPC lipid, for example, has a T_c of -17 °C. AuNPs induced its leakage likely due to the change of local lipid packing and thus T_c. However, AuNPs did not induce fusion of DOPC liposomes.[116,117] As shown below, Zn^{2+} induced fusion of DOCP liposomes and likely the mechanism of leakage is different for Zn^{2+}.

2.3.6 Reversibility of liposome aggregations

The surprising effect of EDTA on leakage of DOCP liposome prompted us to revisit liposome size. We described above that Zn^{2+} can increase the size of DOCP liposomes (Figure 2.3a-d). To investigate if the binding process is reversible, we added EDTA to the DOCP/Zn^{2+} mixture and monitored the size change by DLS (Figure 2.7f). While a decrease in the aggregate size was observed from ~700 to ~300 nm by EDTA, it did not fully go back to the original size of the liposome (~100 nm). This may indicate that besides aggregation, Zn^{2+} possibly induces other changes of the DOCP, e.g., liposome fusion.

2.3.7 TEM and a model of interaction

To have a better understanding, we then performed negative stain TEM. We observed aggregated DOCP liposomes in the presence of Zn^{2+} with different morphologies. For example, multilayered structures were observed (Figure 2.8b and c). These liposomes either have a size of around 100 nm or larger. Two DOCP liposomes can be tightly linked by Zn^{2+}, and they deform to maximize

the contact area. Some liposomes may break in this process and fuse onto the other ones (or on the fused larger liposomes) to form multilayered structures sandwiching Zn^{2+}. This also explains the leakage observed, but not all the liposomes broke from the dye leakage experiment (Figure 2.7a). The nonbroken liposomes are likely protected from further interaction with Zn^{2+}, which might be why adding more Zn^{2+} yielded no more leakage (Figure 2.7d).

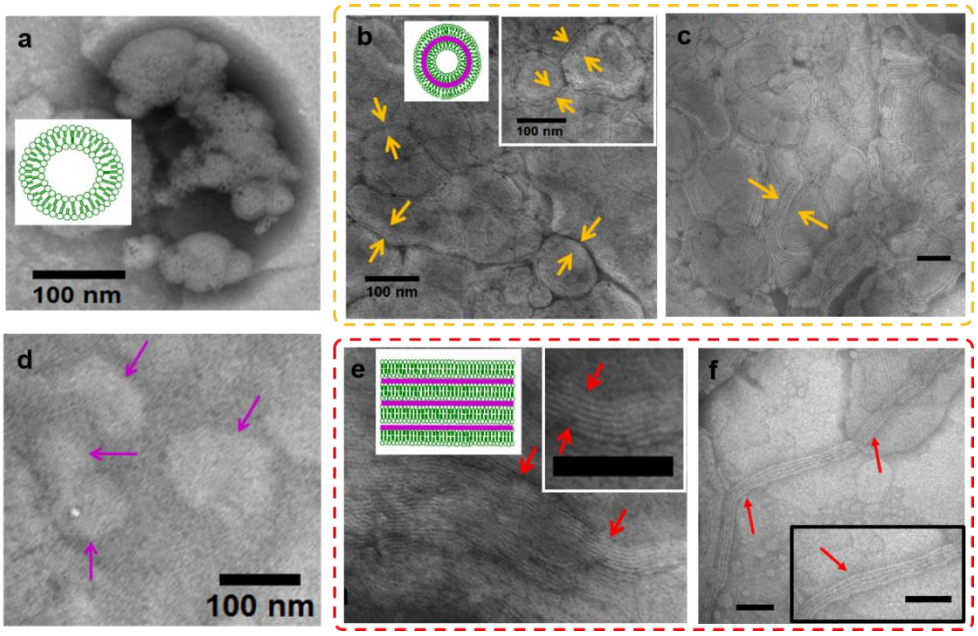

Figure 2.8 Negative stain TEM and schematic illustration of possible products of DOCP liposome mixed with 2 mM Zn^{2+}. (a) DOCP liposomes without Zn^{2+}. (b and c) Fused multilayered liposomes with Zn^{2+} sandwiched between each bilayer. (d) Negative TEM micrograph of DOPC mixture with 2 mM Zn^{2+} at pH 6. (e and f) Lipid multilayers sandwiching Zn^{2+}. Note that Zn^{2+} was still associated with the lipid headgroups instead of with the hydrophobic tails. Pink arrows indicate the individual liposome feature. Yellow arrows indicate the multilayered structures. Red arrows indicate the ribbon-like structures. All the samples were negative stained with phosphotungstic acid before imaging. Scale bars = 100 nm.

In some regions, multilayered structure with ribbon-like structures up to micrometer length was also observed (Figure 2.8 e and f). This structure is formed by fully broken liposomes sandwiching Zn^{2+} (cartoon in Figure 2.8e). Such stacked structure is also reminiscent of the result published by Sasaki and co-workers.[128] In their work, the stacked structures were induced by the strong interaction between Cu^{2+} and metal ligand embedded in the liposome. A control experiment of Zn^{2+}-free DOCP liposomes stained by phosphotungstic acid was also performed, and a completely different feature was observed (Figure 2.8a). This supports that the lamellar structures observed with Zn^{2+} was not due to artifacts from the negative staining agent. In contrast, when DOPC mixed with Zn^{2+} at the same condition, individual liposomes were observed (Figure 2.8d), indicating weak interaction between DOPC and Zn^{2+}.

From TEM, we can see that DOCP liposomes need to bend extensively to interact with each other to form these structures. The energy of bending is likely to be overcompensated by Zn^{2+} binding. In the final product, the structures in Figure 2.8b and c do not have highly curved regions, while in Figure 2.8e and f, we can expect some highly bended regions in the ends. However, since these layered structures were very long, the fraction of lipid suffering from the curvature was very small, making the process overall energetically favorable.

2.3.8 Further discussion

This work has showed the interesting effects of Zn^{2+} on DOCP liposomes. We want to emphasize the following aspects of this study. 1) Bridging phosphate versus terminal phosphate. The striking difference between DOPC and DOCP in terms of interacting with Zn^{2+} has indicated the metal binding difference in different phosphate groups in lipid settings. With DLS, ITC, and calcein leakage assays, we have clearly showed that terminal CP phosphate binds Zn^{2+} much more strongly than the bridging phosphate in PC liposomes. Such difference is known in other biopolymers such as DNA,[144] and now we demonstrated it in lipids. 2) Zn^{2+} versus Ca^{2+}. In this study, we focused on Zn^{2+}, and comparisons were made with Ca^{2+} in many assays. It is impossible to cover all metal ions in one study, and a simple comparison of these two has articulated the importance of metal ions. While Ca^{2+} is known

to bind to phosphate strongly, Zn^{2+} binding is even stronger. 3) Zn^{2+} versus ZnO. We have previously studied the adsorption of DOPC and DOCP liposomes by ZnO NPs.[47,49,111] In both cases, strong interactions were observed. For the Zn^{2+} ion binding, a very large difference was observed for these two lipids. In the case of ZnO NPs, two surfaces interact and can form polyvalent binding to amplify even weak binding. Compared to binding to metal oxides, binding to individual metal ions is weaker. In this case using Zn^{2+}, only DOCP showed binding but not DOPC.

2.4 Summary

In summary, the interaction of Zn^{2+} with DOPC and DOCP liposomes was systematically studied using various techniques including DLS, fluorescence spectroscopy, ITC, and TEM. These two lipids have different headgroup chemistries, and the phosphate in DOCP has stronger affinity for Zn^{2+}. The DLS data showed that Zn^{2+} increased the size of DOCP liposomes, while it had little effect on DOPC liposomes. The size change could not be reversed by removing Zn^{2+} with EDTA, suggesting liposome fusion also occurred. The calcein leakage tests indicated Zn^{2+} could induce leakage of DOCP liposomes. Negative stain TEM suggested that Zn^{2+} caused the fusion and stacking of DOCP liposomes in addition to simple aggregation. The thermodynamic parameters of Zn^{2+} binding to DOCP were measured by ITC, showing an overall endothermic reaction. While DOCP is not a natural lipid, it can be a useful metal ligand as demonstrated here, allowing Zn^{2+}-responsive content release. It has expanded the chemistry of metal binding from amine (e.g., PE lipids),[99,129] serine (e.g., PS lipids),[40] and carboxyl to also phosphate. These groups have different metal preference, since phosphate prefers hard metals, while PE and PS bind soft metals better. By combining different lipids, we might rationally tune metal binding of lipid membranes.

Chapter 3 Cu^{2+}-Directed Liposome Membrane Fusion, Positive-Stain Electron Microscopy, and Oxidation

The results presented in this chapter have been published as:

Yibo Liu and Juewen Liu, Cu^{2+}-Directed Liposome Membrane Fusion, Positive-Stain Electron Microscopy, and Oxidation, *Langmuir*, **2018**, 34, 7545-7553.

3.1 Introduction

After studying the binding of Zn^{2+} with liposomes in Chapter 2, we studied the binding of another transition metal ions, Cu^{2+}, with liposomes. Lipids are a critical component of biological membranes, and they interact with various chemicals to exert responses such as fusion, fission, pore formation, and phase separation.[76,119,120] Instead of directly using cell membranes, liposomes have been prepared with controllable sizes and compositions, allowing the study of fundamental interactions as well as practical applications.[31,57,122,151,152] Although most previous work focused on proteins or small molecular ligands, metal binding has attracted more and more recent attention.[40,41,94,99,128,129] Processes such as oxidative stress, membrane damage, and fusion have been related to metal binding.[13,88]

Natural lipid headgroups contain many metal ligands, and more can be obtained by chemical synthesis.[46,50,153] Extensive studies have been carried out on Ca^{2+} because of its biological relevance.[81,85,91,94,95] Recently, more research has been carried out on transition metals.[40,41,99,129,133,154] Although their free cellular concentrations are much lower than that of Ca^{2+} and Mg^{2+}, transition metals may bind to lipids with a higher affinity.[34,40,41,99,129,133] The rich spectroscopic properties and high electron density of transition metals are also useful for detailed physical characterization. We recently reported interesting binding properties of Zn^{2+} to zwitterionic DOPC liposomes and headgroup inverted DOCP liposomes.[48] Zn^{2+} caused irreversible fusion and stacking of DOCP liposomes, whereas it had little effect on DOPC. Lu and co-workers demonstrated a strong binding between Hg^{2+} and PE lipids,

resulting in a leakage of PE-containing liposomes.[129] Cremer's group reported Ni^{2+} binding to PE lipids thousand-fold tighter than that to PC lipids.[34]

Cu^{2+} is a widely studied transition metal because of its biological importance.[155,156] The strong redox property of Cu^{2+} poses an oxidative stress, whereas its fluorescence quenching property allows convenient monitoring of lipid binding. Cremer and co-workers studied Cu^{2+} binding to PS and PE containing lipid bilayers supported on a silica surface.[40,99] They reported an extremely strong binding of Cu^{2+} by PE potentially enhancing the oxidation of a lipid double bond. Sasaki and co-workers used pyrene- and iminodiacetic acid-modified lipids to detect Cu^{2+}.[128]

Given these progresses, a systematic understanding of freely dispersed liposomes remains to be completed. Compared to supported bilayers, free liposomes may show additional features such as fusion and leakage.[31,50,107,134] Herein, we compared the binding of Cu^{2+} to a few liposomes with various metal-binding properties. Interestingly, Cu^{2+} might act as a positive-stain agent, although a high concentration of Cu^{2+} with a long incubation caused fusion and leakage of some liposomes. The oxidation of an external substrate by Cu^{2+} was inhibited in the presence of high affinity lipids.

3.2 Materials and Methods

3.2.1 Chemicals

All the phospholipids were purchased from Avanti Polar Lipids (Alabaster, AL). $CuCl_2$, disodium calcein, Triton X-100, 2,4-dichlorophenol (2,4-DP), and 4-aminoantipyrine (4-AP), HEPES were purchased from Sigma-Aldrich. EDTA and sodium chloride were from Mandel Scientific (Guelph, ON, Canada). Milli-Q water was used to prepare all the buffers, solutions, and suspensions.

3.2.2 Preparation of liposomes

Liposomes were prepared using the standard extrusion method.[47,49] DOPC, DOCP, DOPS [1,2-dioleoyl-*sn*-glycero-3-phospho-L-serine (sodium salt)], and DOPG [1,2-dioleoyl-*sn*-glycero-3-phospho-(1'-*rac*-glycerol) (sodium salt)] (2.5 mg) were dissolved in chloroform. For rhodamine (Rh)-

labeled liposomes, 1 wt % (~0.6 mol %) Rh-PE (1,2-dioleoyl-*sn*-glycero-3-phosphoethanolamine-N-(lissamine rhodamine B sulfonyl)) (ammonium salt) was incorporated. After evaporating chloroform by blowing N_2, the samples were dried in a vacuum oven at room temperature overnight to fully remove chloroform. The dried lipid films were stored at -20 °C in a N_2 atmosphere prior to use. To prepare liposomes, the lipid films were hydrated with 0.5 mL of buffer A (10 mM HEPES, pH 7.6 with 100 mM NaCl), yielding a lipid concentration of 5 mg mL^{-1}. The resulting cloudy suspension was extruded 21 times through a two-stacked polycarbonate membrane with a pore size of 100 nm. To encapsulate calcein, the lipid films were hydrated with 100 mM calcein overnight followed by extrusion. Free calcein was removed by passing 35 µL of the sample through a PD-10 column using buffer A for elution. The first 600 µL of the fluorescent fraction were collected.

3.2.3 DLS measurements

The Cu^{2+} solution (10 mM) was gradually titrated to liposome suspension (100 µg mL^{-1}) in a buffer of 10 mM HEPES, 100 mM NaCl, pH 7.6. The designed Cu^{2+} concentrations were 10, 100, and 500 µM. Then, the EDTA solution was added to the mixture, giving the final concentration of 10 mM. The hydrodynamic diameter was determined on Malvern Zetasizer Nano ZS 90 with a He-Ne laser (633 nm) at 90° and 25 °C.

3.2.4 Fluorescence quenching assays

The Cu^{2+} solution was gradually titrated in the Rh-liposome (50 µg mL^{-1}) in 10 mM HEPES, 100 mM NaCl, pH 7.6. The Cu^{2+} stock solution (100 µM or 1 mM) was used for this titration. The reversibility of the binding was tested by adding 10 mM EDTA to the mixture of Rh-DOPS (50 µg mL^{-1}) and Cu^{2+} (10 µM). The fluorescence spectra were recorded using a Varian Eclipse fluorometer (Ex: 560 nm; Em: 592 nm).

3.2.5 Liposome leakage tests

To monitor the leakage of liposomes, 3 μL of purified calcein-loaded liposomes were added to 597 μL of buffer (10 mM HEPES, 100 mM NaCl, pH 7.6) in a quartz cuvette at room temperature. The background fluorescence was monitored for 5 min before adding Cu^{2+} ions (typically 10 μL of 1 mM or 10 mM Cu^{2+}). The fluorescence was monitored for another 15 min. At 20 min, 10 μL of 100 mM EDTA was added. At 30 min, 10 μL of 5% Triton X-100 was added to fully rupture the liposomes. The leakage kinetic tests were carried out by adding EDTA at different liposomes and Cu^{2+} incubation time. Calcein was excited at 485 nm, and the emission was monitored at 525 nm using a Varian Eclipse fluorescence spectrophotometer.

3.2.6 TEM

TEM micrographs were recorded on a Philips CM10 transmission electron microscope. A 10 μL liposome (100 μg mL^{-1}) and Cu^{2+} (20 μM) mixture was spotted on a 230 mesh holey carbon copper grid, and extra solution on the grid was removed by a filter paper. The sample is dried in air overnight before imaging. For the time-dependent study, the TEM samples were prepared immediately, 5, 10, and 30 min after mixing Cu^{2+} and DOPS. A 10 μL drop of phosphotungstic acid (2%, 6.9 mM) was spotted on the grid. After 60 s, the extra solution was removed by a filter paper and the sample was dried in air before imaging.

3.2.7 Catalytic activity assays

The catalytic performance was measured by the chromogenic reaction of 2,4-DP with 4-AP. Cu^{2+} (20, 50, or 100 μM) was mixed with liposomes (100 μg mL^{-1}) in 50 mM MES at pH 6.8 for 30 min. For control experiments, only Cu^{2+} was dissolved in buffer. Then, 4-AP and 2,4-DP with a final concentration of 100 μg mL^{-1} was introduced to the mixture. The digital pictures were taken after 1 h incubation.

3.3 Results and Discussion

3.3.1 Cu^{2+} binding measured by fluorescence quenching

To have a systematic understanding, the following lipids were included in this study. DOPS (Figure 3.1a) has a carboxyl group and an amine group that can chelate Cu^{2+} tightly.[40,41] With also a phosphate, the PS headgroup is overall negatively charged. Exposure of PS lipids to the outer leaflet of the cell membrane is an indication of apoptosis.[36,157] For negatively-charged DOPG, its phosphate group is the only possible metal-binding site (Figure 3.1b). DOCP is a synthetic lipid with a fully exposed terminal phosphate also carrying a negative charge (Figure 3.1c),[46] and it has been shown to be useful for binding to metal oxide surfaces.[31,47,49] In addition to these three anionic lipids, we also included DOPC (Figure 3.1d), which is charge neutral. For each lipid, we prepared their single component liposomes using the extrusion method through a membrane with 100 nm pores. From DLS, these liposomes all had an average size of ~100 nm (Figure 3.1e) and their ζ-potential values were consistent with their respective expected surface charges (Figure 3.1f).

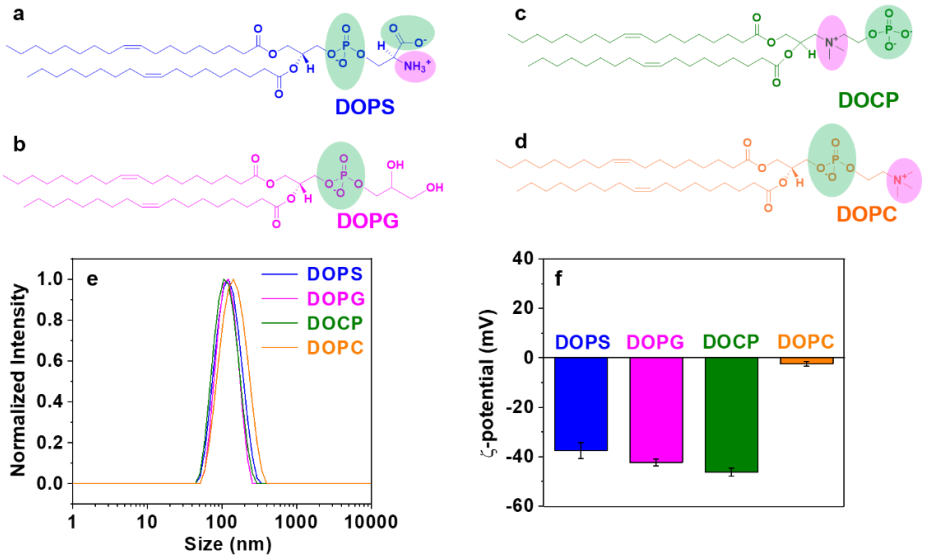

Figure 3.1 Structures of the lipids used in this study: (a) DOPS, (b) DOPG, (c) DOCP, and (d) DOPC. The negatively-charged groups are highlighted in green, and the positively-charged ones in pink. (e) Normalized DLS size distributions of liposomes (100 μg mL^{-1}) at pH 7.6. (f) ξ-potential of the liposomes at pH 7.6 (10 mM HEPES, 100 mM NaCl).

Taking advantage of the strong fluorescence quenching property of Cu^{2+},[40] we included Rh-labeled PE lipids (1 wt % or 0.6 mol %) in all of the liposomes to follow Cu^{2+} binding. Cu^{2+} was gradually titrated (Figure 3.2a-d), and we observed significant quenching of the DOPS sample, reaching 70-80% quenching with 10 μM Cu^{2+} (Figure 3.2e). Cremer and coworkers proposed energy transfer to be responsible for such quenching.[40,41,99] The final quenching reaching more than 50% is likely caused by the lipid bilayer asymmetry,[158] and also some of Rh in the inner leaflet might also be partially quenched.

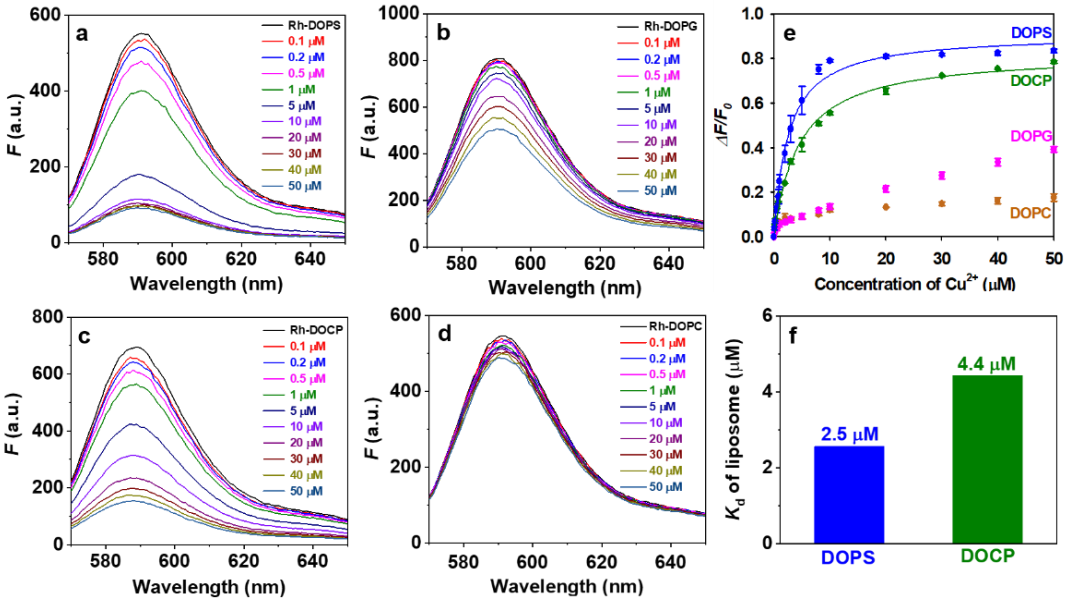

Figure 3.2 Fluorescence spectra of Rh-labeled (a) DOPS, (b) DOPG, (c) DOCP, and (d) DOPC liposomes in the presence of different concentrations of Cu^{2+} at pH 7.6 (50 μg mL^{-1} liposome in 10 mM HEPES, 100 mM NaCl). (e) Adsorption isotherm of Cu^{2+} with the liposomes based on fluorescence quenching. (f) Apparent K_d of Cu^{2+} binding by the two liposomes.

We fitted the DOPS quenching profile to the binding of Cu^{2+} ion with a K_d of 2.5 μM (Figure 3.2f). This apparent K_d is much higher than that reported in the supported bilayer system by Cremer and co-workers (e.g., a K_d of 0.11 μM for 1% POPS and 6.4 pM for 20% PS).[41] This difference was attributable to the much higher lipid concentration in our system. We have a total PS concentration of 62 μM (50 μg mL^{-1}). In the supported bilayer system, a single lipid bilayer had a very small amount of lipid. In addition, they used a flow system that can replenish the bound Cu^{2+}. Our homogeneous assay did not allow us to measure such strong binding, and the purpose here is not to re-make such accurate measurements, but to compare the different lipids.

We then performed the same titration with the other three liposomes (Figure 3.2e). A similar but slightly weaker quenching was observed with the DOCP liposome (K_d = 4.4 μM), suggesting that the exposed terminal phosphate is also a good Cu^{2+} ligand. DOPG also bound to Cu^{2+}, although only

40% fluorescence was quenched with 50 µM Cu^{2+} (Figure 3.2e). With a further increase of Cu^{2+}, the quenching could reach ~100% (Figure 3.3). At low Cu^{2+} concentrations (below 50 µM), the quenching of the DOPG sample was much less than the quenching of DOPS and DOCP. This indicated a weaker interaction between Cu^{2+} and DOPG. The full quenching of the DOPG sample at 500 µM Cu^{2+} (Figure 3.3) was probably caused by the rupture of the DOPG liposomes (*vide infra*). We did not fit the binding curve of DOPG because the binding was far from saturation at 50 µM Cu^{2+} and the solution became turbid (also indicated by DLS, see data below) at higher Cu^{2+} concentrations, which could scatter light and affect fluorescence. For DOPC, only around ~20% quenching was observed with 50 µM Cu^{2+} (Figure 3.2e). The binding between the liposomes and Cu^{2+} was reversible. When EDTA was added to the Rh-DOPS/Cu^{2+} complexes (the tightest among the four liposomes), the Rh fluorescence can be totally recovered (Figure 3.4).

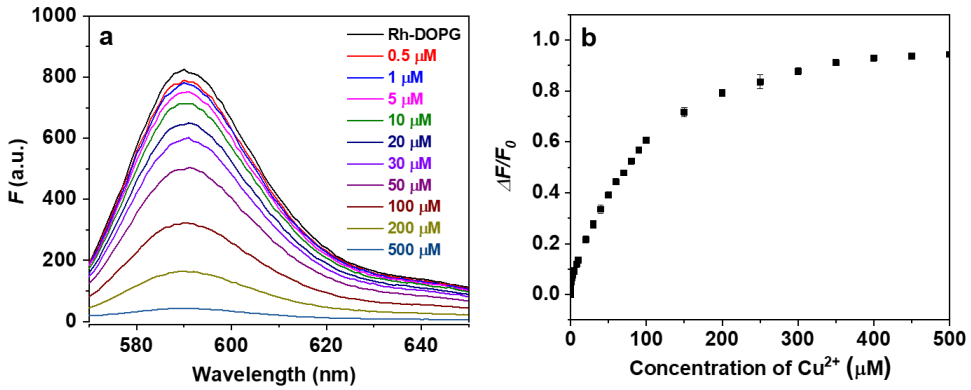

Figure 3.3 (a) Fluorescence spectra of Rh-labeled DOPG liposomes in the presence of different concentration of Cu^{2+} upto 500 µM at pH 7.6 (50 µg mL^{-1} liposome in 10 mM HEPES, 100 mM NaCl). (b) Adsorption isotherm of Cu^{2+} with DOPG liposomes based on fluorescence quenching.

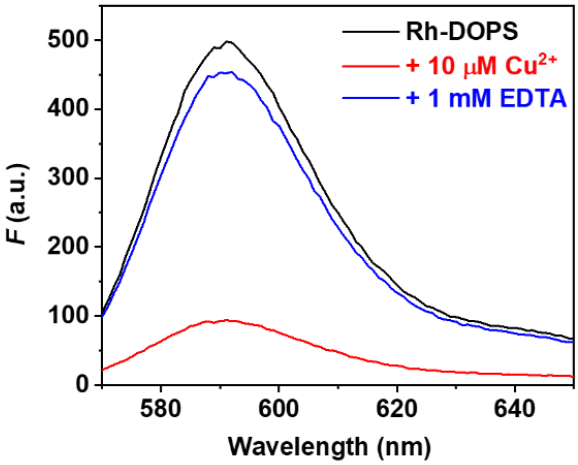

Figure 3.4 Fluorescence spectra of adding EDTA to the Rh-DOPS/Cu^{2+} complexes.

3.3.2 Positive- and negative-stain TEM

The above fluorescence assay suggested binding of Cu^{2+} to the liposomes with different affinities, and the integrity of some liposomes might be compromised. To directly observe the morphology of liposomes after Cu^{2+} binding, we examined the samples using TEM. Normally, liposome imaging requires either cryo-TEM or a negative stain with a heavy metal salt such as uranium, tungsten, and molybdenum.[159] They are called negative stain because these salts stain the non-sample regions so that the liposomes have a negative contrast. Because Cu^{2+} is also a heavy metal, we first imaged its mixture with the liposomes directly. Interestingly, we observed features of positive stains for all of the liposomes. Significantly fused structures were observed with DOCP (Figure 3.5b) and DOPS (Figure 3.5c) liposomes, reaching larger than 500 nm. Because the samples were imaged after drying, some peanut structures could be formed during the drying process otherwise fused liposomes should still be spherical.

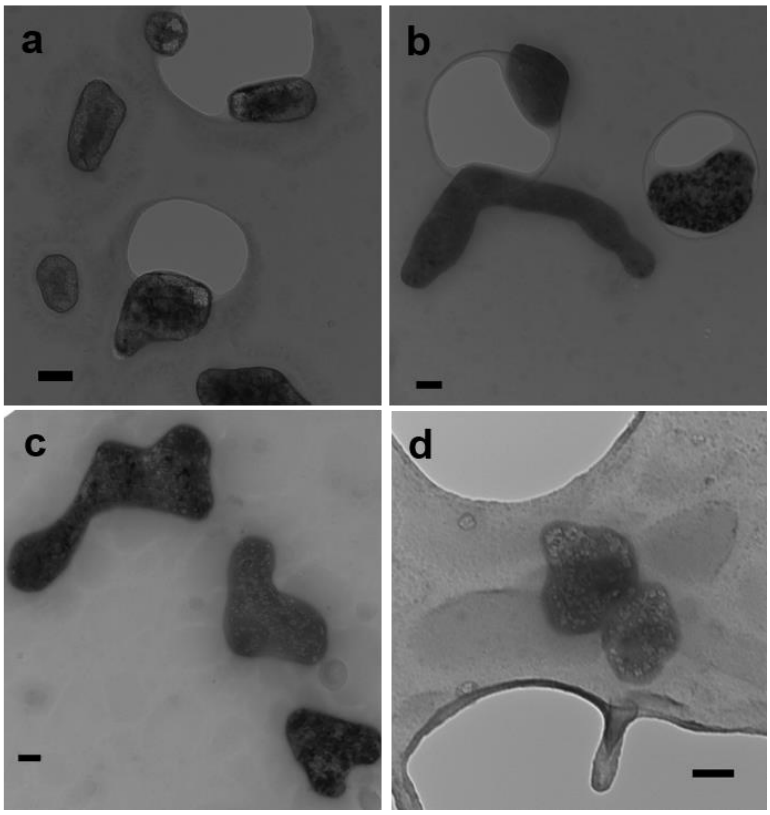

Figure 3.5 TEM micrographs of (a) DOPC, (b) DOCP, (c) DOPS, and (d) DOPG liposomes (100 μg mL^{-1}) mixed with Cu^{2+} (20 μM) for 30 min at pH 7.6 (10 mM HEPES, 100 mM NaCl).

In contrast, DOPC and DOPG liposomes appeared less fused with a size of 100-300 nm (Figure 3.5a and d), consistent with their weaker Cu^{2+} binding from the above fluorescence quenching assay under this Cu^{2+} concentration (20 μM). We suspect that strong Cu^{2+} binding led to fusion of DOPS and DOCP liposomes, although we cannot fully rule out fusion of DOPC and DOPG liposomes at this moment, especially for DOPG liposomes whose size was obviously larger than 100 nm under TEM. It is quite intriguing that even DOPC was positively stained by Cu^{2+}, although it is charge neutral and has very weak Cu^{2+} binding.

DOCP liposomes were ruptured forming layered structures in the presence of Zn^{2+} (Figure 3.6a),[48] whereas in the presence of Cu^{2+}, fused liposome structures were observed (Figure 3.5b). Therefore, different metals can provide quite different interactions with the same liposome. To have a

full understanding, Zn^{2+} was then added to DOPS liposomes and we observed individual liposomes stained with metal instead of layered structures (Figure 3.6b). Therefore, Zn^{2+} coordination to the PS headgroup and CP headgroup was sufficiently different, leading to different products.

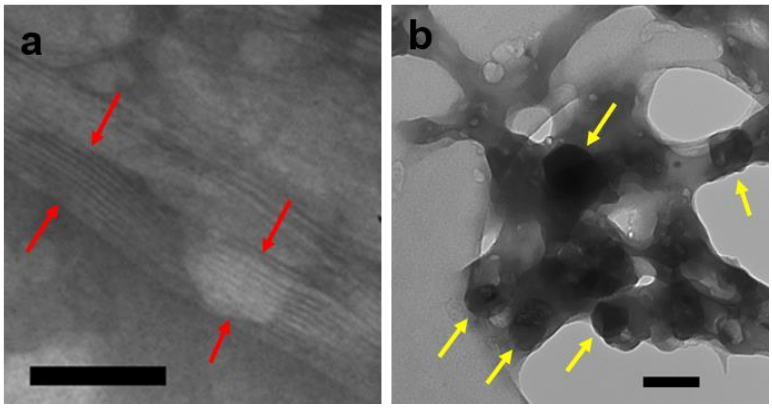

Figure 3.6 (a) Negative-stain TEM micrograph of DOCP liposomes (100 μg mL^{-1}) and Zn^{2+} (2 mM). (b) TEM micrograph of DOPS liposomes (100 μg mL^{-1}) mixed with Zn^{2+} (2 mM) at pH 7.6 (10 mM HEPES 100 mM NaCl). The red arrows in (a) point to the layered features. The yellow arrows in (b) point to the liposome features. Scale bar = 100 nm.

3.3.3 Liposome fusion followed by TEM

To understand the potential fusion process, we then carried out a time-dependent TEM study using Cu^{2+} and DOPS liposomes. Immediately after mixing (e.g., less than 1 min), most features were of ca.100 nm assigned to individual liposomes (Figure 3.7a). This suggested fast adsorption of Cu^{2+} on the liposomes, but little fusion took place at this time. Therefore, a short mixing may retain the liposome size, and Cu^{2+} may serve as a positive-stain agent under this condition. After 5 min (Figure 3.7b), although liposomes of ca.100 nm were still easily found, some fused structures with size larger than 200 nm were observed. At 10 min, most of the species were fused (Figure 3.7c) and finally at 30 min, all of the structures were several hundred nanometers and liposomes of 100 nm were barely found

(Figure 3.7d). Because all of these samples were dried the same way, this time-dependent difference cannot be due to drying. This study further confirmed Cu^{2+}-induced fusion of DOPS liposomes.

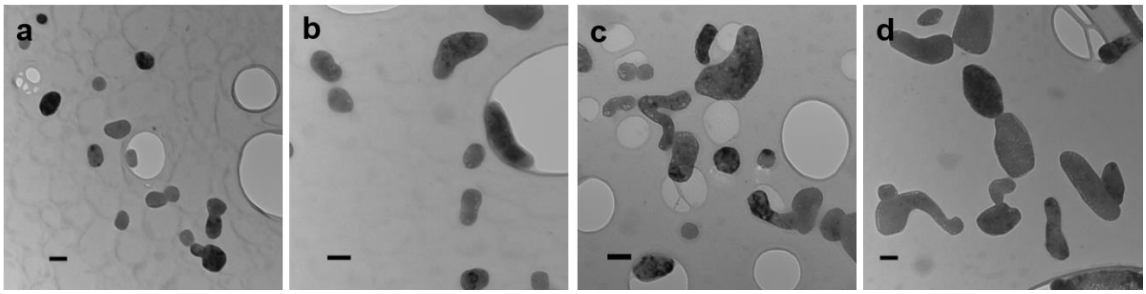

Figure 3.7 Time-dependent TEM micrographs of the 20 μM Cu^{2+} and DOPS (100 μg mL^{-1}) mixture at (a) less than 1, (b) 5, (c) 10, and (d) 30 min after mixing at pH 7.6. Scale bar = 100 nm.

3.3.4 Liposome fusion followed by DLS

The above TEM studies indicated liposome fusion by Cu^{2+}. To further confirm this and to understand reversibility of liposome size change, we followed the reaction by DLS. Started with an initial size of ~100 nm, the three negatively-charged liposomes had a little size change with 100 μM Cu^{2+} (Figure 3.8b-d), whereas a significant size increase occurred with 500 μM Cu^{2+}. The increased size was slightly reduced after adding EDTA to mask Cu^{2+}, but not fully restored (Figure 3.8e) consistent with irreversible liposome fusion observed from TEM and the fluorescence quenching experiment.

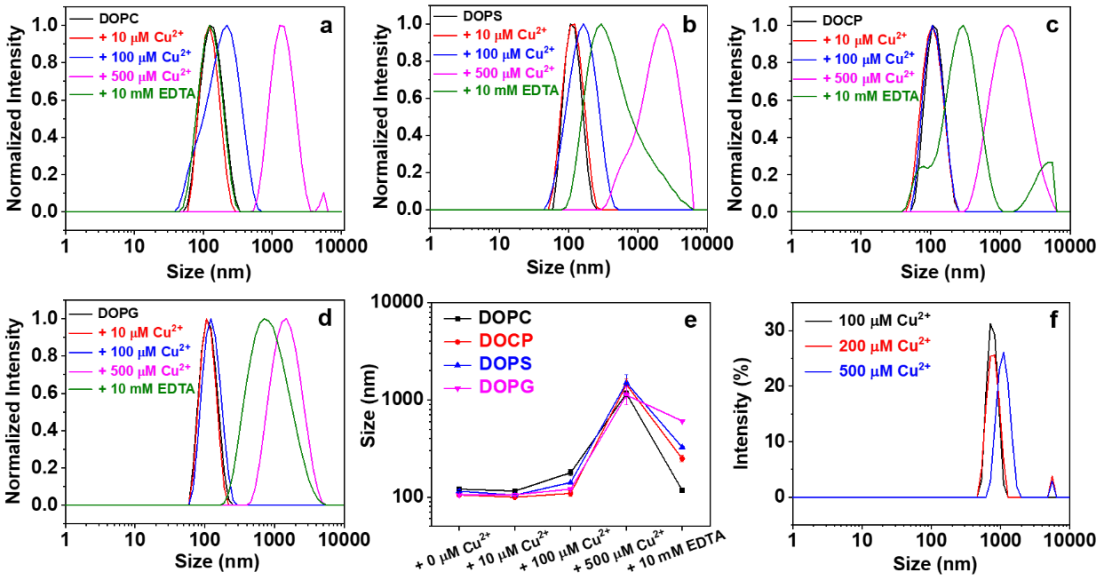

Figure 3.8 Normalized DLS size distributions of (a) DOPC, (b) DOCP, (c) DOPS, and (d) DOPG liposomes (100 μg mL^{-1}, ~ 125 μM lipid molecules) with different concentrations of Cu^{2+} in 10 mM HEPES, pH 7.6 with 100 mM NaCl. (e) Average hydrodynamic diameter of the liposomes as a function of Cu^{2+} concentration and after adding 10 mM EDTA. (f) DLS size distributions of different concentrations of Cu^{2+} at pH 7.6 (10 mM HEPES, 100 mM NaCl).

Interestingly, Cu^{2+} also induced a size change of the DOPC sample, but EDTA fully restored the DOPC sample to the original size of ~100 nm, indicating that the aggregation process for DOPC was reversible and the liposomes did not fuse or break during this process (Figure 3.8a and e black trace). We attributed its size increase to hydrolysis of Cu^{2+} forming $Cu(OH)_2$ or CuO at pH 7.6 because free 100 μM Cu^{2+} without any liposome also has a DLS signal (Figure 3.8f). Control experiments at pH 5 indeed showed no sign of DOPC binding to Cu^{2+}, whereas DOPS still had a slight size increase (ca. 200 nm) (Figure 3.9). DOPS binds Cu^{2+} less strongly at lower pH because its amine group needs to be deprotonated before it can bind Cu^{2+}.[40,41]

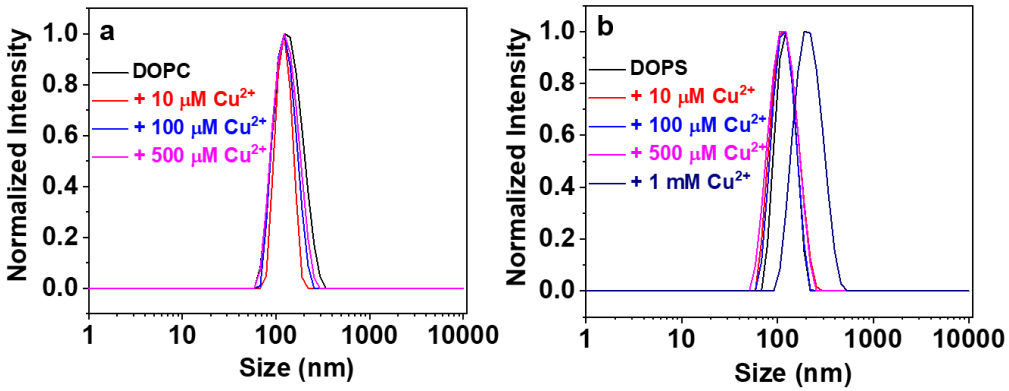

Figure 3.9 Normalized DLS size distributions of (a) DOPC and (b) DOPS liposomes (100 μg mL^{-1} or ca. 125 μM lipids) with different concentrations of Cu^{2+} in 50 mM acetate, pH 5 with 100 mM NaCl.

Taken together, all of the three negatively-charged liposomes fused forming larger liposomes in the presence of a high concentration of Cu^{2+}, whereas the neutral DOPC liposome did not fuse. This is consistent with the TEM data. From the fluorescence quenching assay, DOPS and DOCP liposomes were quenched much more than DOPG did, and this is a reflection of the tighter Cu^{2+} binding by DOPS and DOCP. Comparing DOPG and DOPC, both can only use their lipid phosphate group for chemically interacting with Cu^{2+}. Fusion of DOPG liposomes but not DOPC might be because the additional electrostatic interaction between Cu^{2+} and DOPG.

3.3.5 Cu^{2+}-induced liposome leakage

Membrane integrity is an important property of liposomes. Considering fusion of some liposomes in the presence of Cu^{2+}, we then tested liposome integrity using a calcein leakage assay. The liposomes were prepared with ~100 mM calcein loaded, and its fluorescence was self-quenched at such a high concentration. If the membrane is disrupted, calcein is released into the whole solution, resulting in fluorescence enhancement. For our experiments, the background fluorescence was monitored for 5 min before Cu^{2+} was introduced. Cu^{2+} quenched the fluorescence in all of the samples because of its binding to the free calcein (residual-free calcein or leaked). To avoid this artifact, we added EDTA at

20 min to chelate Cu^{2+} and fluorescence increase at this moment was an indication of leakage. Finally, at 30 min, Triton X-100 was added to fully rupture the liposomes and release all the calcein, so that we can calculate the percentage of leakage induced by Cu^{2+}. Here, we added two different concentrations of Cu^{2+} to the liposomes, 16.7 µM and 166.7 µM.

No leakage was observed with DOPC even with 166.7 µM Cu^{2+} (Figure 3.10a). In contrast, DOCP leaked around 60% of its calcein with just 16.7 µM Cu^{2+}, and full leakage occurred with 166.7 µM Cu^{2+} (Figure 3.10c). These are consistent with the TEM data. DOPS and DOPG liposomes showed no leakage with 16.7 µM Cu^{2+}, whereas both leaked with 166.7 µM Cu^{2+} (Figure 3.10b and d). Leakage of DOPG but not DOPC again suggested the importance of electrostatic interactions with Cu^{2+}.

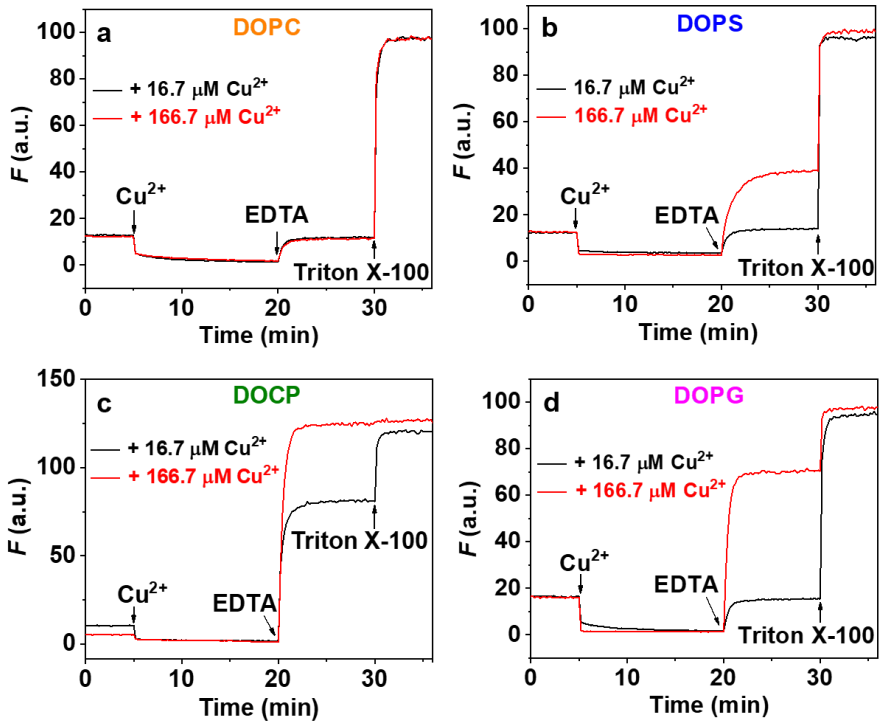

Figure 3.10 Leakage tests of (a) DOPC, (b) DOPS, (c) DOCP, and (d) DOPG liposomes loaded with 100 mM calcein in the presence of Cu^{2+} at pH 7.6 (10 mM HEPES, 100 mM NaCl).

While both DOPS and DOCP liposomes bind to Cu^{2+} tightly, DOPS required more Cu^{2+} to leak. The binding of DOPS to Cu^{2+} is accompanied with the release of its amine proton, and this proton release has retained the overall negative charge of the liposome after Cu^{2+} binding. This was described as an unquenchable surface potential by Cremer and co-workers.[41] Therefore, with a low Cu^{2+} concentration, the surface of DOPS liposomes remained negatively charged. As a result, crosslinking of DOPS liposomes by Cu^{2+}, which was necessary for fusion, was less likely at low Cu^{2+} concentrations because of charge repulsion. The total lipid concentration was only ~0.5 μM in this system,[160] but 16.7 μM Cu^{2+} did not leak DOPS or DOPG liposomes. For these two liposomes, 166.7 μM Cu^{2+} was required. We reason that after Cu^{2+} binding to the high affinity amino ligands in the PS liposomes, further binding to the weaker sites in PS was needed for fusion to take place. Such weaker sites are likely to be related to its phosphate group, which is chemically the same as the phosphate in the PG lipid. On the other hand, Cu^{2+} binding can neutralize the surface charge of DOCP liposomes, and it appears that Cu^{2+} more easily bridged two DOCP liposomes and promoted fusion even at low Cu^{2+} concentrations. In comparison, no leakage was observed for DOPS in the presence of 166.7 μM Zn^{2+} (Figure 3.11a), whereas Zn^{2+} can rupture DOCP liposomes, further indicating the interesting coordination chemistry in these systems.

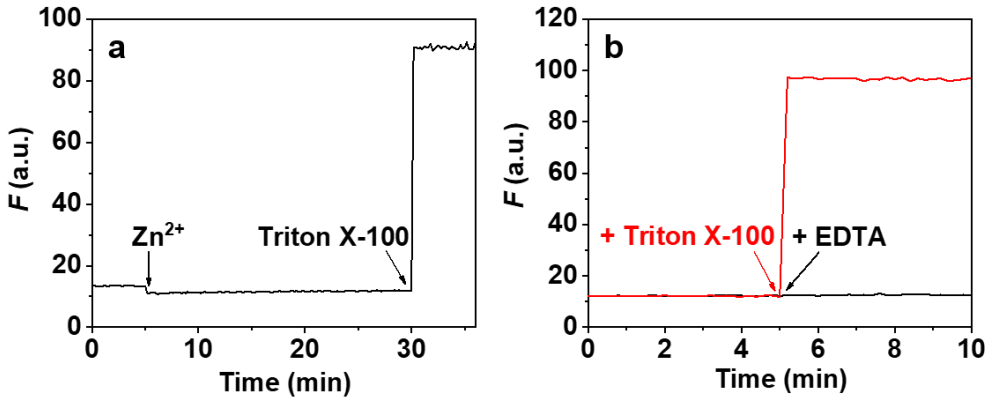

Figure 3.11 (a) Leakage test of calcein-loaded DOPS liposomes in the presence of 166.7 μM Zn^{2+}. (b) Leakage tests of clacein DOPS with Triton X-100 (red curve) and EDTA (black curve).

Because Cu^{2+} strongly quenched calcein fluorescence, in the above experiments, we only monitored the total released calcein after 15 min incubation. To understand the kinetic profile, we also added EDTA after different incubation time periods (Figures 3.12a and b). Leakage of both DOCP and DOPS liposomes reached a steady state within 3 min, indicating that the leakage processes were rapid (Figure 3.12c). As a control, we also added EDTA to calcein-loaded DOPS liposomes and no leakage occurred (Figure 3.11b). The leakage observed here suggested that liposome fusion in the presence of Cu^{2+} was not a clean process, and the interior contents were released. In contrast, cell fusion is a clean and well-regulated process and the contents do not leak.[161] Because DOPS leaked with Cu^{2+} but DOPC did not, we then mixed these two lipids at different ratios (5, 10, and 50 wt % DOPS) and prepared liposomes. The more DOPS added, the more leakage occurred (Figure 3.12d), and even 5% DOPS still showed a moderate leakage.

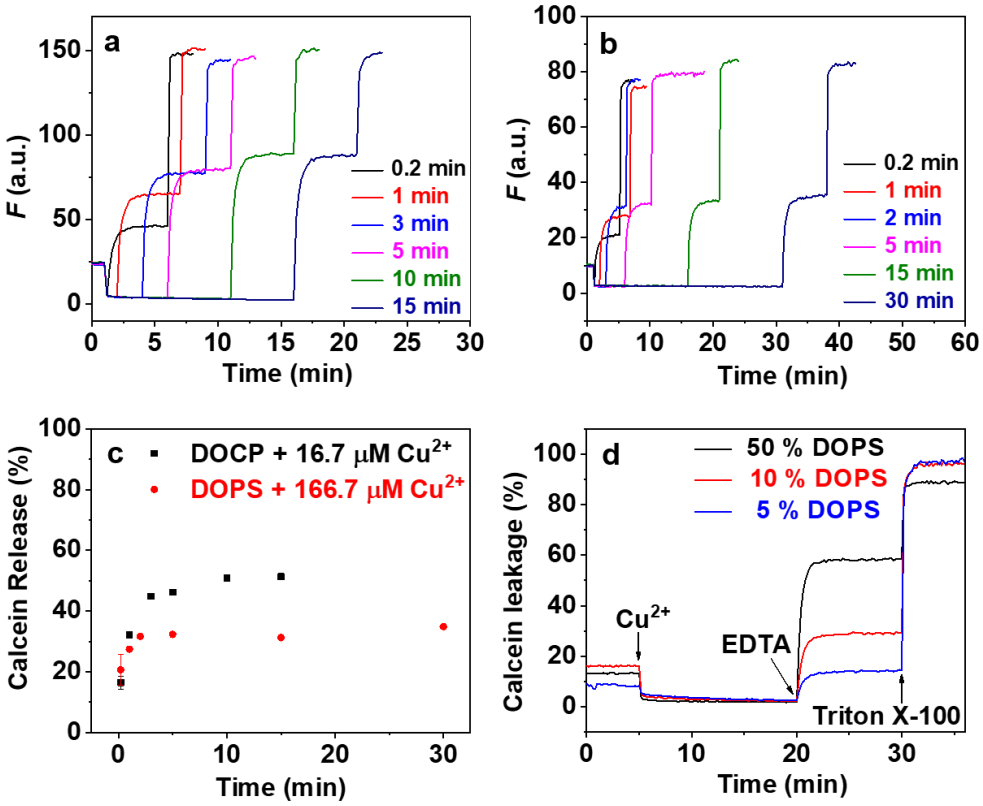

Figure 3.12 Leakage of (a) calcein-loaded DOCP liposomes after incubating with 16.7 μM Cu^{2+}, (b) calcein-loaded DOPS liposomes after incubating with 166.7 μM Cu^{2+} for different times before EDTA was added. The first rise of fluorescence over the initial background was due to Cu^{2+}-induced leakage. Finally, Triton X-100 was added to fully release calcein in each sample. (c) Kinetic leakage test of calcein DOCP with 16.7 μM Cu^{2+} and calcein DOPS with 166.7 μM Cu^{2+}. (d) Leakage tests of calcein-loaded liposomes with DOPC/DOPS mixed lipids containing 50%, 10% and 5% DOPS lipids, respectively. A final of 166.7 μM Cu^{2+} was added to induce leakage. The liposome concentration was estimated to contain a total of 0.5 μM lipid molecules.[160]

Because Cu^{2+} could hydrolyze to form $Cu(OH)_2$, to rule out that leakage was induced by $Cu(OH)_2$, we added pre-prepared $Cu(OH)_2$ to liposomes and monitored the leakage. At 166.7 μM $Cu(OH)_2$, no liposome leakage was observed (Figure 3.13), indicating that $Cu(OH)_2$ could not damage

the liposome membrane. Therefore, leakage was attributed to the direct interaction between Cu^{2+} ions and the lipids.

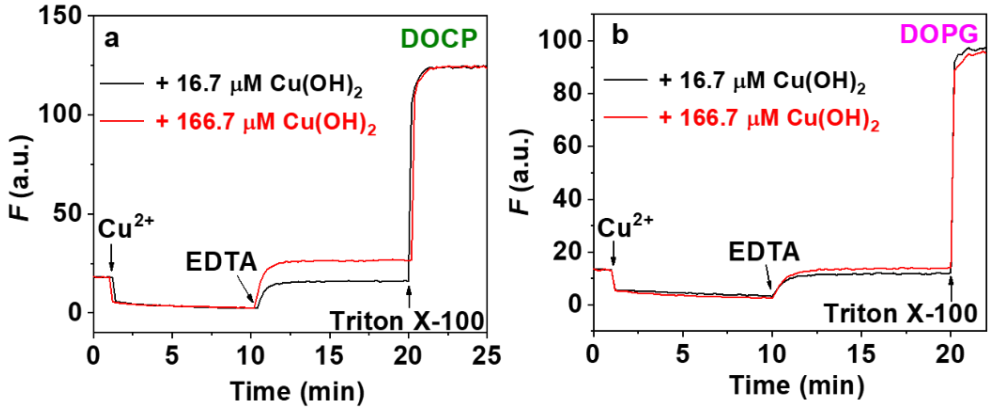

Figure 3.13 Leakage tests of calcein-loaded (a) DOCP and (b) DOPG liposomes with $Cu(OH)_2$ in 10 mM HEPES 100 mM NaCl, pH 7.6.

3.3.6 Oxidative property of Cu^{2+} inhibited by lipid binding

The above studies mainly used fluorescence to probe Cu^{2+} binding to the liposomes. Free Cu^{2+} ions have catalytic properties. For example, it can oxidize 2,4-DP and the product can react with 4-AP forming a red adduct with an absorption peak at 510 nm.[162] Using this reaction, we developed a colorimetric reaction to study Cu^{2+} binding. This experiment was carried out at pH 6.8 using MES buffer instead of pH 7.6 HEPES used in the above experiments because this reaction has optimal performance at this pH from our previous experiments.[162] Figure 3.9 shows that the binding of Cu^{2+} by the liposomes even occurred at pH 5, and pH 6.8 should also be an appropriate condition for this study. With increasing Cu^{2+} concentration, stronger red color was observed, suggesting more efficient reaction (Figure 3.14, column 1). The mixture of Cu^{2+} with DOPC and DOPG produced red color similar to free Cu^{2+}, indicating that the interactions with PC and PG liposomes did not affect the oxidation properties of Cu^{2+}. However, in the presence of DOPS and DOCP, the color change was strongly inhibited, which

was attributed to the strong binding of Cu^{2+} by the lipid headgroups. DOPS had even stronger binding because it inhibited the color more than DOCP did.

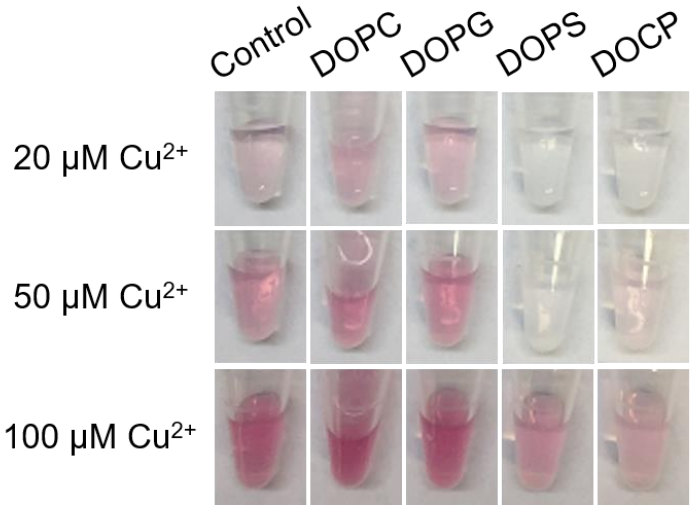

Figure 3.14 Catalytic properties of Cu^{2+} and Cu^{2+}/liposome complexes at pH 6.8. The red color is a reflection of oxidized products.

Cremer and co-workers studied the binding of Cu^{2+} by PE lipids also using an oxidation reaction. They monitored the oxidation of a dye embedded in the lipid bilayer region instead of that in the aqueous phase, and H_2O_2 was also added in addition to Cu^{2+}. The oxidation rate was 8.2 times faster with 70 mol % of the Cu^{2+}-binding PE lipids than that without them, indicating that Cu^{2+} can bind to PE lipids and the binding could recruit Cu^{2+} to the liposome surface to enhance oxidation in the lipid membrane.[99]

In our system, we compare the effect of added lipids for oxidizing foreign substrates and our reaction rates were proportional to the concentration of free Cu^{2+}. Therefore, our results were a reflection of Cu^{2+} binding affinity. Because the location of the substrates was different in these two experiments, it is not surprising that Cu^{2+} binding to PS lipids in our system showed an opposite effect compare to the binding of Cu^{2+} by the PE lipids.

3.3.7 Models of Cu^{2+} and liposome interactions

Taken together our results, we proposed reaction models of Cu^{2+} with each type of the liposome. Cu^{2+} and DOPC only interacted weakly because no liposome leakage and little Rh fluorescence quenching were observed (Figure 3.15a). Interactions still took place when dried because positive DOPC liposome stain was observed from TEM. Likely, Cu^{2+} interacts with the PC phosphate group via weak electrostatic interactions.

In contrast, Cu^{2+} could leak DOCP liposomes at relatively low Cu^{2+} concentrations. Such leakage was believed to be related to a nonclean fusion process, and fusion was also confirmed by TEM. We proposed that Cu^{2+} could readily bridge DOCP liposomes and cause fusion and leakage of the liposomes. The strong interaction between CP and Cu^{2+} was from the terminal phosphate group in the CP headgroup.

Even Cu^{2+} might bind to DOPS tighter than binding to DOCP, a higher Cu^{2+} concentration was needed to bridge DOPS liposomes. This is explained by that Cu^{2+} binding did not change its negative surface charge (Figure 3.15c).[41] We believe that at lower Cu^{2+} concentrations, intravesical binding occurred first without leakage. With Cu^{2+} saturating the tight binding serine sites, further Cu^{2+} addition might associate with weaker binding sites (e.g., the phosphate) to neutralize surface charge and allow liposomes to approach each other to fuse (Figure 3.15c). In the case of DOPG liposome, fusion also took place. Its binding to Cu^{2+} might be slightly stronger than DOPC does but is weaker than the other two. The binding of Cu^{2+} to individual liposome was observed at lower Cu^{2+} concentration and liposome fusion occurred at higher Cu^{2+} concentrations likely due to electrostatic interactions with the lipid phosphate group (Figure 3.15d).

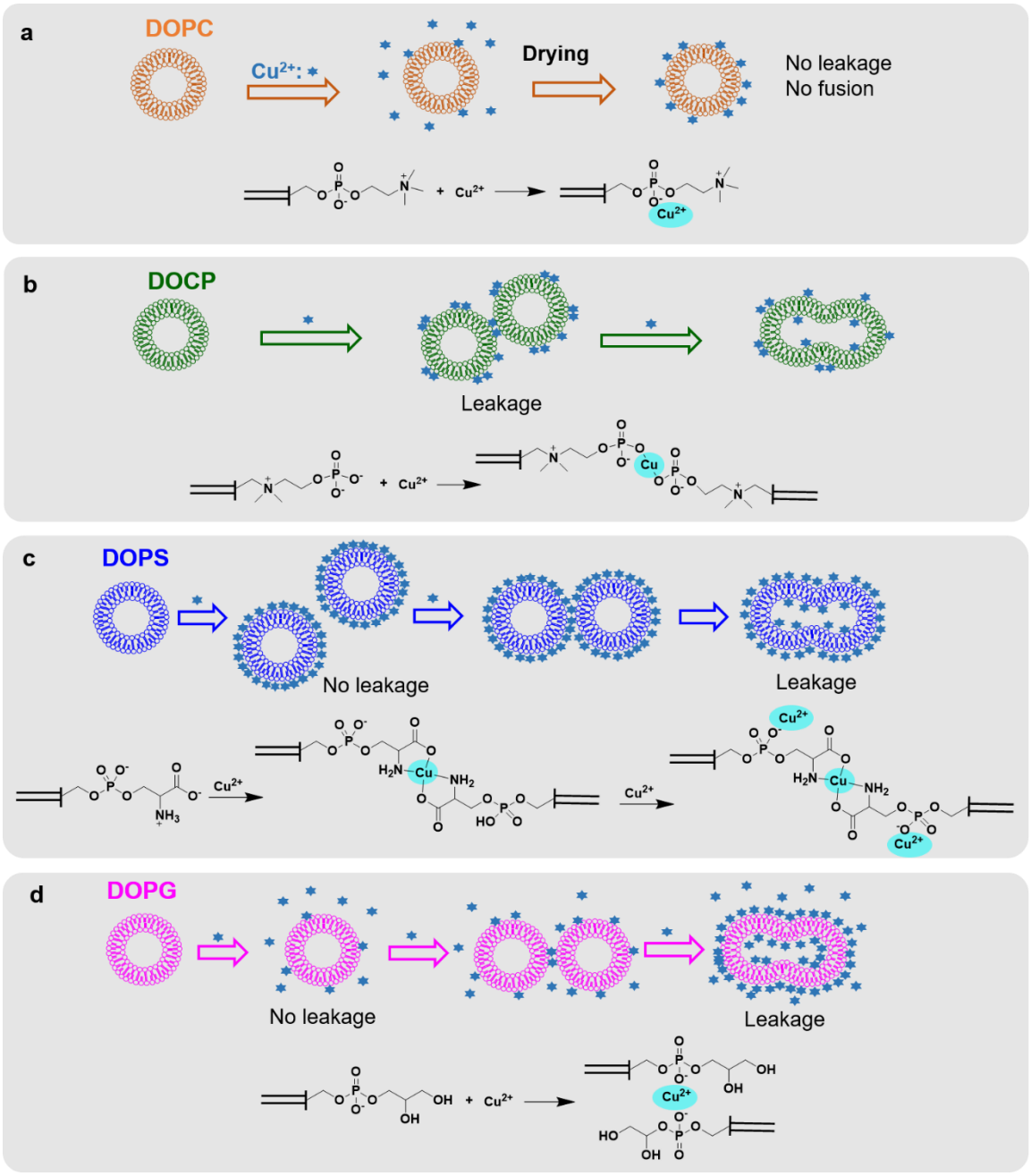

Figure 3.15 Scheme to summarize the model of Cu^{2+} binding to the four liposomes both at the liposome level and at the individual lipid level for (a) DOPC, (b) DOCP, (c) DOPS, and (d) DOPG.

3.3.8 Further discussion

This work shows different interactions of Cu^{2+} with four kinds of liposomes. The following interesting aspects were discovered: (1) The effect of charge. DOPG, DOPS, and DOCP are all negatively-charged liposomes. From fluorescence quenching, leakage tests, and TEM characterizations, DOCP and DOPS interacted with Cu^{2+} much stronger than DOPG did. Therefore, charge is not the determining factor for the interaction between lipids and Cu^{2+}, and coordination of lipid headgroup is more important. On the other hand, anionic DOPG still bound Cu^{2+} more strongly than zwitterionic DOPC did. Because both could only interact with Cu^{2+} via the phosphate group, electrostatic interaction still contributes to Cu^{2+} binding but its importance is less compared to strong metal coordination. (2) Metal binding groups. Although the headgroups of both DOCP and DOPS strongly coordinate with Cu^{2+}, they showed different behaviors in the leakage tests. This indicates that the chemical nature of the lipid headgroup plays important roles in metal/lipid interactions. Importantly, Cu^{2+} binding to DOPS does not change the surface charge because of a concomitant release of protons,[41] whereas to DOCP does, and this is reflected from the leakage properties. (3) Cu^{2+} versus Zn^{2+}. Previously, we have studied the interaction between DOCP and Zn^{2+}.[48] Our results showed the formation of multilayered structures, and this is quite different from DOCP interaction with Cu^{2+}. In this work, we also compared Cu^{2+} and Zn^{2+} for interacting with DOPS liposomes and they also behaved differently. This result demonstrated that different metals interact with the lipids quite differently. Similar results have also been observed that different transition metals could direct the self-assembly of amphiphiles with different morphologies, and work has also been done on toxic metals with liposomes.[68,163,164]

3.4 Summary

In summary, the interaction between Cu^{2+} and four types of liposomes has been systematically studied using fluorescence quenching, DLS, TEM, calcein leakage, and colorimetric assays. Fluorescence quenching showed that DOPS and DOCP have a high affinity toward Cu^{2+}, whereas DOPC and DOPG have weaker binding. The DLS results revealed that Cu^{2+} could induce a size increase

of the three negatively-charged liposomes at higher concentration, and adding EDTA could not completely reverse the process. This suggested that Cu^{2+} induced fusion of DOCP, DOPS, and DOPG liposomes, whereas it had little effect on DOPC. TEM showed Cu^{2+} could positively stain the liposome features under a normal TEM. Leakage tests indicated that the integrity of DOPC was not affected by Cu^{2+}, whereas Cu^{2+} could easily leak DOCP, DOPS, and DOPG liposomes at appropriate concentration. Finally, the tight binding between Cu^{2+} with liposomes inhibited the catalytic properties of Cu^{2+}. Our model has shown that each lipid has a distinct mechanism of interacting with Cu^{2+}. This work demonstrated some important factors in metal binding by liposomes, and these results may direct further biological and analytical applications.

Chapter 4 Growing a Nucleotide/Lanthanide Coordination Polymer Shell on Liposomes

The results presented in this chapter have been published as:

Yibo Liu and Juewen Liu, Growing a Nucleotide/Lanthanide Coordination Polymer Shell on Liposomes, *Langmuir*, **2019**, 35, 11217-11224.

4.1 Introduction

After studying liposome binding to divalent transition metal ions such as Zn^{2+} (Chapter 2) and Cu^{2+} (Chapter 3), we then studied the binding of trivalent lanthanide ions, which were rarely used to interface with liposomes.[165,166] Liposomes are lipid vesicles dispersed in aqueous solutions. With an aqueous internal compartment, a hydrophobic shell and excellent biocompatibility, liposomes have been engineered for drug delivery,[50,167] biosensing,[53,62] and mimicking the cell membrane. However, their density is close to that of water making it difficult to centrifuge and separate. At the same time, liposomes are relatively fragile and tend to merge with each other or leak its content.

To increase the stability of liposomes, a few strategies have been attempted. For example, solid or porous NPs were used to support liposomes,[168,169] forming supported lipid bilayers.[31,151] These supported bilayers are sometimes difficult to fully seal the NPs, although the membrane becomes mechanically stronger.[170] The second method is to covalently cross-link the lipids (e.g., with diacetylenic lipids).[171] While stability is enhanced, cross-linked lipids are difficult to degrade and most other lipids cannot be cross-linked. Finally, it is possible to coat liposomes with a shell.[172] Decoration of liposomes with very small NPs can also increase membrane stability as demonstrated by Zhang and Granick,[173] which was attributed to the local gelation of the underlying lipids.[32,116,117]

We are interested in coating liposomes with an inorganic nanoshell, and this has been demonstrated in a few systems. For example, Jin and Gao coated liposomes with a gold nanoshell and controlled content release with light.[174] Liposome-templated silica nanoshells were also reported by a

few groups.[175,176] Song et al. synthesized a suite of liposome templated platinum nanocages as highly efficient catalysts.[177] Schmidt and Ostafin grew a layer of calcium phosphate on liposomes for drug delivery.[178]

Coordination polymers or materials are self-assembled metal/organic structures,[69,179-181] and nucleotides are particularly interesting ligands to prepare such materials. In the past few years, many nucleotide-based coordination materials have been reported, showing applications such as biosensors, drug delivery vehicles, enzyme capsules, and smart materials.[162,182,183] In particular, lanthanide/nucleotide has been one of the most extensively studied systems.[184] With different combinations of lanthanides and nucleotides/nucleosides, a variety of interesting materials were obtained for sensitized lanthanide luminescence and enhanced contrast of magnetic resonance imaging. In addition, their adaptive inclusion of guest molecules has been demonstrated for biological applications.[181,185]

Because many lipids have metal coordination ligands such as phosphate, serine, or synthetically introduced groups, liposomes might also serve as a good template for growing coordination materials. Many research efforts have been reported on lipid binding to metal ions such as Cu^{2+},[40,41,99,134,186] Zn^{2+},[48] Hg^{2+},[129,163,164] Ca^{2+},[187] and Na^{+}.[188] Work has also been carried out on lanthanides, and they were mainly focused on fundamental interactions.[165,166,189-194] To investigate liposome-templated growth, we first studied the adsorption of Gd^{3+} by two types of negatively-charged liposomes. We chose Gd^{3+} as a representative lanthanide ion because it is commonly used for its magnetic properties. We then demonstrated liposome-templated growth of a nucleotide/lanthanide shell, which showed enhanced stability toward leakage induced by NPs.

4.2 Materials and Methods

4.2.1 Chemicals

All the phospholipids were purchased from Avanti Polar Lipids (Alabaster, AL). $GdCl_3$, disodium calcein, Triton X-100, ZnO NPs (catalog number: 721077), and HEPES were purchased from

Sigma-Aldrich. Adenosine-5'-monophosphate disodium salt (AMP) was purchased from Alfa Aesar (Ward Hill, MA). EDTA and sodium chloride were purchased from Mandel Scientific (Guelph, ON, Canada). Milli-Q water was used to prepare all the buffers, solutions, and suspensions.

4.2.2 Preparation of gadolinium/adenosine monophosphate coated liposome (liposome@Gd^{3+}/AMP)

To prepare Gd^{3+}/AMP coated liposome, a liposome suspension (100 μg mL^{-1}) was incubated with Gd^{3+} (500 μM) for 30 min and then AMP (500 μM) was added. After 30 min incubation, the mixture was centrifuged at 10,000 rpm for 10 min to collect the precipitated liposome@Gd^{3+}/AMP, and the pallet was washed with buffer A. To prepare calcein loaded DOPS@Gd^{3+}/AMP, 100 μL of purified calcein-loaded DOPS liposome was mixed with 5 μL Gd^{3+} (10 mM) and 5 μL AMP (10 mM), and the remaining procedures were the same as described above.

4.2.3 ζ-potential measurements

A liposome suspension (100 μg mL^{-1}) mixed with metal ions (Gd^{3+}, Zn^{2+}, and Ca^{2+}) in buffer A (final metal concentrations: 10, 50, 100, 200, and 500 μM) was measured using a Malvern Zetasizer Nano ZS 90 with a He-Ne laser (633 nm) at 90° and 25 °C. The data were analyzed by Malvern Dispersion Technology Software 4.20.

4.2.4 TEM

TEM micrographs were recorded on a Philips CM10 transmission electron microscope. A 10 μL liposome (100 μg mL^{-1}) and Gd^{3+} (20 μM) mixture or liposome@Gd^{3+}/AMP (100 μg mL^{-1} based on liposome concentration) was spotted on a 230 mesh holey carbon copper grid and the extra solution on the grid was removed by filter paper. The samples were dried in air overnight before imaging.

4.2.5 Liposome leakage tests

To monitor the integrity of liposome membranes, 3 μL of purified calcein-loaded liposomes were added to 600 μL buffer A in a quartz cuvette at room temperature. The background fluorescence was monitored for 5 min before adding 10 μL of Gd^{3+} ions (1 or 10 mM). The fluorescence was

monitored for another 15 min. At 20 min, 10 µL of 100 mM EDTA was added. At 30 min, 10 µL of 5% Triton X-100 was added to fully rupture the liposomes. For the stability toward Gd^{3+}/AMP, 10 µL of AMP (10 mM) was added at 15 min as an additional step. For the stability against Triton X-100, 10 µL of various concentration (0.005, 0.05 and 0.5%) of Triton X-100 was added to calcein-loaded DOPS or DOPS@Gd^{3+}/AMP at 2 min. Then, at 10 min, 10 µL of 5% Triton X-100 was added to all the samples. In the case of DOPS@Gd^{3+}/AMP, 10 µL of 100 mM EDTA was added at 7 min as an additional step. For the stability toward ZnO NPs, 10 µL of ZnO (1 mg mL^{-1}) was added to calcein-loaded DOPS or DOPS@Gd^{3+}/AMP at 2 min, 10 µL of 5% Triton X-100 was added at 18 min. In the case of DOPS@Gd^{3+}/AMP, 10 µL of 100 mM EDTA was added as an extra step. Calcein was excited at 485 nm, and the emission was monitored at 525 nm using a Varian Eclipse fluorescence spectrophotometer. The percentage of leakage was calculated by $I_{released}/I_{total} \times 100\%$.

4.3 Results and Discussion

4.3.1 DOPS and DOCP liposomes

Two kinds of liposomes were studied: DOPS and DOCP, because they are both negatively charged and contain strong metal-binding ligands. DOPS (Figure 4.1a) has a carboxyl and an amine group that can chelate metal ions.[40,41] In addition, it has a bridging phosphate resulting in an overall negative charge. PS lipids mainly reside in the inner leaflet of cell membranes, and its flip to the outer leaflet is an indication of apoptosis. DOCP is a synthetic lipid with a terminal phosphate (Figure 4.1a). Compared to a bridging phosphate, a terminal phosphate binds the metal species stronger. For example, DOCP liposomes adsorb strongly on various metal oxides.[47,49] These two liposomes were, respectively, prepared by the extrusion method, and they both had a hydrodynamic size of ca.100 nm from DLS (Figure 4.1b). Their ζ-potential values were consistent with their respective surface charges (Figure 4.1c). For some control experiments, we also studied a few other types of liposomes, such as DOPC and DOPG (Figure 4.1a).

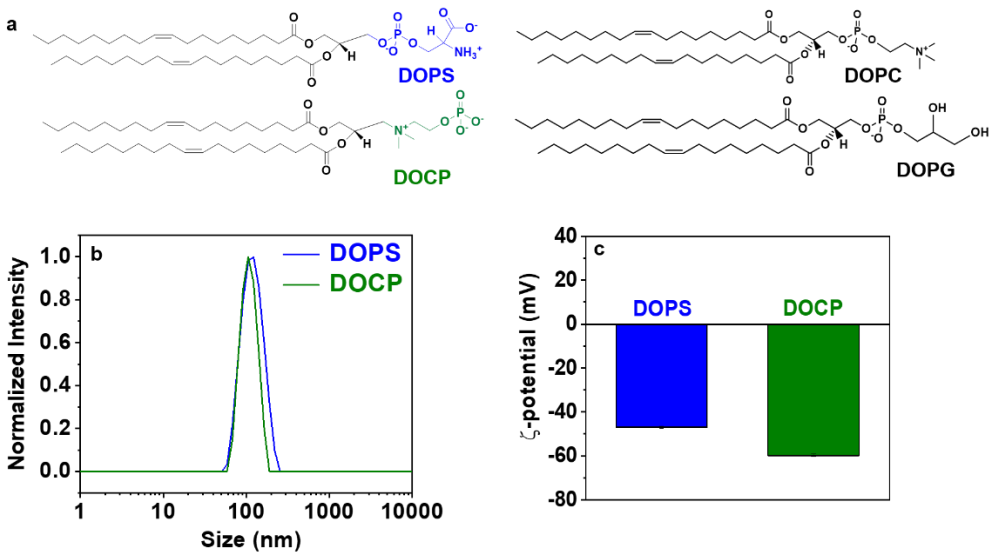

Figure 4.1 (a) Chemical structures of DOPS, DOCP, DOPC and DOPG lipids. (b) Normalized DLS size distributions and (c) ξ-potential of DOPS and DOCP liposomes at pH 7.6 (10 mM HEPES 100 mM NaCl).

4.3.2 Gd^{3+} binding characterized using TEM

After preparing the liposomes, we studied Gd^{3+} adsorption using TEM. Non-stained liposomes are not visible under normal TEM, and usually liposomes need to be observed with a negative stain. We previously showed that Cu^{2+} could bind to liposomes and display positive stain features.[186] With addition of Gd^{3+}, we also observed positive stain features consistent with metal binding to both the DOPS (Figure 4.2a) and DOCP liposomes (Figure 4.2b). Most of the features were ca. 100 nm, close to the original size of the liposomes. Some peanut-shaped structures may be caused by liposome fusion or the drying processes during the preparation of the TEM specimens, and some dark spots might be because the metal species come together during drying. It is unclear whether the adsorbed metal ions can aggregate on the liposomes in the solution phase or not. These features are different from those with Cu^{2+}, for which we observed extensively fused liposome structures with much larger sizes

(> 500 nm) (Figure 4.2c). The TEM results suggested that Gd^{3+} could bind to both DOPS and DOCP liposomes without causing extensive fusion, although a moderate fusion may still take place.

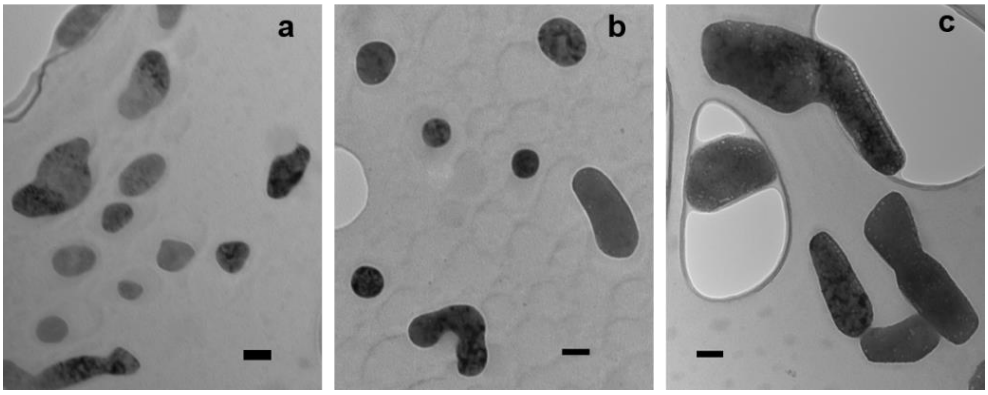

Figure 4.2 TEM micrographs of (a) DOPS liposomes with Gd^{3+}, (b) DOCP liposomes with Gd^{3+}, and (c) DOCP liposomes with Cu^{2+} (100 μg mL^{-1} liposome, 20 μM metal ion). Scale bars = 100 nm.

4.3.3 Gd^{3+} binding reverses the surface charge of liposomes

We then followed the surface charge of the liposomes upon adding Gd^{3+} (Figure 4.3). The ζ-potential of liposome/Gd^{3+} complexes increased gradually with increasing Gd^{3+} concentration and became positive with more than 150 μM Gd^{3+} (Figure 4.3a). In this experiment, the lipid concentration was 124 μM. Because slightly more than half of the lipids were on the outer leaflet of the membrane, at the PZC, the lipid headgroup and Gd^{3+} had a ratio of ∼2:1, true for both the DOPS and DOCP liposomes. However, when the liposomes were mixed with Zn^{2+}, the sample remained negative even with 2 mM Zn^{2+} (Figure 4.3c). Similarly, even with 10 mM Ca^{2+}, charge reversal did not occur (Figure 4.3d). Therefore, Gd^{3+} is unique in the sense that it was the only metal showing charge reversal for the DOCP and DOPS liposomes. This is consistent with the previously-reported charge reversal of DOPS by La^{3+} binding.[166]

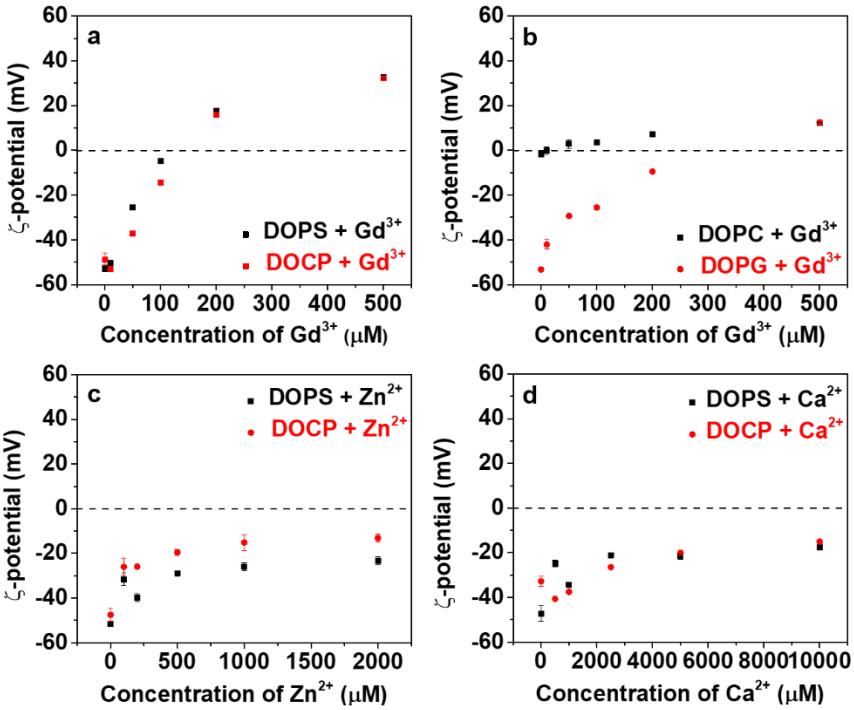

Figure 4.3 ξ-potential of DOPS and DOCP liposomes titrated with (a) Gd^{3+}, (c) Zn^{2+}, and (d) Ca^{2+}. (b) ξ-potential of DOPG and DOPC liposomes titrated with Gd^{3+}. The experiments were carried out at pH 7.6 (10 mM HEPES, 100 mM NaCl).

Cremer and co-workers reported that the binding of Cu^{2+} to the PS headgroup releases two protons from the amine group. Thus, the surface potential remained negative after Cu^{2+} binding. The release of protons was also reported upon lanthanide binding to the PS lipid.[166] With three formal positive charges, after neutralizing the negative charges on the liposome, a positive charge may still remain, rendering Gd^{3+} overcompensating the surface potential. This work also indicates that we can control the surface charge of liposomes by using different metal ions. We also tested other trivalent metal ions, Fe^{3+} and Cr^{3+}, however, these metal ions did not show charge reversal properties at the same concentration with Gd^{3+} (500 μM) (Figure 4.4). This is probably because these metals have a weaker binding affinity compared to lanthanides. In addition, we also measured the ζ-potential of DOPC or

DOPG liposomes in the presence of Gd^{3+} (Figure 4.3b). The ζ-potential reached slightly positive values (~12 mV) with 500 μM Gd^{3+}. These lipids have weak metal coordination ability because they only have a bridging phosphate for metal binding. Their slight positive charge might be from weakly adsorbed metal ions. Therefore, the strong binding of Gd^{3+} with lipids is necessary for reversing the charge to a high positive potential (> 30 mV).

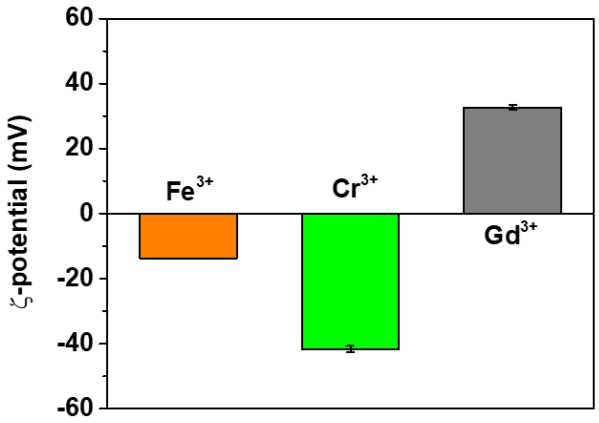

Figure 4.4 ξ-potential of DOPS liposomes (100 μg mL^{-1}) in the presence of 500 μM Fe^{3+}, Cr^{3+} and Gd^{3+} at pH 7.6.

4.3.4 Gd^{3+} leaks DOCP but not DOPS liposomes

After confirming the strong binding of Gd^{3+} by both DOCP and DOPS liposomes, we then studied its effect on membrane integrity. For this purpose, a leakage assay was carried out. The liposomes were loaded with 100 mM calcein dye, but its fluorescence was self-quenched at such a high concentration. If the membrane was disrupted, calcein would release to the whole solution to induce fluorescence increase.[31] The background fluorescence was monitored for 5 min before Gd^{3+} was added. The background was not zero due to a small amount of free calcein outside the liposomes. For both liposomes, adding Gd^{3+} caused an immediate fluorescence drop to the zero fluorescence level and this

was attributed to Gd^{3+} binding to free calcein and quenching the fluorescence. Note that the free calcein concentration was very low (well below 20 nM), and most of the added Gd^{3+} ions were not associated with free calcein, and they can interact with the liposomes. At this point, leakage due to Gd^{3+} binding to the liposomes may take place, but this leakage was not reflected from the fluorescence enhancement because of calcein binding to Gd^{3+}. After 15 min, EDTA was added to the samples to chelate Gd^{3+} and release the free calcein. The fluorescence difference between this point and the initial background was due to the leakage (Figure 4.5a). Finally, at 30 min, Triton X-100 was added to fully rupture the liposomes, and this can allow the calculation of the percentage of leakage induced by Gd^{3+}. Note, after adding EDTA to release free calcein, Gd^{3+} is unlikely to be associated with lipids considering the extreme high association constant of Gd^{3+}/EDTA ($\sim 5 \times 10^{16}$ M^{-1}),[195] compared to Gd^{3+}/nucleotide ($\sim 1 \times 10^{5}$ M^{-1}).[196]

For the DOCP liposomes, we observed significantly increased fluorescence with 16.7 μM Gd^{3+}, much higher than the initial background (Figure 4.5a). With 10-fold more Gd^{3+}, the increase was even higher. Because we observed liposome features under TEM (Figure 4.2b), the overall structure of the DOCP liposomes was not disrupted and leakage should occur locally. We also studied the kinetics of DOCP leakage by adding EDTA after different incubation times with Gd^{3+} (Figure 4.5c), and the fraction of leakage increased gradually with time. We calculated the fraction of leakage at each time point and plotted the data in Figure 4.5d, where leakage reached 60% in 2 h, indicating a slow process. In comparison, leakage of DOPS liposomes by Cu^{2+} stopped within 3 min.[186] Interestingly, the DOPS liposomes did not leak even with 166.7 μM Gd^{3+} (Figure 4.5b). The nonleaky property was previously observed with La^{3+} binding to PS liposomes.[166] Because both the CP and PS headgroups are negatively charged, their difference in leakage can only be attributed to the way of metal binding. This time-dependent leakage in Figure 4.5c also indicated that the leakage was due to Gd^{3+}/ liposome interactions instead of the added EDTA.

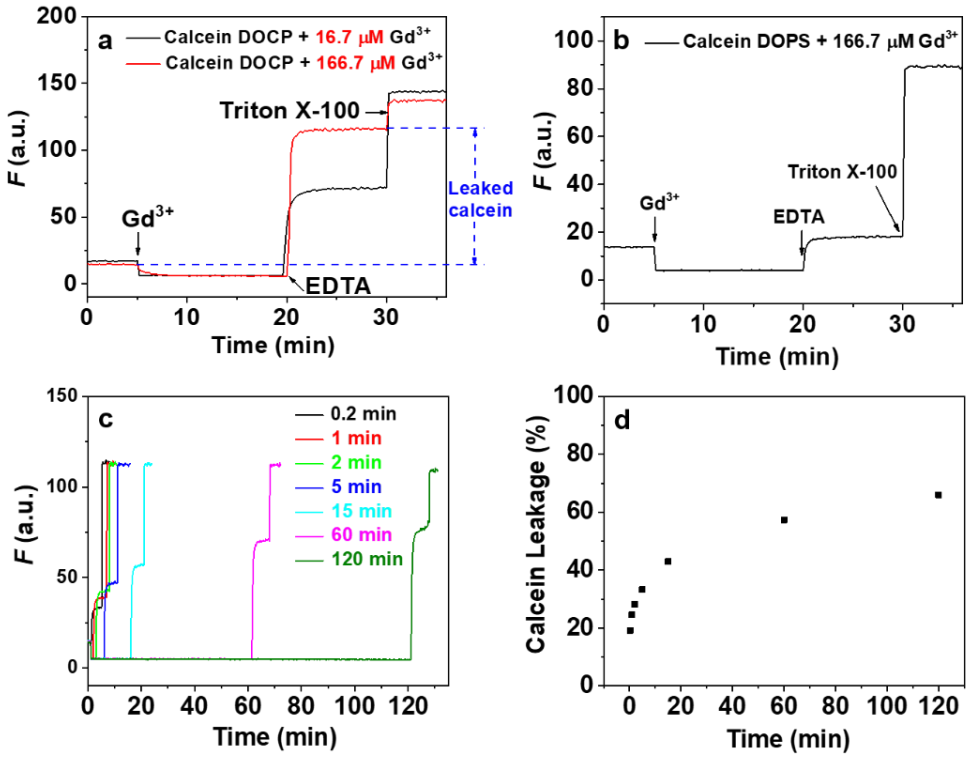

Figure 4.5 Leakage of (a) DOCP and (b) DOPS liposomes loaded with 100 mM calcein in the presence of Gd^{3+} at pH 7.6 (10 mM HEPES, 100 mM NaCl). The blue line indicates the fluorescence increase due to the leaked calcein. (c) Leakage of the calcein-loaded DOCP liposomes after incubating with 16.7 μM Gd^{3+} for different time periods before EDTA was added. The first rise of fluorescence over the initial background was because of Gd^{3+}-induced leakage, and the second rise was due to Triton X-100. (d) Kinetic of calcein leakage from the DOCP liposomes induced by 16.7 μM Gd^{3+}. The total lipid molecule concentration was estimated to be ~0.5 μM.[160]

4.3.5 Coating a Gd^{3+}/AMP shell

Because Gd^{3+} did not disrupt the membrane integrity of the DOPS liposomes, we used DOPS to test liposome-templated growth of a coordination polymer shell. To ensure that the shells were growing on the liposome templates instead of randomly undergoing nucleation in solution, we incubated Gd^{3+} with the DOPS liposomes first and then AMP was added (Figure 4.6). After adding

AMP, a turbid suspension was obtained, and we centrifuged the sample to collect the pallet. Under TEM, dark spherical shells were observed (Figure 4.7a), indicating that the DOPS liposomes templated the shell. These features were quite different from those of Gd^{3+} mixed with DOPS liposomes (Figure 4.2a), where the structures did not have a well-defined shape. In addition, DOPS@Gd^{3+}/AMP can be centrifuged to isolate and purify the product. After washing and re-dispersion by sonication, the dark shells remained (Figure 4.7b). For comparison, we also used noncharged zwitterionic DOPC liposomes to template the growth. However, the structure appeared more fragile, and the spherical shape of the liposomes were less retained (Figure 4.7c), indicating that the binding of Gd^{3+} with lipids might be critical for the templated growth. In addition, for samples added with AMP first, no well-defined structure was observed (Figure 4.7f), further proving the critical role of Gd^{3+} coordination to lipids. We also tested a few other negatively-charged liposomes. DOCP liposomes could form dark circles (Figure 4.7d) similar to those observed with DOPS liposomes, but as described above, the content leaked from the DOCP liposome upon mixing Gd^{3+}. Dark rings were occasionally observed for DOPG liposomes, but the majority of the products were random precipitants (Figure 4.7e). DOPG is negatively charged, but it only has a bridging phosphate for metal binding. Overall, it appears that DOPS is an optimal liposome template.

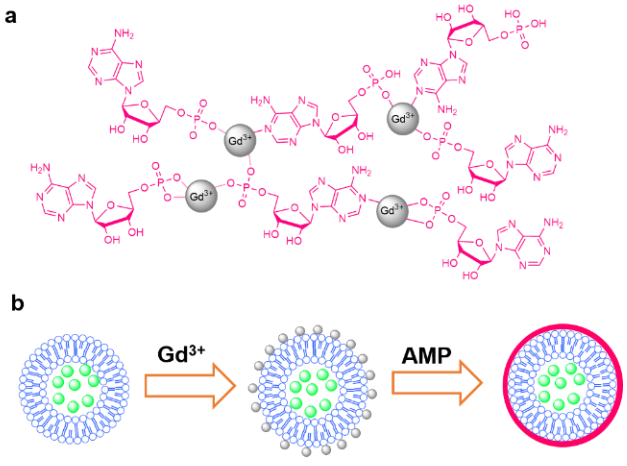

Figure 4.6 Schematic illustration of (a) the structure of Gd^{3+}/AMP coordination polymer and (b) the formation of DOPS@Gd^{3+}/AMP. The content inside the liposomes was retained during this process.

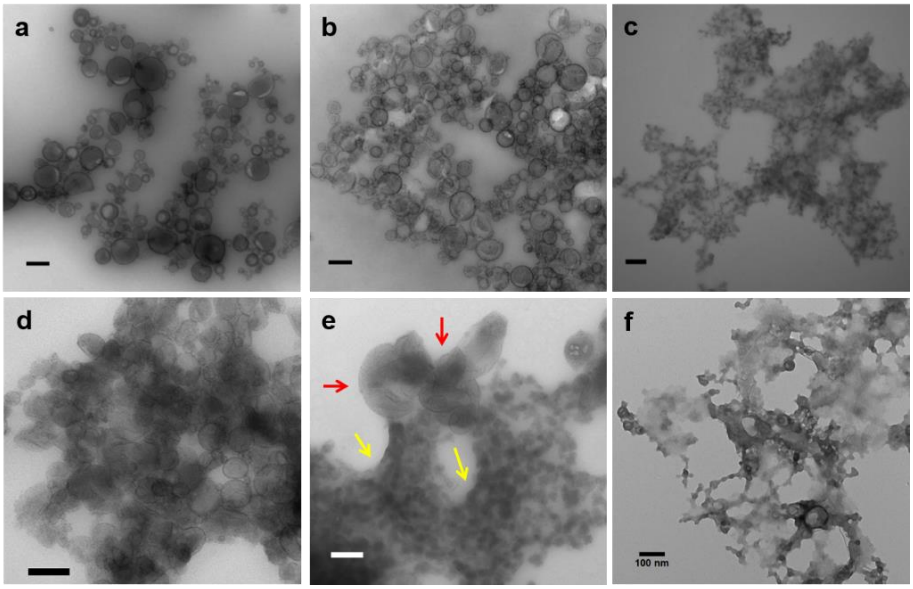

Figure 4.7 TEM micrographs of DOPS coated with 500 µM Gd^{3+}/AMP (a) before and (b) after washing with buffer. TEM micrographs of (c) DOPC, (d) DOCP, and (e) DOPG liposomes (100 µg mL^{-1}) coated with 500 µM Gd^{3+}/AMP. (f) A TEM micrograph of DOPS@Gd^{3+}/AMP prepared by mixing DOPS with AMP first. The molar ratio of Gd^{3+} to AMP was 1:1 for all these experiments. Liposome concentration is 100 µg mL^{-1}. Scale bars = 100 nm. The red arrows in (e) indicate the DOPS@Gd^{3+}/AMP products, while yellow arrows indicate random Gd^{3+}/AMP NPs formed independent of the liposomes.

We then studied the effect of the Gd^{3+}/AMP concentration on the final structures. We fixed the DOPS liposome concentration at 100 µg mL^{-1} (exposed PS headgroup concentration: ca. 62 µM), and varied the Gd^{3+} and AMP concentrations (the ratio of Gd^{3+} to AMP was fixed at 1:1). When 200 µM Gd^{3+}/AMP was used, dark rings can be observed around the liposomes (Figure 4.8a). However, the liposomes appeared to be soft and irregular in shape. This was likely due to deformation during drying, suggesting that the shell was not rigid. When 1 mM Gd^{3+}/AMP was used, the liposomes were round in shape and thicker shells were observed (Figure 4.8b, red arrows). However, free Gd^{3+}/AMP NPs were also produced (Figure 4.8b, yellow arrows). It appears that 500 µM Gd^{3+}/AMP is an optimal

concentration, where the Gd^{3+}/AMP shells were rigid and they grew mainly on the liposome surface (Figure 4.7a).

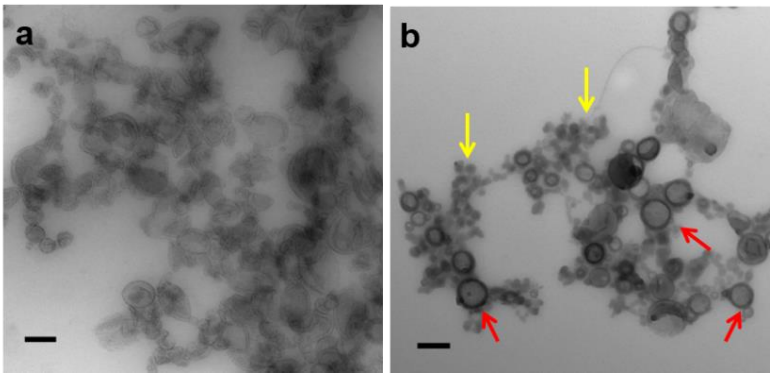

Figure 4.8 TEM micrographs of DOPS liposomes coated with (a) 200 µM and (b) 1 mM Gd^{3+}/AMP. The molar ratio of Gd^{3+} to AMP was 1:1. Liposome concentration is 100 µg mL^{-1}. Scale bars = 100 nm. The red arrows in (b) indicate the DOPS@Gd^{3+}/AMP products, while yellow arrows indicate random Gd^{3+}/AMP NPs formed independent of the liposomes.

4.3.6 Membrane integrity after Gd^{3+}/AMP coating

After coating the Gd^{3+}/AMP shell, we then studied the membrane integrity using the calcein leakage assay. We added Gd^{3+} at 5 min and AMP at 15 min. EDTA was added at 20 min to release calcein from Gd^{3+} (Figure 4.9). Because the fluorescence after EDTA was the same as the initial background, no leakage occurred, indicating forming the shell did not leak the DOPS liposomes. Finally, Triton X-100 was added to fully rupture the liposomes. Therefore, forming the shell on the DOPS liposome can fully retain the content inside the liposomes. We checked the TEM of the samples after adding Triton X-100, and the shell feature remained (Figure 4.10a). The coated Gd^{3+}/AMP shell can be destroyed by adding inorganic phosphate or EDTA due to their strong affinity to Gd^{3+} (Figure 4.10b and c). Note in this case, the liposome remained intact, and only the shell was disrupted.

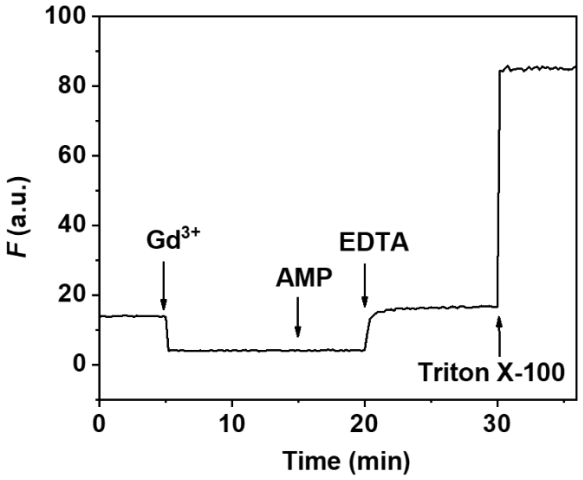

Figure 4.9 Leakage test of calcein-loaded DOPS liposomes mixed with Gd^{3+} and AMP.

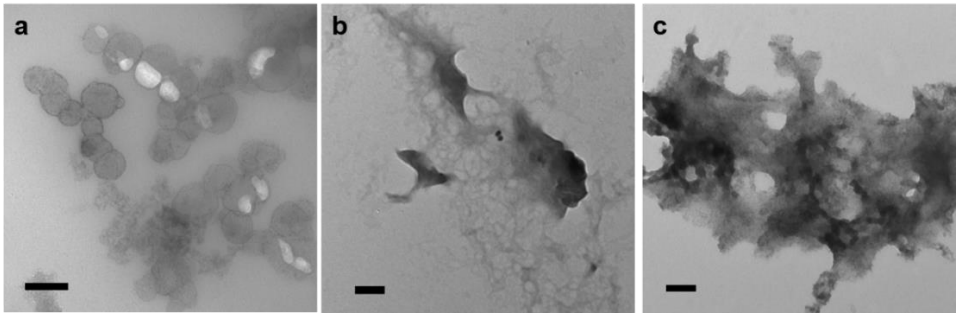

Figure 4.10 TEM micrographs of DOPS@Gd^{3+}/AMP mixed with (a) 0.5% Triton X-100, (b) 10 mM EDTA, (c) 10 mM inorganic phosphate for 30 min. Scale bars = 100 nm.

4.3.7 Probing porosity of the Gd^{3+}/AMP shell using Triton X-100 and ZnO NPs

After coating the Gd^{3+}/AMP shell on DOPS liposomes, we were interested in whether the shell can increase the stability of the sealed liposomes. First, we tested the stability against Triton X-100, a surfactant commonly used to induce the leakage of liposomes. We added different concentrations of Triton X-100 to the free calcein-loaded DOPS liposomes and also to DOPS@Gd^{3+}/AMP. Leakage of the free liposomes increased with the increase of the Triton X-100 concentration (Figure 4.11a). For

DOPS@Gd^{3+}/AMP, we had to add EDTA to chelate Gd^{3+} before analysis of leakage because Gd^{3+} can quench calcein fluorescence. When 0.05% Triton X-100 was added, the fluorescence only recovered to the background level of DOPS after adding EDTA (Figure 4.11b). However, more Triton X-100 also induced higher leakage and the fraction of leakage was similar to that of the free DOPS liposomes (Figure 4.11c). Our control experiment indicated that Triton X-100 did not disrupt the Gd^{3+}/AMP shell (Figure 4.10a). Overall, the Gd^{3+}/AMP shell did not prevent liposome leakage induced by Triton X-100. This might be attributable to the small size of Triton X-100, which can diffuse through the Gd^{3+}/AMP layer, suggesting that the shell was porous.

To test this hypothesis, we then used a larger material to induce leakage. It was reported that ZnO NPs can leak liposomes,[49] likely due to its cationic surface.[65] As expected, ZnO NPs with a size of 20 nm induced ca. 85% leakage of the free DOPS liposomes (Figure 4.11d and e).[149] When ZnO was added to DOPS@Gd^{3+}/AMP, after adding EDTA, fluorescence only recovered to slightly higher than the background level (Figure 4.11d, ~12% leakage, note in this case, no Triton X-100 was added). These results indicate that the Gd^{3+}/AMP shell could protect the liposomes from ZnO NPs, likely due to its large size. The effect of the pore size and the size of the leaking agents is depicted in Figure 4.11f. In this experiment, we compared Triton X-100 and ZnO for their liposome leakage, while EDTA was added only to free the released calcein from Gd^{3+} so that the amount of released calcein can be quantified.

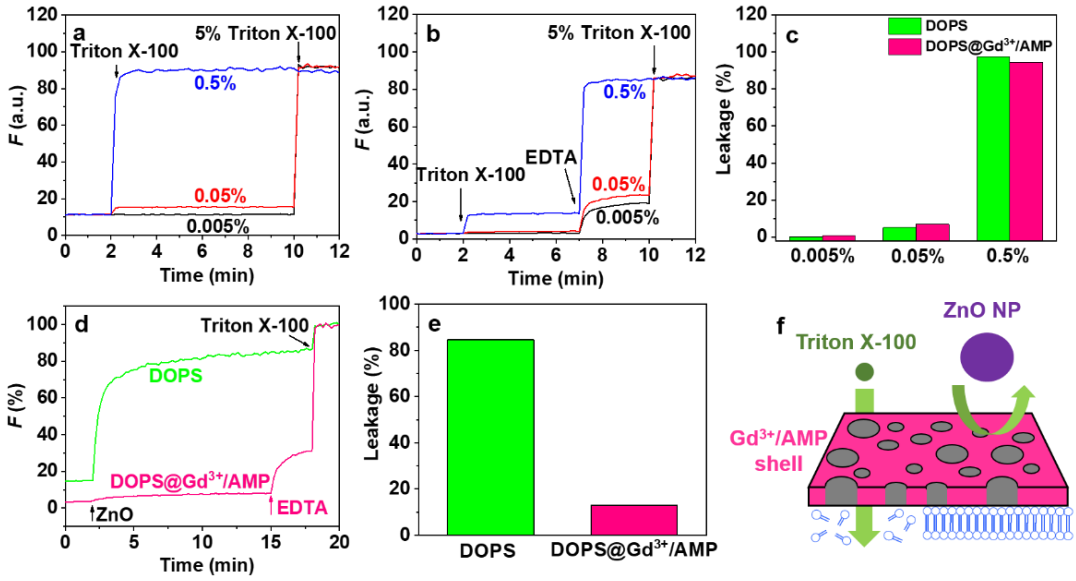

Figure 4.11 Leakage tests of calcein-loaded (a) DOPS liposomes and (b) DOPS@Gd^{3+}/AMP in the presence of different concentrations of Triton X-100. (c) Fraction of leakage with different Triton X-100 concentrations. (d) Leakage tests of calcein-loaded DOPS liposomes and DOPS@Gd^{3+}/AMP after adding 10 μL of 1 mg mL^{-1} ZnO NPs. (e) Fraction of leakage of calcein-loaded DOPS liposomes and DOPS@Gd^{3+}/AMP induced by ZnO NPs. (f) Schematic illustration of Triton X-100 could penetrate through the porous Gd^{3+}/AMP coating, but larger ZnO NPs cannot.

4.4 Summary

In summary, we studied the binding of Gd^{3+} by the DOPS and DOCP liposomes using TEM, ζ-potential measurements, and calcein leakage assays. TEM showed the adsorption of Gd^{3+} on DOPS and DOCP liposomes, but they did not cause a significant fusion of the liposome to form much larger vesicles. Gd^{3+} binding reversed the surface charge of both liposomes, and such charge reversal was not observed with Zn^{2+} or Ca^{2+}. Gd^{3+} induced leakage of the DOCP liposomes but not DOPS liposomes. Taking advantage of this, AMP was added to form a Gd^{3+}/AMP shell on DOPS liposomes, and the content inside the liposomes was retained during this process. The shell increased the stability of the

DOPS liposome against ZnO NPs, although similar leakage was observed in the presence of Triton X-100. This was attributed to the porous nature of the Gd^{3+}/AMP shell. This work demonstrates a simple method to form a porous shell on liposomes, and also reveals interesting surface metal binding interactions on liposomes.

Chapter 5 Adsorption of Nanoceria by Phosphocholine Liposomes

The results presented in this chapter have been published as:

Yibo Liu and Juewen Liu, Adsorption of Nanoceria by Phosphocholine Liposomes, *Langmuir*, **2016**, 32, 13276-13283.

5.1 Introduction

The previous chapter studied liposome binding of free lanthanide ions and the subsequent growth of its nucleotide coordination materials. This chapter further studied liposome interactions with lanthanide containing metal oxide NPs. CeO_2 NP or nanoceria is an important material used as catalysts, gas sensors, UV filters, and solid oxide fuel cells.[197] Its unique properties are attributed to the surface Ce^{3+} ions, providing a redox couple with Ce^{4+}.[198,199] The Ce^{3+} sites are accompanied by oxygen vacancies near the surface. Therefore, small CeO_2 NPs of several nanometers possess enhanced activities because of a large surface-to-volume ratio.[200-202]

With high biocompatibility, nanoceria is also an attractive material for various biological applications.[198,200] For example, it was reported that nanoceria can scavenge ROS in living systems with superoxide dismutase and catalase-like activities.[198,203-205] In a few cases, nanoceria protected cells from oxidative stress induced by ROS or radiation.[206-210] It was also reported that nanoceria protects normal cells but not cancer cells.[211] On the other hand, CeO_2 nanorods with a high aspect ratio had proinflammatory effects.[212] In vivo studies revealed that nanoceria fights against inflammation, ischemic stroke, and radiation-induced damages.[207,213] With so many biological applications, however, only a few studies have touched upon its interaction with biological molecules,[214] especially biomembranes.[206,212]

To enter cells, nanoceria has to first cross the cell membrane. Therefore, it is important to study its interaction with membranes.[31,76,215] Lipids are the main component on the cell membrane. The outer membrane of eukaryotic cells is rich in PC lipids. The interactions of PC membranes with various nanomaterials have been studied,[31,32,151,152] in particular, with various oxides.[47,107,111,160] A primary

example is the spontaneous fusion of PC liposomes onto silica forming SLBs driven by van der Waals force.[101,104,169] By contrast, PC liposomes adsorb onto TiO_2 NP via a stronger force, likely bonding with the lipid phosphate group.[47,84,107,109,111] Most of the metal oxide NPs studied so far have a size of several tens of nanometers or larger. Compared to metal oxide NPs, an interesting feature of nanoceria is its small size, which may exert a different behavior. For example, very small silica NPs behave completely different when mixed with PC liposomes compared with the larger NPs.[216] Although larger nanoceria can also be made, small particles (below 10 nm) are required for catalytic activity and biomedical relevance.[200-202] In this work, we explore the interaction between nanoceria of ~ 5 nm and PC liposomes in terms of adsorption, stability, and membrane integrity.

5.2 Materials and Methods

5.2.1 Chemicals

All phospholipids were purchased from Avanti Polar Lipids (Alabaster, AL). CeO_2 dispersion (catalog number: 289744, 20% dispersed in 2.5% acetic acid), disodium calcein, and Triton X-100 were purchased from Sigma Aldrich. HEPES, sodium acetate, phosphate, and sodium chloride were purchased from Mandel Scientific (Guelph, ON, Canada). Milli-Q water was used to prepare all buffers and suspensions.

5.2.2 ζ-potential and DLS measurements

The ζ-potential of CeO_2 NPs (100 μg mL^{-1}) was measured at various pH values in water using a Malvern Zetasizer Nano ZS90 instrument with a He-Ne laser (633 nm) at 90° collecting optics. HCl and NaOH were used to adjust the pH. The size was measured with CeO_2 (1 mg mL^{-1} in 25 mM acetate buffer, pH 4) and with DOPC liposomes (100 μg mL^{-1} in 25 mM HEPES buffer, pH 7.6).

5.2.3 Liposome adsorption studied using fluorescence quenching

A CeO_2 suspension was gradually titrated into the Rh-liposome (50 μg mL^{-1}, 1 mL) in a buffer (25 mM acetate, pH 4, or 25 mM acetate with 150 mM NaCl, pH 4, or 25 mM HEPES, pH 7.6). CeO_2

stock solutions (1 or 10 mg mL^{-1}) were used for this titration. The fluorescence spectra were recorded using a Varian Eclipse fluorometer (Ex: 560 nm; Em: 592 nm).

5.2.4 Phosphate inhibition studies

CeO_2 NPs (10 mg mL^{-1}) were first incubated in a phosphate buffer (100 mM) for 30 min to cap the surface with phosphate. Then, 5 or 10 µL of the above mixture was added to the Rh-labeled liposomes (25 µg mL^{-1}, 1 mL), and the fluorescence was measured. To study the displacement, CeO_2 NPs were added to 1 mL of the Rh-labeled liposome (25 µg mL^{-1}). Then, 20 µL of the phosphate buffer (500 mM, pH 7.6 or 4) was added, and the fluorescence was measured.

5.2.5 Complex stability tests

To the Rh-labeled liposome (50 µg mL^{-1}, 200 µL) in a buffer (25 mM acetate, pH 4 or 25 mM HEPES, pH 7.6), a small amount of CeO_2 was added to reach a final concentration of 1, 2, 5, 10, 25, 50, 100, or 200 µg mL^{-1}. After 30 min incubation, the mixture was centrifuged at 10,000 rpm for 10 min to collect the supernatant. The supernatant was diluted 10 times, and its fluorescence was measured. To redisperse the DOPC/CeO_2, the complex was prepared in HEPES buffer (25 mM, pH 7.6) as above and centrifuged at 10,000 rpm for 10 min. The pellets were collected and redispersed in 200 µL of acetate buffer (50 mM, pH 4). After sonication, the suspension was again centrifuged, and the supernatant was collected and diluted 10 times for fluorescence measurement. In another case, the complexes were prepared in acetate buffer (25 mM, pH 4). After 30 min incubation, 150 mM NaCl was added to destabilize the DOPC/CeO_2 complexes. After centrifugation at 10,000 rpm for 10 min, the pellets were collected and redispersed in 200 µL of HEPES (50 mM, pH 7.6) by sonication. These samples were again centrifuged at 10,000 rpm for 10 min, and the supernatant was collected and diluted 10 times for fluorescence measurement.

5.2.6 Liposome leakage tests

To monitor the CeO_2 NP-induced liposome leakage, 3 μL of the above purified calcein-loaded liposomes were added to 597 μL of HEPES buffer (25 mM, pH 7.6) in a quartz cuvette at room temperature. The background fluorescence was monitored for 5 min before adding various amounts of CeO_2 NPs (e.g., 10 or 20 μL of 1 mg mL^{-1} CeO_2 or 5 μL of 10 mg mL^{-1} CeO_2). The fluorescence was monitored for another 20 min followed by adding 20 μL of phosphate buffer (500 mM, pH 7.6). At 25 min, 10 μL of 5% Triton X-100 was added. Calcein was excited at 485 nm, and the emission was monitored at 525 nm.

5.2.7 TEM and cryo-TEM

TEM measurements were recorded on a Philips CM10 transmission electron microscope. CeO_2 solution (10 μL) was spotted on a 230 mesh holey carbon copper grid, and the extra solution on the grid was removed using a filter paper. The sample was dried in air before measurement. Cryo-TEM samples were prepared by mixing the DOPC liposomes (50 μg mL^{-1}) and CeO_2 (50 μg mL^{-1}) in acetate buffer (25 mM, pH 4). The sample (5 μL) was spotted on a plasma-treated carbon-coated copper TEM grid. The grid was blotted with two pieces of filter paper for 2 s and quickly plunged into liquid ethane. The sample was then loaded to a liquid N_2-cooled cold stage, imaged using a 200 kV field emission transmission electron microscope (FEI Tecnai G2 F20), at -175 °C.

5.2.8 Differential scanning calorimetry (DSC)

To measure the T_c, DPPC liposomes (100 μg mL^{-1}) and DPPC/CeO_2 (mass ratio of 1:1 and 1:5) were used. The samples were degassed before injection into the DSC sample cell, whereas the reference cell was filled with the corresponding buffer. Each sample was scanned from 25 to 65 °C at the rate of 1 °C min^{-1} using a VP-DSC instrument (MicroCal). Six scans were carried out for each sample, and the fifth scan was plotted.

5.3 Results and Discussion

5.3.1 Characterization of nanoceria and liposomes

DLS characterization based on scattering intensity shows that our CeO_2 NPs have an average hydrodynamic size of 20 nm, whereas the number-based size distribution is centered at ca. 5 nm (Figure 5.1a). It is known that light scattering strongly favors larger particles, and our data suggest that this nanoceria sample is slightly aggregated. Although many previous works prepared nanoceria capped by various ligands and polymers to facilitate dispersion,[210,217,218] we are interested in understanding the native surface property. As a result, our nanoceria did not have a strong capping ligand, explaining the moderate aggregation. A TEM micrograph shows that the size of the individual nanoceria is below 5 nm and some aggregates can also be observed (Figure 5.1a, inset), which is consistent with the DLS data. Its crystallinity was confirmed using high-resolution TEM (HRTEM) (Figure 5.1b). Such small particles were used to ensure a high catalytic activity.[200-202]

Next, we studied the surface charge of nanoceria with a careful pH titration. At pH lower than 7, nanoceria is positively charged, whereas the surface becomes negative at a higher pH (Figure 5.1c). Therefore, at physiological pH, nanoceria is nearly charge neutral, which may affect its colloidal stability because of the lack of charge stabilization.

The structure of a DOPC lipid is shown in Figure 5.1d. Its headgroup contains a negatively-charged phosphate and a positively-charged choline. Therefore, this zwitterionic PC lipid is overall charge neutral, which is confirmed by the ζ-potential measurement (Figure 5.1e). The neutral charge avoids the electrostatic interactions with nanoceria. On the basis of our previous studies, the lipid phosphate group is likely to be important for the interaction with nanoceria.[47,49,111,160] Our liposomes were prepared using the standard extrusion method through 100 nm pores, which is consistent with the DLS measurement of ca. 120 nm (Figure 5.1f).

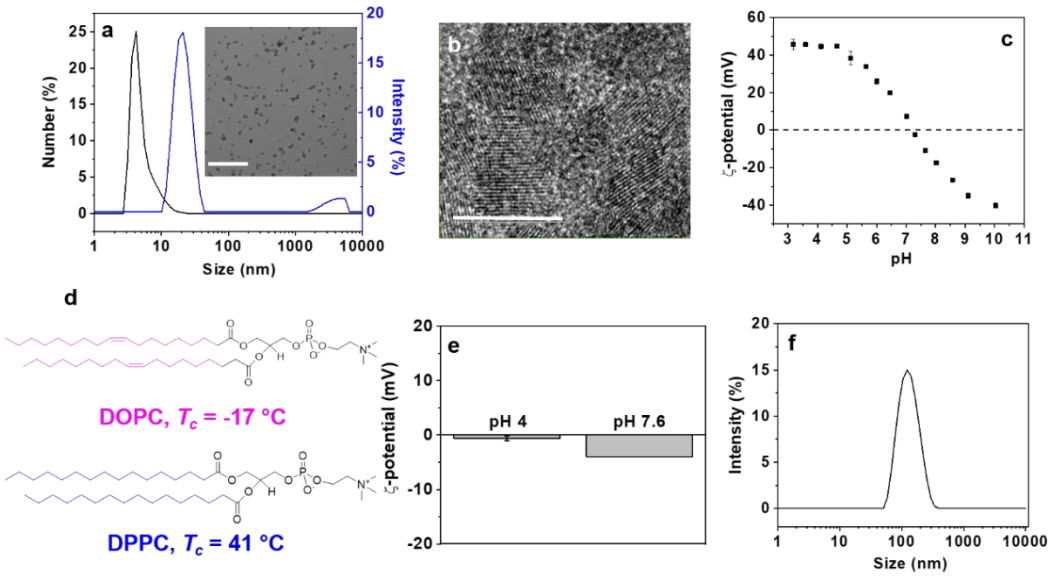

Figure 5.1 (a) DLS size distributions of the CeO_2 NPs dispersed in 25 mM acetate (pH 4) with both number- and scattering intensity-based distributions. Inset: TEM micrograph of the sample (scale bar: 100 nm). (b) HRTEM micrograph of the CeO_2 NPs showing their crystalline structure (scale bar: 10 nm). (c) ζ-potential of the CeO_2 NPs as a function of pH. (d) Structures of DOPC and DPPC lipids and their phase transition temperature (T_c) values are labeled. (e) ζ-potential of the DOPC liposomes in 25 mM acetate (pH 4) and HEPES (pH 7.6) buffers. (f) DLS size distribution of the DOPC liposomes in 25 mM HEPES (pH 7.6).

5.3.2 Nanoceria adsorbed by DOPC liposomes

To study the interaction, we first measured nanoceria adsorption using the DOPC liposomes containing 1% Rh label. To this liposome sample, we gradually titrated CeO_2 NPs at pH 4 and 7.6. We chose these two pH values because the catalytic activity of CeO_2 is the highest at pH 4,[219] whereas pH 7.6 is the physiological condition.

The fluorescence spectra of the Rh-labeled DOPC liposomes at different nanoceria concentrations are shown in Figure 5.2a, and an overall trend of fluorescence decrease is observed. We

measured the ultraviolet-visible (UV-Vis) spectra of our nanoceria and its mixture with the DOPC liposome at pH 4 (Figure 5.2c), where no light scattering feature was observed. In addition, no light absorption was observed beyond 400 nm. Therefore, the drop in fluorescence cannot be explained by the light-scattering or inner-filter effect. Nanoceria is a strong quencher for many adsorbed fluorophores.[220] Without light scattering, we attribute the fluorescence drop here to the adsorption of nanoceria by the liposome, directly quenching the associated Rh fluorophore.

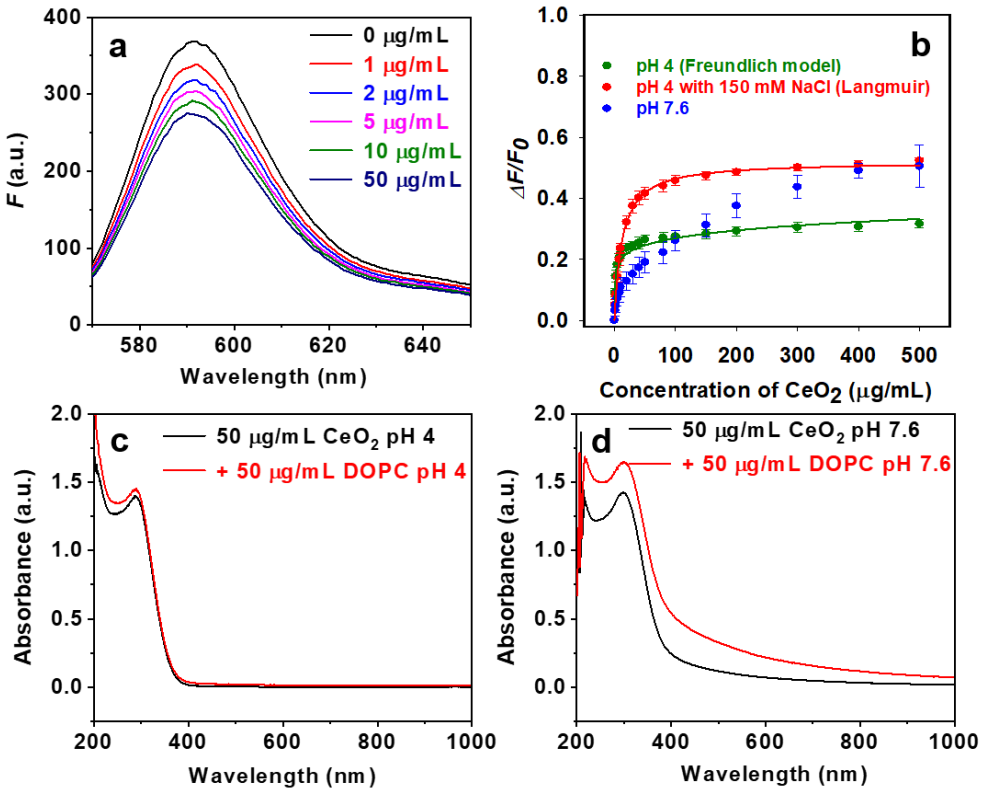

Figure 5.2 (a) Fluorescence spectra of the Rh-labeled DOPC liposomes at different CeO_2 concentrations dispersed in 25 mM acetate, pH 4. (b) Adsorption isotherms of CeO_2 NPs onto 50 μg mL^{-1} Rh-labeled DOPC liposomes at pH 4 without NaCl (green), with 150 mM NaCl (red), and at pH 7.6 without NaCl (blue). UV-Vis spectra of CeO_2 and CeO_2/DOPC complexes at (c) pH 4 and (d) pH 7.6. There is no scattering and absorption observed beyond 400 nm at pH 4, while at pH 7.6 scattering was observed.

The amount of quenching was quantified by plotting the relative fluorescence change ($\Delta F/F_0$) at each CeO_2 concentration. At pH 4, the fluorescence initially dropped quickly. With higher than 20 μg mL^{-1} of CeO_2, however, further quenching was slightly observed (Figure 5.2b, green trace). Even with 500 μg mL^{-1} CeO_2, quenching only reached ca. 30%. Therefore, the surface of the DOPC liposomes was not fully occupied by CeO_2 at pH 4. CeO_2 NPs are positively charged at pH 4 (Figure 5.1c). The initially adsorbed CeO_2 may electrostatically repel the further incoming NPs. To confirm this hypothesis, we then repeated the measurement in the presence of 150 mM NaCl to screen charge interactions (no NaCl was included in the previous experiment). In this case, we indeed observed stronger quenching reaching 50% (Figure 5.2b, red trace). This indicates that more CeO_2 NPs were adsorbed by screening the charge repulsion. The incomplete quenching can be explained by the fact that only around 50% of the Rh-labels were on the outer leaflet of the bilayer, whereas the labels on the inner leaflet were not quenched by CeO_2. This also suggests that CeO_2, although small, did not penetrate through the bilayer membrane.

The pH 4 plots in Figure 5.2b are essentially adsorption isotherms. For quantitative analysis, we fitted the data. At pH 4 without NaCl, a simple Langmuir isotherm failed to account for the data. The cationic CeO_2 NPs repel each other at pH 4, which conflicts with a basic assumption of the Langmuir isotherm that adsorbed molecules do not interact. Thus, we fitted the data with the Freundlich isotherm (Figure 5.2b, green trace), which takes into consideration the lateral repulsion. On the other hand, adsorption at pH 4 with 150 mM NaCl was nicely fitted using the Langmuir isotherm model because lateral electrostatic interactions were screened. Based on this fitting, a dissociation constant (K_d) of 12.4 μg mL^{-1} CeO_2 and a final quenching of 52% at full surface coverage are obtained.

On the other hand, at pH 7.6, the initial stage of quenching was milder, but the final quenching reached > 50% (Figure 5.2b, blue trace). UV-vis spectra of both CeO_2 and its mixture with the DOPC liposomes showed a quite obvious light-scattering effect because of the aggregation of the involved particles (Figure 5.2d). As such, not all of the decreased fluorescence is attributable to direct fluorescence quenching because light scattering can also contribute. Forming large aggregates is quite

common in liposome/NP systems.[19,117,221] This complication makes it difficult for quantitative data fitting, and the higher fluorescence drop beyond 50% at high CeO_2 concentrations might be a pure result of light scattering because the surface might have already been saturated. It is interesting to note that at pH 7.6, an initial high quenching efficiency was observed. At low CeO_2 concentrations, the light scattering effect is small, and this initial quenching is then supportive of the CeO_2 adsorption. No fitting of this data set was performed because of the light scattering effect.

5.3.3 Lipid phosphate-based adsorption

Because cerium is a hard metal that has a strong affinity to phosphate,[220,222,223] we propose that the phosphate group in the lipid might be playing a critical role. To test this, we added free inorganic phosphate ions to the CeO_2 NPs before mixing them with DOPC (Figure 5.3a). In this case, free phosphate inhibited the nanoceria adsorption at both pH 4 and 7.6. This supports the affinity between nanoceria and phosphate. To further test this mechanism, we mixed DOPC and CeO_2 first, followed by adding phosphate to see if phosphate can displace CeO_2 (Figure 5.3b). Fluorescence was recovered at both pH values, indicating that the displacement reaction indeed occurred, also supporting the interaction of CeO_2 with the phosphate group in the PC lipid.

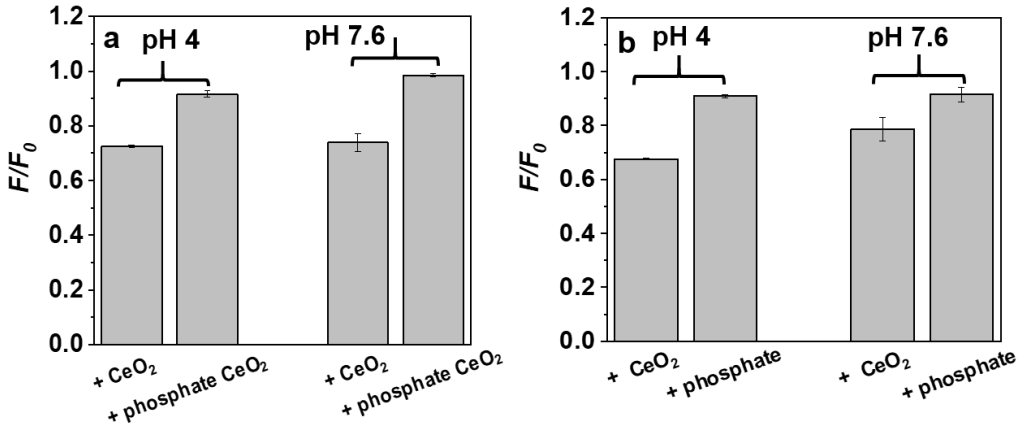

Figure 5.3 (a) Phosphate inhibited the CeO_2 adsorption on the Rh-labeled DOPC liposomes (25 μg mL^{-1}) at pH 4 and 7.6. (b) Phosphate (10 mM) induced the CeO_2 desorption at pH 4 and 7.6.

5.3.4 Aggregation and restabilization of the adsorption complex

After confirming the adsorption of nanoceria by the liposomes, we next studied further aggregation of this system. Because nanoceria may bridge a few liposomes, the system might grow into large aggregates. In this experiment, the Rh-labeled liposomes were incubated with various concentrations of CeO_2. Then, the mixture was centrifuged at 10,000 rpm for 10 min, and the supernatant fluorescence intensity was measured. Free liposomes could not be precipitated under this condition, allowing us to distinguish between well-dispersed liposomes and extensively aggregated structures. At pH 4, the supernatant fluorescence gradually decreased with increasing CeO_2 (Figure 5.4a, pink bars). The lowest fluorescence was achieved at a CeO_2 NP concentration of 10 μg mL^{-1}. Under this condition, the precipitated liposome reached the maximal value. As the concentration of the CeO_2 NPs was further increased, fluorescence started to increase again in the supernatant, suggesting liposome restabilization by the CeO_2 NPs. This may be because at a CeO_2 concentration lower than 10 μg mL^{-1}, the NPs could bridge the liposomes to form aggregates with decreased stability. With more CeO_2 added, the bridging phenomenon was disrupted and the whole liposome surface became positively charged due to the adsorption of the CeO_2 NPs. Both contribute to the restabilization. At pH 7.6, however, no such restabilization was observed (Figure 5.4a, blue bars) because CeO_2 NPs are charge neutral at this pH, and there is no driving force for the bridges to be disrupted.

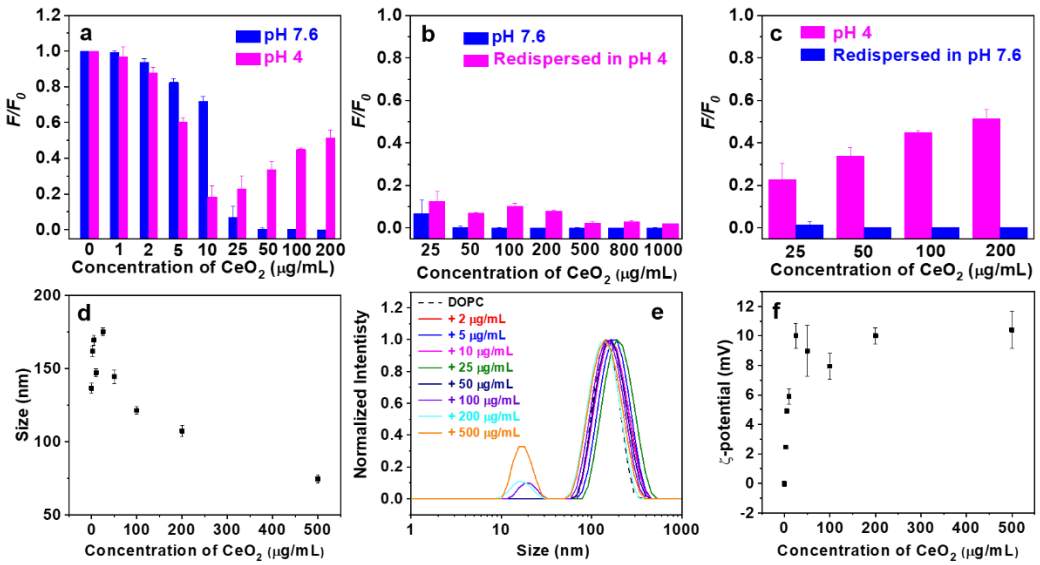

Figure 5.4 (a) Fluorescence of the supernatant after mixing CeO_2 and Rh-DOPC at pH 4 and 7.6 and centrifugation. A finally increased fluorescence at pH 4 suggests restabilization of this system. (b) Complex prepared at pH 7.6 and redispersed at pH 4 failed to show restabilization. (c) Complex prepared at pH 4 and redispersed at pH 7.6. (d) Averaged hydrodynamic size of DOPC/CeO_2 complexes as a function of the CeO_2 concentration at pH 4. (e) DLS size distributions of DOPC/CeO_2 complexes with different CeO_2 amounts at pH 4. (f) ζ-potential of DOPC/CeO_2 complexes as a function of the CeO_2 concentration at pH 4.

We also quantitatively measured the size and the ζ-potential change when adding various amounts of nanoceria to the DOPC liposomes at pH 4 (Figure 5.4d-f). The size initially increased with the CeO_2 concentration up to 25 μg mL^{-1}, whereas further increase in CeO_2 made the size smaller (Figure 5.4d). It is interesting to note that the largest size was still below 200 nm, suggesting that this system did not aggregate extensively at pH 4. With more than 100 μg mL^{-1} CeO_2, another peak just above 10 nm was observed, attributable to the free CeO_2 NPs (Figure 5.4e). The ζ-potential gradually increases with increasing CeO_2 concentration and reaches a plateau at 25 μg mL^{-1} (Figure 5.4f). This

suggests that beyond this point, all measured surfaces were CeO_2, either as free NPs or adsorbed on the liposome.

In addition, when CeO_2 and DOPC were first mixed at pH 7.6 and then redispersed at pH 4, significantly less supernatant fluorescence was observed compared with those prepared at pH 4 directly (Figure 5.4b). This suggests that the majority of complexes formed at pH 7.6 was stably crosslinked by the CeO_2 NPs. In comparison, when the CeO_2/DOPC complexes were prepared at pH 4 and redispersed at pH 7.6, no fluorescence was observed in the supernatant (Figure 5.4c). This indicates that the complexes were readily aggregated at pH 7.6, attributable to the lack of charge in the CeO_2 NPs at this pH.

On the basis of the above understanding, we proposed an interaction model. At pH 4, both the DOPC liposome and CeO_2 NPs are well-dispersed in solution. At low CeO_2 concentrations, CeO_2 NPs moderately crosslink the liposomes, resulting in small aggregates (< 200 nm) that can be precipitated by centrifugation. With further increase in the CeO_2 NPs, each liposome surface is densely covered by CeO_2, and the crosslinking is disrupted, leading to restabilization (Figure 5.5a). At pH 7.6, CeO_2 aggregation occurred even in the absence of DOPC. Upon mixing, immediate crosslinking is formed by the aggregated CeO_2 NPs, and they remained as aggregates even after adjusting the pH to 4 (Figure 5.5b).

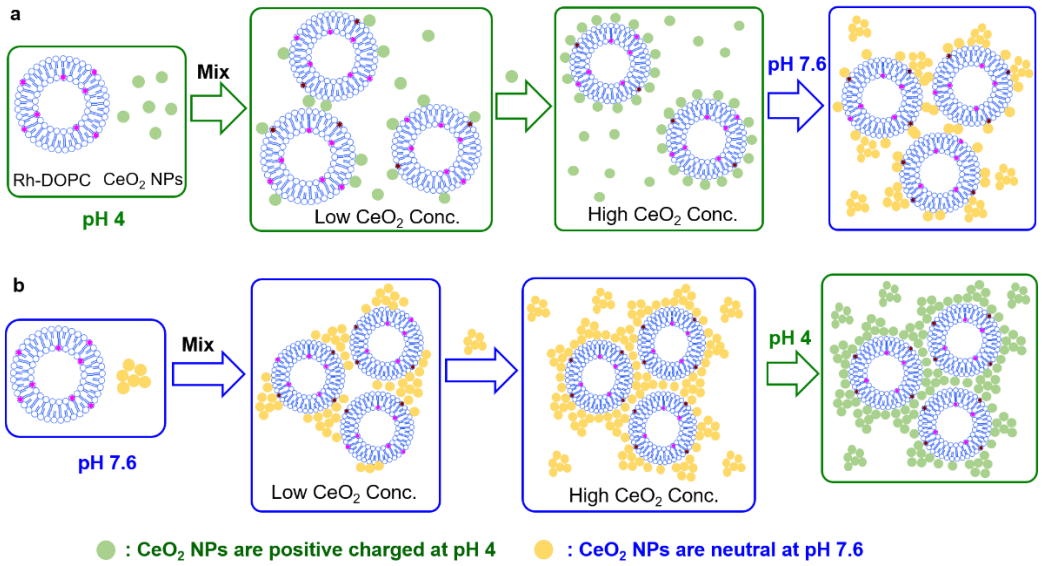

Figure 5.5 Schematic illustration of the adsorption of DOPC and CeO_2 at (a) pH 4 and (b) pH 7.6. At pH 4, there is a redispersion of the system by adding more CeO_2 NPs because of charge repulsion. At pH 7.6, CeO_2 NPs are nearly charge neutral and are readily aggregated. The aggregates can further bridge the liposomes to form even larger aggregates.

5.3.5 Nanoceria induces liposome leakage

A key question regarding the NP/membrane interaction is membrane integrity, which can be probed by a leakage assay. In this work, 100 mM calcein was encapsulated in each DOPC liposome, and most of the free calcein molecules outside of the liposome were removed. With such a high calcein concentration, its fluorescence is self-quenched. If the lipid membrane is disrupted, calcein is released into the whole solution, yielding fluorescence enhancement. After mixing the calcein-loaded liposomes with nanoceria, we observed an immediate fluorescence quenching, suggesting that nanoceria adsorbed the free calcein molecules outside of the liposome (note that some free calcein still exists in our system). Adding Triton X-100 to fully rupture the membrane, however, still failed to induce the fluorescence enhancement and further quenching was observed (Figure 5.6a), which is also attributable to the calcein adsorption by nanoceria. To confirm this, we added nanoceria to a free calcein solution, and indeed, we

observed efficient fluorescence quenching (Figure 5.6b). Therefore, direct monitoring of fluorescence cannot be used here.

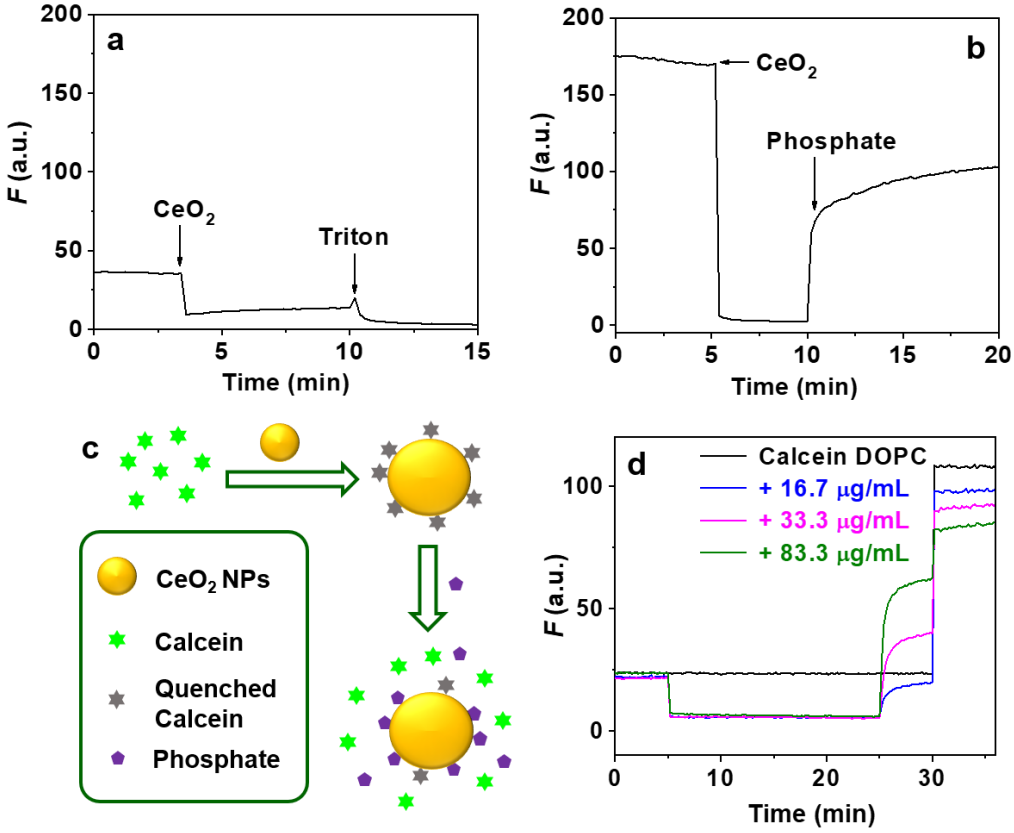

Figure 5.6 (a) Calcein-loaded DOPC leakage test by adding CeO_2 NPs. Triton X-100 was added to fully disrupt the liposomes. The quenching of fluorescence is due to the calcein adsorption by CeO_2. (b) Phosphate displacement of free calcein adsorbed on CeO_2 NPs. (c) Schematic illustration of calcein fluorescence recovery by adding phosphate. (d) Leakage tests of the calcein-loaded DOPC liposomes by adding CeO_2 at 5 min. At 25 min, phosphate was added, and at 30 min, Triton X-100 was added.

From our above studies, we know that nanoceria has a strong affinity to phosphate. We reason that phosphate might displace calcein from the nanoceria surface, as schematically shown in Figure 5.6c. To confirm this, we added phosphate to the above control sample and indeed observed a

fluorescence increase (Figure 5.6b). With this in mind, we next added various concentrations of nanoceria to the calcein-loaded DOPC liposomes at 5 min (Figure 5.6d). All of the samples showed fluorescence quenching to the background level. At 25 min, we added phosphate and observed a strong fluorescence enhancement. With more CeO_2 added, higher fluorescence was observed after the phosphate addition, and the recovered level was higher than the original level (e.g., fluorescence before 5 min). This indicates that the liposome leaked upon addition of CeO_2 and the leaking process is CeO_2 concentration-dependent. Further addition of Triton-X100 fully ruptured the liposomes and released all of the encapsulated calcein.

5.3.6 Cryo-TEM characterization

This is the first time we observed DOPC liposome leakage when mixed with a nonsilica and a noncationic oxide.[49] At pH 7.6, CeO_2 is near charge neutral (slightly negatively charged), and thus the leakage is unlikely due to membrane damage by cationic nanomaterials.[49,65] From the surface chemistry standpoint, CeO_2 is more similar to TiO_2 in terms of containing a hard Lewis acid metal favoring a strong phosphate interaction, which is demonstrated in this work. Therefore, we want to understand whether this is due to fully ruptured liposomes or local membrane damages. For this purpose, TEM was used. Using the normal TEM, we observed that the distribution of CeO_2 (Figure 5.7a) is quite different from that in the absence and presence of liposomes (inset of Figure 5.1a). Although we can see the CeO_2 NPs distributed around a liposome-shaped contour, we cannot resolve the liposomes. Using cryo-TEM, we indeed observed CeO_2 adsorption, and the liposome structure was still largely maintained, although deformation of liposomes from a perfect spherical structure was also observed (Figure 5.7b).

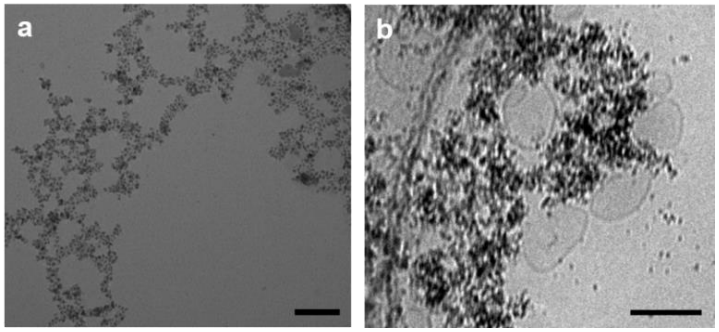

Figure 5.7 TEM image (a) and cryo-TEM (b) of the DOPC liposomes mixed with the CeO_2 NPs (scale bars = 100 nm).

As such, the leakage must be due to the local interaction between CeO_2 and the liposomes. As a further control, we tested the calcein-loaded DPPC liposomes, and CeO_2 NPs failed to leak them (Figure 5.8a). DPPC and DOPC have the same headgroup chemistry, and the only difference is that DPPC is in the gel phase at room temperature with a T_c of 41 °C. On the other hand, DOPC has a T_c of -17 °C and is fluid at room temperature. Therefore, the leakage of DOPC liposomes is likely to relate to the T_c.

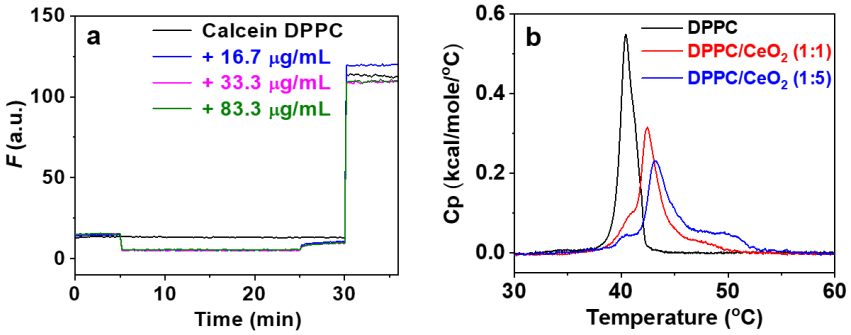

Figure 5.8 (a) Calcein leakage tests of the DPPC liposomes with CeO_2 added at 5 min, phosphate added at 25 min, and Triton X-100 added at 30 min. The buffer was 25 mM HEPES (pH 7.6). The final fluorescence after adding phosphate was lower than the initial fluorescence regardless of the CeO_2 concentration, suggesting that no leakage occurred. (b) DSC traces of the DPPC liposomes as a function of the CeO_2 concentration. The ratio refers to the mass concentration of DPPC and CeO_2.

One possibility is that the adsorption is very strong, and it can increase the T_c of the lipid at the spot of adsorption.[32] We observed such a phenomenon with AuNPs.[116,117] In that case, we attributed it to the strong van der Waals force between gold and liposomes. Here, the CeO_2 NPs were brought very close to the liposome surface by the lipid phosphate interaction. If this hypothesis is true, CeO_2 NPs should increase the T_c of the liposomes. Therefore, we used DSC to measure the DPPC liposomes (Figure 5.8b). Free DPPC has a T_c of 41 °C as expected. After adding a 1:1 mass ratio of CeO_2 NPs, its T_c shifted to 42.5 °C. Further increase in the CeO_2 concentration by 5-fold increased the T_c to 43.2 °C with a significant peak broadening. We reason that at the spot of adsorption, the DOPC lipids underwent a fluid-to-gel phase transition, and calcein can leak during this transition period. Once adsorbed, the liposomes become stable again.[32,116,117,173] The DPPC liposome is already in the gel phase, and thus adding nanoceria would not induce the phase transition, and thus no leakage took place.

Although this is a model study performed in a reduced physical system, it still has interesting biological implications. For example, nanoceria alone cannot enter the membrane, and it has to be internalized by cells through active transportation, likely via endocytosis.[206,212] In acidic endosomes and lysosomes, the surface charge of nanoceria changes from neutral to positive, and this is likely to have an influence on its membrane interactions. Nanoceria can strongly bind to the phosphate group in lipids, and this is likely to be true for all phospholipids. Such an interaction can even change T_c and induce a transient membrane leakage.

5.4 Summary

In summary, the interaction between PC liposomes and CeO_2 NPs was systematically studied using a suite of techniques. We are interested in nanoceria because of its antioxidation activity widely tested in many cellular and animal studies in recent years. Two types of liposomes, DOPC and DPPC, were included in this study. They have the same headgroup chemistry but different T_c values. The fluorescence quenching experiments indicated that the CeO_2 NPs are adsorbed by DOPC at both pH 4 and 7.6. The interaction between the phosphate in the lipid headgroup and CeO_2 is mainly responsible

for the adsorption. At pH 4, the CeO_2 NPs are positively charged, whereas at pH 7.6, they are nearly charge neutral. Such electrostatic factors showed a strong influence on the observed adsorption isotherms. When CeO_2 NPs are positively charged, the complexes can be restabilized with a relatively higher amount of CeO_2 NPs. CeO_2 could induce the leakage of DOPC. This is the first time we observed that the DOPC liposome is leaked by a noncationic metal oxide, and the leakage is attributed to the CeO_2 adsorption-induced local fluid-to-gel phase transition. This work provides a fundamental understanding of the interaction between lipid bilayers and CeO_2 NPs at the molecular level, which may offer insights into the CeO_2 interaction with cell membranes.

Chapter 6 Leakage and Rupture of Lipid Membranes by Charged Nanoparticles

The results presented in this chapter have been published as part of:

Yibo Liu and Juewen Liu, Leakage and Rupture of Lipid Membranes by Charged Polymers and Nanoparticles, *Langmuir*, **2020**, 36, 810-818.

6.1 Introduction

After studying the adsorption of CeO_2 NPs with liposomes in the last chapter, we further studied the effects of charge of NPs on liposome membrane integrity. Understanding membrane leakage and disruption by nanomaterials is fundamentally and practically important.[76,224,225] Compromised membrane integrity is often associated with cytotoxicity, whereas controlled leakage is useful for sensing, signal amplification, and controlled release.[111,226-229] Many leakage studies were performed using cell membranes,[230-235] but the complexity of cell surfaces and the need to keep cells viable make it difficult to gain fundamental understanding. In this regard, reduced physical systems based on model membranes are appealing.

Membrane leakage can be induced by amphiphilic molecules that either make pores or dissolve lipids.[236] Their mechanism of action is easy to understand and thus not discussed here. Another type of membrane disruptors are polymers and nanomaterials.[231,237-245] A comprehensive study was performed over a decade ago using PC bilayers supported on freshly cleaved mica. A wide range of cationic peptides, polymers, dendrimers, and inorganic NPs were studied; all disrupted the supported membrane.[65,237-241] Some recent works were carried out using dye-loaded liposomes, also demonstrating cationic NPs inducing more rapid leakage.[243,244] A thermodynamic model was proposed to explain the interaction between charged NPs and membranes; although it did not specify the type of charge on NPs, both cationic and anionic NPs could interact with lipid membranes.[242] Thus it is unclear why cationic materials appeared more effective in leaking membranes.

At the same time, cationic NPs were also reported to stabilize lipid membranes and prevent leakage.[173,246] For example, latex beads induced local gelation of fluid PC membranes and thus decreased leakage.[32] We found that when the interaction is too strong, such as using citrate-capped AuNPs, a transient leakage was observed.[116,117] The interaction strength can be modulated by capping AuNPs to separate the gold core from the liposome surface.[118] Small cationic NPs were reported to stabilize liposomes (even more effective than anionic NPs),[247] which is in direct conflict with the notion of their membrane disruptive effect.

Electrostatic interactions were believed to govern the leakage process,[243,244] although the membranes studied were often made of zwitterionic PC lipids with an overall neutral charge. In principle, they should have a similar interaction with cationic and anionic nanomaterials because electrostatic interactions should be nearly zero. Then, why cationic nanomaterials appeared to be more membrane disruptive? Is there a fundamental difference between cationic and anionic materials for interacting with zwitterionic liposomes? We herein performed a systematic study on this topic. Instead of using different materials to test the effect of charge, we tuned the charge by varying pH. It appears that charge alone is unimportant, and the key is the interaction strength. For supported bilayers, the surface for supporting the bilayers could cause artifacts associated with data interpretation.

6.2 Materials and Methods

6.2.1 Chemicals

All phospholipids were purchased from Avanti Polar Lipids (Alabaster, AL). Disodium calcein, Triton X-100, ZnO NPs (catalog number: 721077), TiO_2 (20 nm, catalog number: 718467, 500 nm, CAS No.: 13463-67-7), Fe_3O_4 (catalog number: 637106), and HEPES were purchased from Sigma-Aldrich. EDTA and sodium chloride were purchased from Mandel Scientific (Guelph, ON, Canada). Milli-Q water was used to prepare all buffers, solutions, and suspensions.

6.2.2 ξ-potential and DLS measurements

The surface charge and hydrodynamic size of the liposomes and metal oxides were measured at a concentration of 100 μg mL^{-1} at different pH (10 mM HEPES, 100 mM NaCl). The data were collected on a Malvern Zetasizer Nano ZS90 with a He-Ne laser (633 nm) at 90° collecting optics.

6.2.3 ZnO surface modification

Surface-capped ZnO NPs were prepared by incubation ZnO (2 mg mL^{-1}) with polyethylenimine (PEI), polyethylene glycol (PEG), imidazole, and phosphate (10 mM for imidazole and phosphate, and 10 mg mL^{-1} for PEI and PEG) overnight. The resulting NPs were washed with Milli-Q water to remove unbound ligands. The surface-capped ZnO was redispersed in Milli-Q water with a concentration of 1 mg mL^{-1}.

6.2.4 Adsorption of metal oxides with Rh-labeled liposomes

To study liposome adsorption, 200 μL metal oxide NPs (200 μg mL^{-1}) with different pH (10 mM HEPES without and with 100 mM NaCl) were mixed with 1 μL Rh-labeled liposome (5 mg mL^{-1}). After incubating for 30 min, the mixtures were centrifuged at 10,000 rpm to precipitate the liposome/metal oxide complexes. The adsorption efficiency of the liposomes was calculated from the decrease of fluorescence intensity in the supernatant. Before the fluorescence measurement, the pH was adjusted to 7.6 by diluting 50 μL of the supernatant in 550 μL of 25 mM HEPES (pH 7.6). The fluorescence spectra were collected on a Varian Eclipse fluorometer with excitation at 560 nm and emission at 592 nm.

6.2.5 Liposome leakage tests

To monitor liposome leakage with metal oxides at pH 7.6, 3 μL of calcein-loaded liposomes were added to 600 μL of the buffer. At 2 min, metal oxide (10 μL, 2 mg mL^{-1}) solution was added. The fluorescence was monitored for another 18 min. At 20 min, 10 μL of 5% Triton X-100 was added to fully rupture the liposomes. To study the leakage caused by metal oxides at different pH, 2 μL of

calcein-loaded liposomes were added to 100 µL of 10 mM HEPES (or with 100 mM NaCl) of different pH. To this solution, 2.5 µL of 2 mg mL^{-1} metal oxide suspension with corresponding pH was added and incubated for 30 min. The fluorescence of the solutions containing the liposomes alone at each pH was used as the background, whereas the fluorescence of the liposomes treated with Triton X-100 at each pH was set for full leakage. As calcein fluorescence is pH sensitive (fully quenched at pH 4 and weakened at pH 11.5), the pH of the samples was adjusted to pH 7.6 before fluorescence measurement by diluting 50 µL of the resulting solution with 550 µL of 25 mM HEPES (pH 7.6). No background leakage was observed when incubated in buffers of different pH. The percentage of leakage was calculated by $F_{Released}/F_{Total} \times 100\%$. Calcein was excited at 485 nm, and the emission was monitored at 525 nm.

6.2.6 Cryo-TEM

Large TiO_2 NPs (500 nm) were used for cryo-TEM, and they were treated with 0.1 M NaOH before use. The liposome/metal oxide complexes were prepared by incubating the liposomes (200 µg mL^{-1} for most samples; 100 µg mL^{-1} for DOPC/ZnO with EDTA) and metal oxides (200 µg mL^{-1}) at different pH overnight. The free liposomes were removed by centrifugation, and the pellets were redispersed in the buffer. Cryo-TEM experiments were carried out by spotting liposome/metal oxide suspension on a carbon-coated copper TEM grid (treated with plasma to ensure that the surface was hydrophilic) in a humidity-controlled chamber. The grid was blotted with two filter papers to remove extra samples and quickly plunged into liquid ethane. The sample was then loaded to a liquid N_2-cooled cold stage. The samples were imaged with a 200 kV field emission TEM (FEI Tecnai G2 F20) at -178 °C.

6.3 Results and Discussion

6.3.1 Liposomes, nanomaterials, and the leakage assay

To systematically understand the interactions between liposomes and charged materials, we studied two types of lipids: DOPC and DOPS (Figure 6.1a), three types of metal oxide NPs, ZnO, TiO_2, and Fe_3O_4. Under physiological conditions, the zwitterionic DOPC is nearly charge neutral and not expected to have strong electrostatic interactions with nanomaterials. A careful ξ-potential measurement, however, showed a small negative charge below pH 9, and the negative charge increased slightly at pH 11.5 (Figure 6.1b). DOPS is a negatively-charged lipid, and its amine and carboxyl groups can chelate metal ions.[40,41,186] By using DOPS, we can study the effect of electrostatic attraction and metal coordination. In addition, we also include DPPC. It has the same headgroup as DOPC, but its saturated tails afford a higher T_c of 41 °C (T_c of DOPC is -17 °C). Thus, DPPC exists in the gel phase at room temperature, whereas DOPC and DOPS are in the fluid phase. All liposomes have a hydrodynamic size of ca. 100 nm (Figures 6.1 c and d).

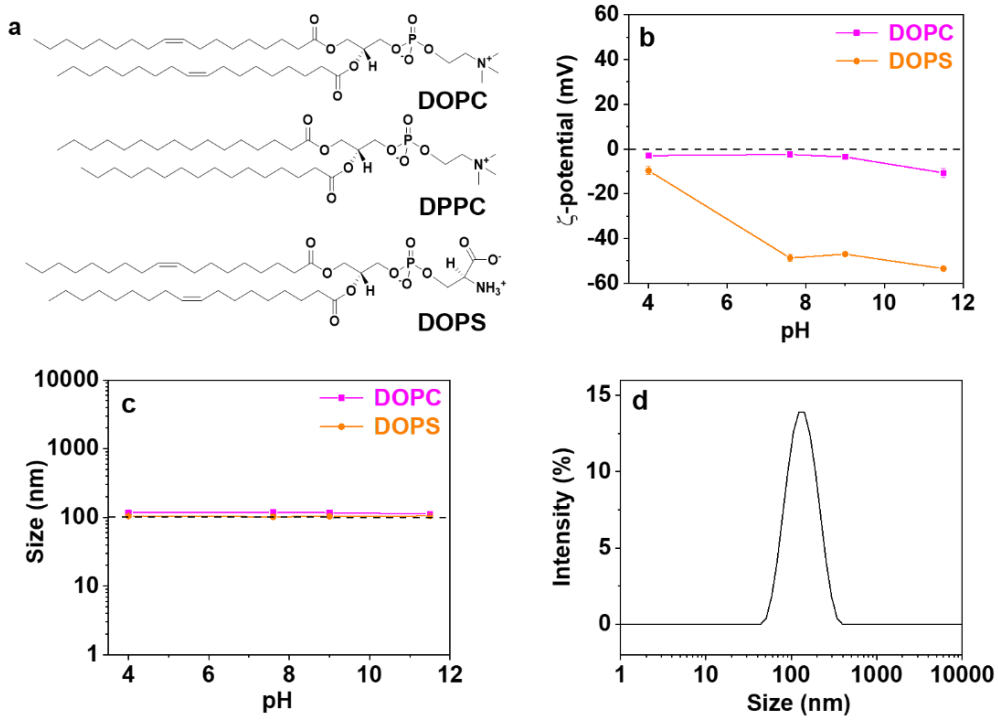

Figure 6.1 (a) Structures of the lipids used in this work. (b) ξ-potential and (c) hydrodynamic size of DOPC and DOPS liposomes at different pH (10 mM HEPES 100 mM NaCl). (d) Hydrodynamic size of DPPC at pH 7.6.

In previous studies, the effect of charge was studied by using different types of nanomaterials. However, aside from charge, different materials could be different in other aspects, such as the strength of van der Waals interactions. Therefore, we studied the effect of charge here by tuning the pH, which can minimize the difference brought by materials composition. For this purpose, we chose a few metal oxides, ZnO, TiO_2, and Fe_3O_4, as their surface charge can be readily tuned by pH. We intentionally used bare metal oxide NPs without strong surface ligands, so that their native surface properties can be directly probed. For some control experiments, ZnO with pre-adsorbed ligands was also used. All metal oxides were well dispersed in solution after a gentle sonication.

In the previous work, three techniques were used for studying membrane disruption. One was based on microscopy such as AFM, TEM, and confocal fluorescence microscopy looking at SLBs.[65,248]

The pores on membranes would have to be relatively large to be observed. Another assay relied on the leakage of enzymes or dyes.[240] Cell-based enzyme leakage assays could suffer from the toxicity of nanomaterials, leading to a loss of cell viability and leakage, which may cause false positive results. Finally, some advanced spectroscopic methods were reported, such as electron paramagnetic resonance, oriented circular dichroism, X-ray diffraction, and solid-state NMR. These techniques require special sample conditions (frozen, dried, or very concentrated liposomes), making the conclusions less relevant to typical solution phase conditions.

To overcome these problems, we used a dye leakage assay by encapsulating 100 mM calcein dye in liposomes resulting in self-quenched fluorescence. If the membrane was disrupted, calcein would release to the whole solution, inducing fluorescence enhancement. The addition of Triton X-100 would fully rupture the liposomes and release all of the calcein, allowing the calculation of the percentage of leakage.[249] For most experiments, we were more concerned on whether leakage occurred or not instead of how much leakage. It needs to be noted though that leakage only reflects membrane perturbation, and it is not necessarily an indication of formation of permanent pores. To test such processes, cryo-TEM was also used in this study.

6.3.2 Modulating metal oxide charge by pH

We studied the leakage of the DOPC liposomes in the presence of metal oxide NPs. Before this experiment, we individually tested the free metal ions in these oxides, and none caused leakage. We did not test titanium ions, since TiO_2 is stable and unlikely release any ions into solution. Therefore, any observed leakage must be due to the NPs instead of the dissolved metal ions. ZnO is positively charged at pH 7.6, whereas Fe_3O_4 and TiO_2 are negatively charged (Figure 6.2a). Only ZnO leaked the DOPC (Figure 6.2b), which seemed to agree with the notion that cationic NPs can leak liposomes. We then varied the pH (4, 9, and 11.5) to tune the surface charge of the metal oxides. TiO_2 and Fe_3O_4 were positively charged at pH 4, but negatively charged at pH 9 and pH 11.5 (Figure 6.2a). For ZnO, it was positively charge at pH 9 but became negative at pH 11.5. We could not test ZnO at pH 4 because of

its dissolution.[149] We failed to see leakage with the negatively-charged metal oxides (Figure 6.3a), and only positively-charged ZnO (pH 9) and TiO_2 (pH 4) leaked DOPC. However, the positively-charged Fe_3O_4 (pH 4) did not leak the liposomes (Figure 6.3a). Sometimes, a negative leakage value was obtained because some metal oxides quenched the background fluorescence. The integrity of DOPC with the presence of Fe_3O_4 at pH 4 was confirmed using cryo-TEM (Figure 6.4). Therefore, cationic NPs do not guarantee leakage, and other factors also need to be considered.

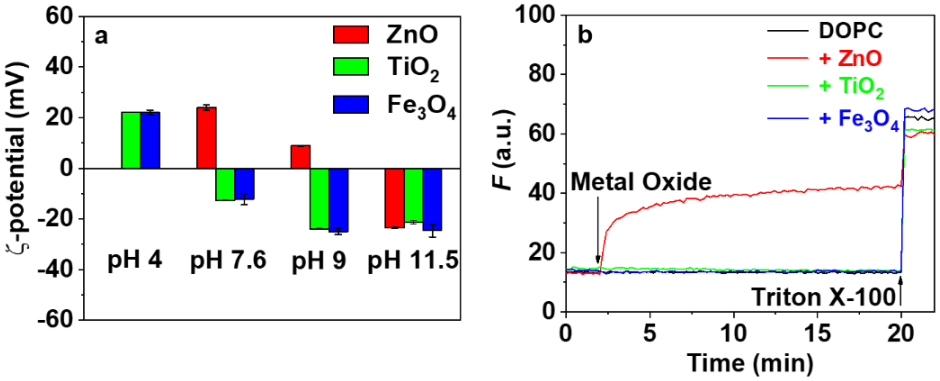

Figure 6.2 (a) ξ-potential of the metal oxides at different pH (10 mM HEPES, 100 mM NaCl). (b) Leakage tests of the DOPC liposomes by metal oxides at pH 7.6 (10 mM HEPES).

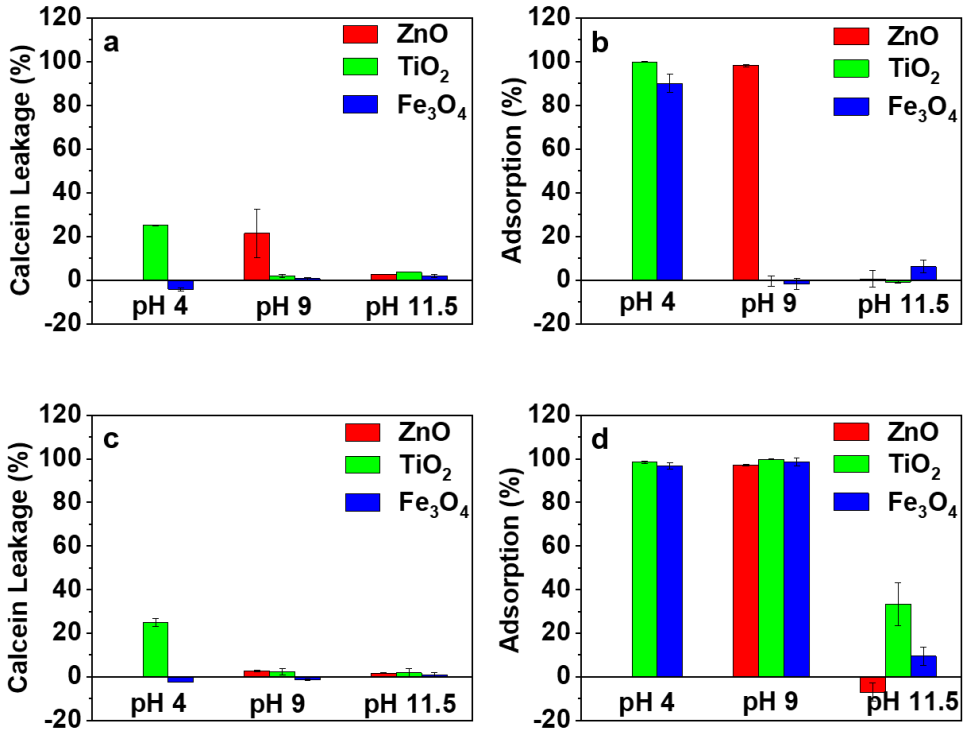

Figure 6.3 Leakage of the DOPC liposomes by metal oxides at different pH (a) without and (c) with 100 mM NaCl. Adsorption of the DOPC liposomes by various metal oxides at different pH (b) without and (d) with 100 mM NaCl.

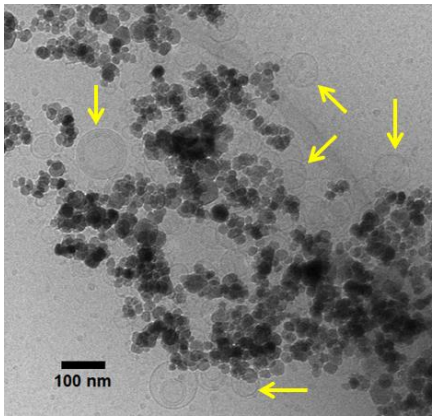

Figure 6.4 Cryo-TEM micrographs of DOPC liposomes mixed with Fe_3O_4 at pH 4.

6.3.3 Adsorption and leakage

In a previous study, we established that the adsorption of metal oxide NPs by PC liposomes was weaker at higher pH.[111] As adsorption is the first step of interaction, it is easy to understand that without adsorption, no leakage occurs. To quantitatively analyze adsorption, we incorporated 1 wt % Rh-PE lipids in our DOPC liposomes and incubated them with each metal oxide. After centrifugation to precipitate the adsorbed liposomes, we measured the fluorescence of the free liposomes to calculate the percentage of adsorption (Figure 6.3b). At pH 4, both TiO_2 and Fe_3O_4 adsorbed on the DOPC liposomes, but only TiO_2 leaked it (Figure 6.3a). Above pH 9, the adsorption of TiO_2 and Fe_3O_4 was inhibited (Figure 6.3b), which can explain the lack of leakage of their samples (Figure 6.3a). At pH 9, ZnO was positively charged, and it adsorbed and leaked DOPC. ZnO became negatively charged at pH 11.5, where it failed to adsorb DOPC and no leakage occurred. Taken together, adsorption of positively-charged oxides does not guarantee leakage, but without adsorption, no leakage can take place.

6.3.4 Tuning interaction strength by varying ionic strength

To study if electrostatic interactions are important, we tuned the ionic strength at pH 7.6 by adding NaCl. First, we confirmed that the addition of NaCl alone did not leak the DOPC liposomes (Figure 6.5a). ZnO leaked the DOPC liposomes without NaCl, whereas 100 mM NaCl inhibited the leakage (Figure 6.6). Thus, electrostatic interactions can influence the leakage of the DOPC liposomes. Although DOPC is zwitterionic, it is slightly negative charged at pH 7.6 (Figure 6.1b). Such electrostatic attraction might bring ZnO further closer to the lipid membrane causing the leakage. It was reported that the insertion of the G5 polyamidoamine dendrimer into lipid bilayers was inhibited by a high salt concentration because of the weakening of electrostatic attraction.[250] As salt had a large effect on the leakage, we also studied leakage and adsorption of the DOPC liposomes under different pH in the presence of 100 mM NaCl (Figure 6.3c and d). In this case, TiO_2 and Fe_3O_4 adsorbed the DOPC liposomes at pH 9 (Figure 6.3d, they did not adsorb DOPC without NaCl at pH 9, Figure 6.3b). However, even when they were adsorbed, still no leakage was observed (Figure 6.3c).

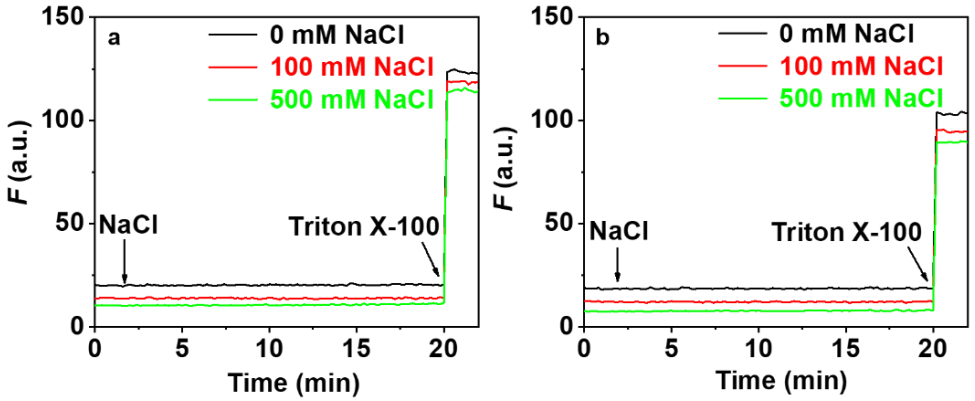

Figure 6.5 Leakage test of the calcein-loaded (a) DOPC and (b) DOPS liposomes with different NaCl concentrations at pH 7.6 (10 mM HEPES). No leakage was observed up to 500 mM NaCl. NaCl was added at 2 min.

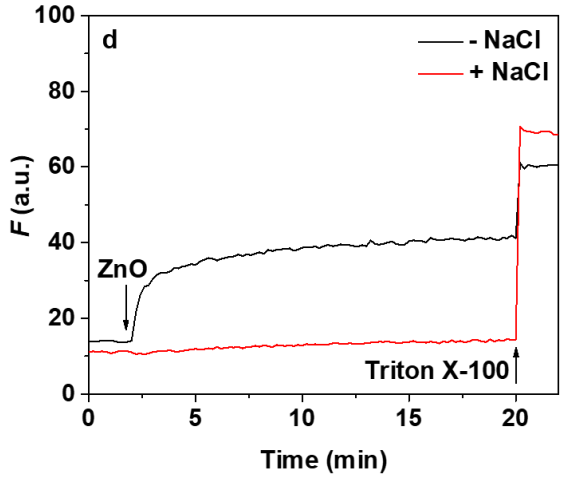

Figure 6.6 Leakage of the calcein-loaded DOPC liposomes with ZnO at pH 7.6 without (black) and with (red) 100 mM NaCl.

6.3.5 Leakage of negatively-charged DOPS liposomes

The above studies all used zwitterionic DOPC liposomes, and charge attraction appeared to be important. To further test the effect of charge, we then studied calcein-loaded DOPS liposomes. At pH 7.6, only ZnO leaked DOPS, whereas TiO_2 and Fe_3O_4 did not (Figure 6.7a). As the latter two were negatively charged, the charge repulsion might inhibit adsorption. To promote adsorption, we included 100 mM NaCl and indeed leakage was observed for TiO_2 (Figure 6.7a, pink trace). We then studied the leakage of DOPS with the presence of 100 mM NaCl at various pH values (Figure 6.7c). Note that the addition of NaCl did not leak the DOPS liposomes (Figure 6.5b). Positively-charged ZnO (pH 9) adsorbed DOPS and leaked it (Figure 6.7 c and d), whereas when it turned to negative (pH 11.5), the adsorption reduced and no leakage occurred.

Interestingly, for TiO_2, it adsorbed and leaked the DOPS liposomes regardless of pH. Even at pH 11.5, both DOPS and TiO_2 were strongly negatively charged, leakage was still observed (Figure 6.7c). This could be attributed to the coordination interaction between the PS headgroup and TiO_2. It was reported that DOPS could form SLBs on TiO_2,[42] which would fully disrupt DOPS liposomes, and thus, it was not surprising to see its leakage. To confirm our hypothesis, we carried out a cryo-TEM study of the DOPS/TiO_2 system prepared at pH 11.5 (Figure 6.7b). The TiO_2 surface was clearly wrapped with a conformal lipid bilayer, indicating that the supported DOPS bilayer was formed even at such a high pH. The Fe_3O_4 NPs failed to induce leakage at any pH, even at pH 4 (Figure 6.7c). At pH 4, these positively-charged oxides should adsorb strongly with the negatively-charged liposomes. This is another example that simple charge attraction alone was insufficient for leakage.

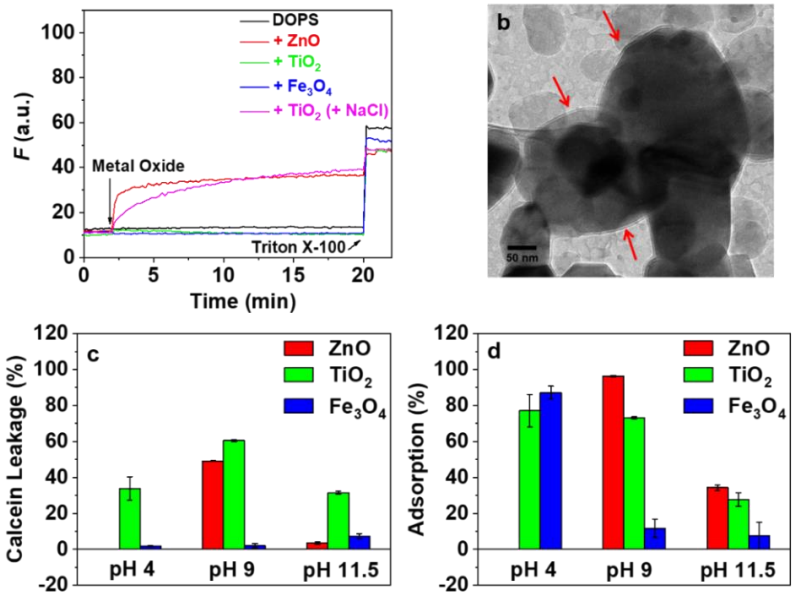

Figure 6.7 Leakage of calcein-loaded DOPS liposomes by various metal oxides NPs at pH 7.6 (10 mM HEPES). Pink trace with 100 mM NaCl. (b) Cryo-TEM micrograph of DOPS liposomes mixed with TiO_2 at pH 11.5. The red arrows point at the SLBs. (c) Leakage of the calcein-loaded and (d) adsorption of the Rh-labeled DOPS liposomes by the metal oxides at the different pH (10 mM HEPES, 100 mM NaCl).

6.3.6 Leakage by ZnO is transient and desorption also caused leakage

Because adsorption was required for leakage, the next question is whether the adsorbed particle can continue to leak, or leakage was transient and occurred only during adsorption. As we can easily dissolve ZnO by adding a metal chelator, such as EDTA, we then studied the dissolution of adsorbed ZnO. We showed in our previous work that the addition of EDTA to the free liposomes (without adsorbed ZnO) caused no leakage.[186]

ZnO leaked the DOPC liposomes as expected (Figure 6.8a, 2-12 min), but the rate of leakage was slow after the first 2 min. We then added EDTA to this sample (Figure 6.8a, 12-20 min), and interestingly, we also observed a rapid leakage. This indicates that leakage caused by adsorption of

ZnO was transient. This was also confirmed using cryo-TEM because after mixing the DOPC liposomes with ZnO, intact liposomes were still observed (Figure 6.8b). As some dyes remained at this stage, the leakage was caused by perturbation of local membranes instead of rupture of the whole liposome. After dissolving ZnO by EDTA, intact liposomes were observed under TEM (Figure 6.8c), confirming that the dissolution-induced leakage was not related to full membrane disruption either. Similar dissolution-induced leakage was also observed previously with negatively-charged AuNPs,[116] and the fundamental mechanism was similar in these materials. Adsorption of ZnO can cause local gelation of the lipids underneath it,[32] and this fluid-to-gel phase transition can cause a transient leakage. Once fully stably adsorbed, the gel phase already formed and the leakage stopped. When removing ZnO, the phase reversed back to fluid, also causing a transient leakage.

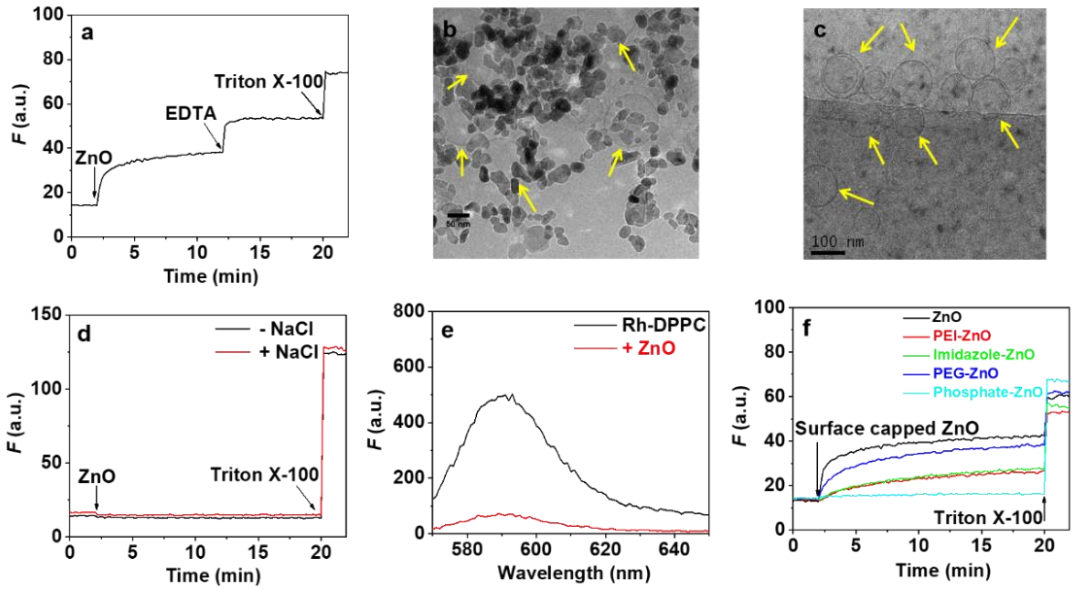

Figure 6.8 (a) Leakage of the calcein-loaded DOPC liposomes by removing adsorbed ZnO using EDTA. Cryo-TEM micrographs of (b) DOPC liposomes mixed with ZnO at pH 7.6, and (c) the DOPC liposomes after adding EDTA to the DOPC/ZnO mixture. The yellow arrows point at intact liposomes. (d) Leakage study of the calcein-loaded DPPC liposomes with ZnO NPs. (e) Fluorescence spectra of supernatant of Rh-DPPC and Rh-DPPC with ZnO. (f) Leakage of the DOPC liposomes with ligand capped ZnO NPs.

To further confirm this hypothesis, we used the gel-phase DPPC liposomes (T_c of 41 °C). No leakage of the DPPC liposomes was observed by ZnO (Figure 6.8d), although they effectively adsorbed the ZnO NPs (Figure 6.8e). This can be explained by the fact that when the liposome was already in the gel phase, further adsorption of ZnO did not change its phase, and it is also consistent with the model of local gelation.[116] This further indicates that liposome leakage is not necessarily correlated with the presence of cationic nanomaterials.

6.3.7 Capping the ZnO NPs

To probe the effect of surface chemistry, we capped the ZnO NPs with various molecules, including phosphate, PEI, PEG, and imidazole (Figure 6.8f). This was to increase the distance between ZnO and the liposome surface. When capped by imidazole or PEI, the leakage was reduced compared to the bare ZnO. When ZnO was coated with phosphate, no leakage occurred. Likely phosphate capping inhibited adsorption of the DOPC liposome. PEG is a weak ligand, and the adsorption of PEG had little effect on the interaction between DOPC and ZnO.[251] We also observed significant leakage in the presence of PEG-capped ZnO. This difference in leakage is a reflection of the surface ligand capping. Thus, one needs to be careful when talking about leakage by a certain material. Surface ligands have a very large influence on its leakage property. In addition, we have seen many examples of fine tuning the surface chemistry of NPs with the same charge, but they showed different behaviors of leakage. The best example is probably capping AuNPs with various ligands.[116] Another interesting example is SiO_2 NPs, which are negatively charged but have favorable interactions with PC liposomes. They can be internalized by liposomes and also form SLBs,[104,168,169,216] which have to break the liposomes. Therefore, charge alone cannot govern the interaction.

6.3.8 A unified understanding

Taken together, we summarize the factors that affect membrane leakage and integrity to unify the observations in the current work and in the literature. Based on the data obtained in this work, we conclude the following. (1) Electrostatic interactions indeed can affect the integrity of PC membranes.

Electrostatic attraction could bring NPs close to the PC membranes (Figure 6.9a left), inducing local gelation.[116] Consequently, a transient liposome leakage may occur. In contrast, with electrostatic interactions screened by NaCl, no leakage occurred (Figure 6.9a right). This is best exemplified in the ZnO/DOPC case (Figure 6.6). However, electrostatic interactions may not be the major force responsible for the leakage. For example, cationic Fe_3O_4 NPs could not leak the liposomes (Figures 6.3a and c, and Figure 6.7c). (2) As pH can change surface charge, it also affects the interaction between NPs and membrane (Figure 6.9b). For example, ZnO adsorbed and leaked the DOPC liposomes at pH 9, but at pH 11.5, the adsorption was inhibited (Figure 6.3b), thus no leakage occurred (Figure 6.3a). (3) The interaction strength can also be tuned by its surface ligand (Figure 6.9c). When ZnO was capped with different molecules, the extent of leakage was also different (Figure 6.8f). (4) If dissolution of the NPs can also induce leakage, then likely the leakage was caused by a local phase transition (Figure 6.9d, left).[32] In another case, the adsorption of NPs would not alter the phase of the lipids if the lipid bilayer exist in the gel phase already (Figure 6.8d), and no leakage would occur (Figure 6.9d, right).

The points above have been verified in our current work. By evaluating the previous literature, we further discussed the following. (5) Different NPs interact with membranes differently. Lipid membranes in the fluid phase could leak due to NPs (if interaction strength is sufficiently strong) (Figure 6.10 left),[116] whereas if the NP binding is not strong enough to cause the phase transition, and the membrane is still in fluid phase after binding, the membranes are likely stabilized (Figure 6.10 right).[173,247] (6) The important forces that induce liposome leakage could be chemical interactions (TiO_2/DOPS),[42] electrostatic interactions (ZnO/DOPC), and van der Waals forces (AuNP/DOPC).[116] In certain cases, adsorption is favorable to an extent to have the next step of fusion, and the best examples are SiO_2/DOPC (Figures 6.10b) and TiO_2/DOPS (Figures 6.7b and 6.10b). (7) Finally, we discussed dispersed liposomes versus SLBs. Large-scale surfaces are unlikely to be fully and perfectly covered by lipid bilayers and various defects are expected. Most such supports are negatively charged (e.g., silica and mica), and cationic materials can enlarge such defects by interacting directly with the surfaces and they appeared to damage the supported membranes. The dye leakage assay can avoid this potential

artifact (Figure 6.10c), and it provides information for transient leakage, for which permanent hole formation is not necessary.

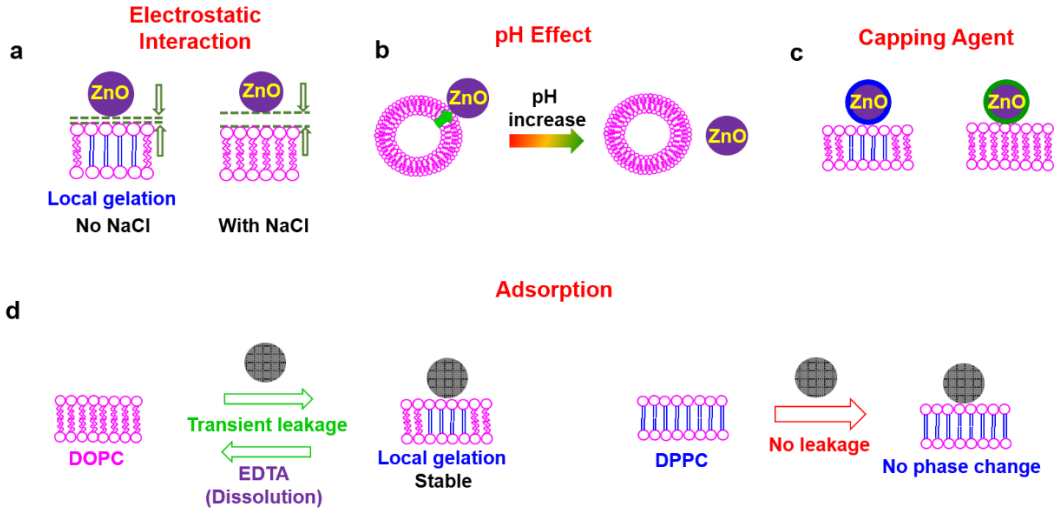

Figure 6.9 Schemes to summarize the factors found out in our current work that affect the membrane integrity in the presence of NPs. (a) Electrostatic attraction can be screened by NaCl, which can modulate the interaction strength and affect membrane leakage. (b) Tuning pH can alter the NP and membrane interaction. When pH is increased, the surface charge of the NPs can be altered, and consequently, the adsorption can be inhibited. (c) Capping NPs with ligands can separate the particle core from the membrane surface, which often leads to decreased interaction strength, and the surface ligands are closely related to the leakage property. (d) Scheme on the left: strong adsorption can cause local gelation of the fluid membrane and thus lead to a transient leakage during the phase transition. Removal of the adsorbed particles in this case can also cause leakage due to phase transition back to the fluid state. Scheme on the right: if the lipid is in the gel phase, adsorption of NPs will not change the lipid phase, thus no leakage occurs.

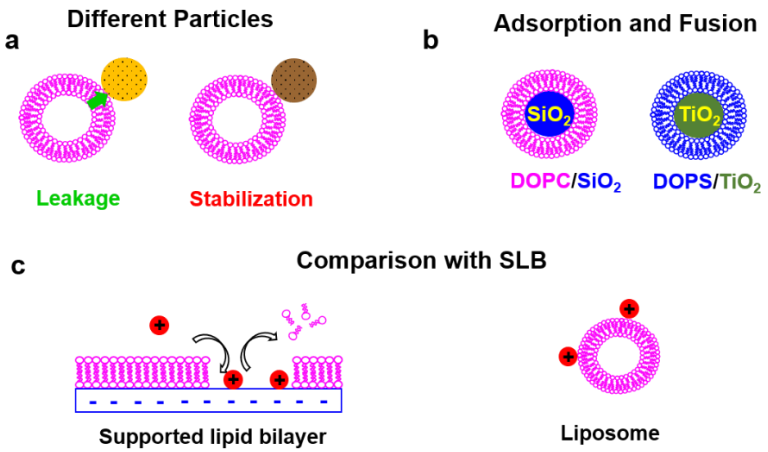

Figure 6.10 Schemes to summarize the factors that affect the membrane integrity in the presence of NPs discussed based on the previous literature. (a) Different particles interact with the membrane differently. NPs could interact with the membrane causing local membrane gelation that leaks the membrane. If the interaction force is not strong enough, no local gelation occurs, in which case, the membrane is stabilized. (b) In some cases, adsorption can cause further membrane fusion forming lipid bilayer supported on NPs to fully leak the content. (c) Comparison of SLBs and liposomes. Because of the negatively-charged support, cationic NPs may drive pore formation or enlarge existing pores, and such artifacts are avoided with dispersed liposomes.

6.4 Summary

In summary, we started with a simple question why cationic materials appeared to be more effective in perturbing lipid membranes. We systematically studied the effect of NP charge and leakage in solution by changing pH, thus avoiding potential interference from other factors such as the use of different materials. At the same time, the ionic strength, materials, surface ligand, and lipid composition were studied. The following main conclusions have been made. (1) The leakage induced by inorganic nanomaterials was dependent on their surface properties. We used a dye leakage assay in the solution phase, and the previously observed damages in SLBs are likely due to the underlying substrate. (2) We

studied both DOPC and DPPC liposomes; they have the same headgroup but different T_c. No leakage was observed with DPPC. Therefore, besides the headgroup, the tail has a significant effect on membrane leakage. (3) The ionic strength was studied by varying the concentration of NaCl. It shows that the electrostatic interactions have some effect on the leakage. As indicated in our data, DOPC leakage was induced by ZnO without NaCl. Since DOPC carried a slight negative charge, cationic ZnO can be attracted to its surface. In contrast, when electrostatic interaction was screened by NaCl, leakage was suppressed. (4) Finally, because DOPS contains strong coordination lipids, even with negatively-charged materials such as TiO_2 at high pH, leakage can be induced. We conclude that charge alone is not the governing factor. Regardless of charge, the particle needs to strongly interact with the liposomes to induce leakage.

Leakage means membrane perturbation, but it does not mean full membrane disruption. Nanomaterials can interact with liposomes in various ways. In general, when a stable adsorption complex is formed, the NPs can in general stabilize liposomes and prevent leakage. Leakage can take place during the initial adsorption process. Depending on the size and interaction strength and other factors, we may see further disruption of the membrane to form SLBs, but this process does not always happen and the interaction can stay at the stage of simple adsorption.

Chapter 7 Conclusions and Future Work

7.1 Conclusions and Original Contributions

In this Thesis, the interactions between liposomes and metal ions and metal oxide NPs have been studied with an emphasis on the lipid headgroup chemistry. In each system, the interaction mechanisms and the effects on liposome aggregation and membrane integrity were systematically studied, interaction forces were carefully identified, and a general interaction model was proposed. Overall, the thesis provides a fundamental understanding of interactions of lipid membranes with metal ions/oxides at a molecular level, which may promote the development of new research topics and applications.

In Chapter 2, the interactions of Zn^{2+} with DOPC and DOCP liposomes were systematically studied. The terminal phosphate in DOCP showed a stronger affinity for Zn^{2+}. While the binding of Zn^{2+} caused irreversible liposomes aggregation, fusion, and leakage of DOCP liposomes, these effects were minimal for DOPC liposomes. The thermodynamic parameters of Zn^{2+} binding to DOCP liposomes showed an overall endothermic reaction. This work highlights the lipid phosphate group in metal binding, expanding the chemistry of metal binding from amine (i.e., PE lipids), serine (e.g., PS lipids), and carboxyl groups.

In Chapter 3, we studied the interaction between Cu^{2+} and four types of liposomes. Fluorescence quenching experiments showed that the binding of Cu^{2+} with DOPS and DOCP were stronger than with DOPC and DOPG. However, all showed a positive-stain feature under normal TEM. In addition, Cu^{2+} could induce fusion and membrane leakage of DOPC, DOPS and DOPG at an appropriate concentration. Finally, the tight binding between Cu^{2+} and liposomes inhibited the catalytic properties of Cu^{2+}. Our model has shown that each lipid has a distinct mechanism of interaction with Cu^{2+}, which depends on the lipid headgroup chemistry.

In Chapter 4, we studied the binding of Gd^{3+} with DOPS and DOCP liposomes. In comparison to the binding of Cu^{2+} with these liposomes (Chapter 3), TEM showed that adsorption of Gd^{3+} on these

liposomes caused no significant membrane fusion. Unique surface potential reversal was observed after Gd^{3+} binding but was not seen during binding of Zn^{2+} and Ca^{2+}. Interestingly, Gd^{3+} induced leakage of the DOCP liposomes but not DOPS liposomes. Taking this advantage, AMP was added to form a Gd^{3+}/AMP shell on DOPS liposomes, and the content inside the liposomes was retained. The shell increased the stability of DOPS liposomes against membrane damageable ZnO NPs but not small surfactant molecules. This work not only demonstrates a simple method to form a shell on liposomes but also reveals detailed mechanisms for binding of lanthanide metal ions on lipid membranes.

In Chapter 5, we studied the interactions between PC liposomes and CeO_2 NPs. The fluorescence quenching experiments indicated that CeO_2 NPs were adsorbed by DOPC at both pH 4 and pH 7.6. At pH 4, the Ce_2O NPs were positively charged, and the complexes could be stabilized with a relatively higher amount of CeO_2 NPs. In contrast, DOPC aggregated at pH 7.6 at all the concentrations tested. The interaction between phosphate in the lipid headgroup and CeO_2 was the main force responsible for the adsorption. CeO_2 could induce the transient leakage of DOPC liposomes. This is the first time that we observed that DOPC liposomes were leaked by a noncationic metal oxide, and the leakage was attributed to the CeO_2 adsorption-induced local fluid-to-gel phase transition. This work provides a fundamental understanding of the interactions between lipid bilayers and CeO_2 NPs at the molecular level, which may offer insight into CeO_2 interaction with cell membranes.

In Chapter 6, we started with a simple question: why do cationic NPs appear to be more effective in perturbing lipid membranes? To answer this question, we studied the effects of NP charge on liposome leakage using the same materials by changing the solution pH. This strategy avoided interference from other factors like using different materials. By systematically varying the parameters, including the ionic strength, materials, surface ligand and lipid composition, we concluded that the leakage induced by inorganic NPs was strongly dependent on their surface properties. Charge alone is not important; the interaction strength is the key factor.

7.2 Future Work

The results presented in this thesis have demonstrated the importance of lipid headgroup chemistry, particularly when metal ions and metal oxide NPs are involved. Simple electrostatic interactions cannot explain all the experimental observations, and more specific chemical interactions must be considered. In turn, such interactions can be rationally harnessed to achieve metal ion adsorption, staining, the growth of metal coordination shells, and the control of liposome leakage. The following ideas can be further explored in the future.

First, lipid headgroup chemistry can be further broadened by rational design of headgroup structures. From the previous studies, phosphate groups were responsible for the interactions of a variety of biomolecules, such as DNA and lipids, with metal-containing materials.[47,111,150,252] Phosphorothioate-modified DNA, in which one non-bridging oxygen is substituted with sulfur, showed different interactions towards metals compared to unmodified DNA because of the different metal preference of oxygen and sulfur.[253] Inspired by this, phosphorothioate-modified lipids can be designed via chemical synthesis, and their interactions with metal-containing materials worth to investigate. With such lipids, the binding with thiophilic metals can be studied,[254] which may provide new fundamental understanding and insights into biomedical applications and material science.

Second, the structure of water molecules near the liposome surface during binding of metal ions/metal oxides may be studied. All membrane constituents are surrounded by water molecules, and many lipid headgroups, such as the PC headgroup, are highly hydrated.[29,30] Without this water to provide hydration, lipids are not able to self-assemble into bilayer membranes. Hydration and dehydration strongly affect the membrane properties, and metal ions/metal oxides can induce the rearrangement of water structures upon approaching.[81,82,84] For example, when liposomes are adsorbed directly via their headgroups on a metal oxide surface, the liposomes need to be sufficiently dehydrated.[83] As a result, the structures of water molecules during these interactions would be interesting to study in the future. To probe the interfacial water structure, advanced spectroscopy such

as vibrational sum frequency spectroscopy (VSFS) could be used. In addition, ITC may also be a promising tool to monitor changes in the thermodynamic parameters involved in hydration/dehydration processes. Dehydration is often accompanied release of a large number of water molecules, which may lead to a substantial increase in entropy.[81]

Third, on the lipid membrane, the configuration of lipid molecules interacting with metal ions/metal oxide NPs can be studied, including the tilt angle of the lipid headgroup, the configuration of the lipid tails, and the lateral organization of the lipid molecules after interacting. My work and some previous studies by others showed that the adsorption of NPs could induce a local lipid phase transition and such a change would likely reflect on the packing of lipid tails.[32,116,150,255] Such information might potentially be difficult to obtain experimentally, and using polarity sensitive dyes such as Laurdan only provides indirect evidence.[32] Higher-resolution techniques, such as nuclear magnetic resonance spectroscopy (NMR) and small-angle X-ray scattering (SAXS), might instead be used. In addition, molecular dynamics simulation can also be a powerful approach.

Fourth, the properties of liposome/metal-containing material complexes can be explored. For instance, nanoceria has a number of enzyme-like catalytic activities and is called a nanozyme.[256] Their catalytic properties after immobilization on a liposome can be studied (Chapter 5). The lipid membrane might be usable to recruit substrates to adsorb nanozymes and it may also act as an inhibitor. The fluidity of the lipid membrane may also be useful for immobilizing multiple nanozymes with different activities for cascade enzyme-like reactions. Another interesting application is the magnetic properties of DOPS@Gd/AMP (Chapter 4), since Gd^{3+} is well-known for its magnetic properties. Thus, the potential applications of DOPS@Gd/AMP in magnetic resonance imaging (MRI) is worth exploring.

Finally, to further broaden the understanding of interactions at the membrane surfaces, interactions with novel metal-containing nanomaterials can be explored, such as metal-organic frameworks (MOF), upconversion NPs, and 2D transition metal dichalcogenides (TMDCs). They have been widely demonstrated for biological applications,[257-259] but understanding of their interactions with cell membranes is lacking.

References

1. Vance, D. E.; Vance, J. E., *Biochemistry of Lipids, Lipoproteins and Membranes*. Elservier: Amsterdam, **1996**.

2. Cheng, X.; Smith, J. C., Biological Membrane Organization and Cellular Signaling. *Chem. Rev.* **2019,** *119* (9), 5849-5880.

3. McMahon, H. T.; Gallop, J. L., Membrane Curvature and Mechanisms of Dynamic Cell Membrane Remodelling. *Nature* **2005,** *438* (7068), 590-596.

4. Edidin, M., Lipids on the Frontier: A Century of Cell-Membrane Bilayers. *Nat. Rev. Mol. Cell Biol.* **2003,** *4*, 414-418.

5. Cho, W.; Stahelin, R. V., Membrane-Protein Interactions in Cell Signaling and Membrane Trafficking. *Annu. Rev. Biophys. Biomol. Struct.* **2005,** *34*, 119-151.

6. Marsden, H. R.; Tomatsu, I.; Kros, A., Model Systems for Membrane Fusion. *Chem. Soc. Rev.* **2011,** *40* (3), 1572-1585.

7. Chan, Y.-H. M.; Boxer, S. G., Model Membrane Systems and Their Applications. *Curr. Opin. Chem. Biol.* **2007,** *11* (6), 581-587.

8. Simons, K.; Vaz, W. L. C., Model Systems, Lipid Rafts, and Cell Membranes. *Annu. rev. Biophys. Biomol. Struct.* **2004,** *33*, 269-295.

9. Butterfield, S. M.; Lashuel, H. A., Amyloidogenic Protein-Membrane Interactions: Mechanistic Insight from Model Systems. *Angew. Chem. Int. Ed.* **2010,** *49* (33), 5628-5654.

10. Bondar, A.-N.; Lemieux, M. J., Reactions at Biomembrane Interfaces. *Chem. Rev.* **2019,** *119* (9), 6162-6183.

11. Chatterjee, S. N.; Agarwal, S., Liposomes as Membrane Model for Study of Lipid Peroxidation. *Free Radical Biol. Med.* **1988,** *4*, 51-72.

12. Niki, E.; Yamamote, Y.; Komuro, E.; Sato, K., Membrane Damage due to Lipid Oxidation. *Am. J. Clin. Nutr.* **1991,** *53* (201S-205S).

13. Martens, S.; McMahon, H. T., Mechanisms of Membrane Fusion: Disparate Players and Common Principles. *Nat. Rev. Mol. Cell Biol.* **2008,** *9* (7), 543-556.

14. Weber, T.; Zemelman, B. V.; McNew, J. A.; Westermann, B.; Gmachl, M.; Parlati, F.; Söllner, T. H.; Rothman, J. E., SNAREpins: Minimal Machinery for Membrane Fusion. *Cell* **1998,** *92*, 759-772.

15. Cebecauer, M.; Amaro, M.; Jurkiewicz, P.; Sarmento, M. J. o.; Šachl, R.; Cwiklik, L.; Hof, M., Membrane Lipid Nanodomains. *Chem. Rev.* **2018,** *118* (23), 11259-11297.

16. Laan, E. v. d. B.-v. d.; Killian, J. A.; Kruijff, B. d., Nonbilayer Lipids Affect Peripheral and Integral Membrane Proteins via Changes in the Lateral Pressure Profile. *Biochim. Biophys. Acta* **2004,** *1666* (1-2), 275-288.

17. McMullen, T. P. W.; Lewis, R. N. A. H.; McElhaney, R. N., Cholesterol-Phospholipid Interactions, the Liquid-Ordered Phase and Lipid Rafts in Model and Biological Membranes. *Curr. Opin. Colloid Interface Sci.* **2004,** *8* (6), 459-468.

18. Al-Ahmady, Z.; Kostarelos, K., Chemical Components for the Design of Temperature-Responsive Vesicles as Cancer Therapeutics. *Chem. Rev.* **2016,** *116* (6), 3883-3918.

19. Wang, F.; Liu, J., Nanodiamond Decorated Liposomes as Highly Biocompatible Delivery Vehicles and A Comparison with Carbon Nanotubes and Graphene Oxide. *Nanoscale* **2013,** *5* (24), 12375-12382.

20. Krause, M. R.; Regen, S. L., The Structural Role of Cholesterol in Cell Membranes: From Condensed Bilayers to Lipid Rafts. *Acc. Chem. Res.* **2014,** *47* (12), 3512-3521.

21. Bacia, i.; Schwille, P.; Kurzchalia, T., Sterol Structure Determines the Separation of Phases and the Curvature of the Liquid-Ordered Phase in Model Membranes. *Proc. Natl. acad. Sci. U.S.A.* **2005,** *102* (9), 3272-3277.

22. Feigenson, G. W.; Buboltz, J. T., Ternary Phase Diagram of Dipalmitoyl-PC/Dilauroyl-PC/Cholesterol: Nanoscopic Domain Formation Driven by Cholesterol. *Biophys. J.* **2001,** *80* (6), 2775-2788.

23. Veatch, S. L.; Keller, S. L., Separation of Liquid Phases in Giant Vesicles of Ternary Mixtures of Phospholipids and Cholesterol. *Biophys. J.* **2003,** *85* (5), 3074-3083.

24. Almeida, R. F. M. d.; Fedorov, A.; Prieto, M., Sphingomyelin/Phosphatidylcholine/Cholesterol Phase Diagram: Boundaries and Composition of Lipid Rafts. *Biophys. J.* **2003,** *85* (4), 2406-2416.

25. Brown, D. A.; London, E., Structure and Origin of Ordered Lipid Domains in Biological Membranes. *J. Membr. Biol.* **1998,** *164* (2), 103-114.

26. Sezgin, E.; Levental, I.; Mayor, S.; Eggeling, C., The Mystery of Membrane Organization: Composition, Regulation and Roles of Lipid Rafts. *Nat. Rev. Mol. Cell Biol.* **2017,** *18* (6), 361-374.

27. Koynova, R.; Caffrey, M., Phases and Phase Transitions of the Phosphatidylcholines. *Biochim. Biophys. Acta* **1998,** *1376* (1), 91-145.

28. Cevc, G.; Marsh, D., *Phospholipid Bilayers*. Wiley-Interscience: New York, **1987**.

29. Chen, S.; Zheng, J.; Li, L.; Jiang, S., Strong Resistance of Phosphorylcholine Self-Assembled Monolayers to Protein Adsorption: Insights into Nonfouling Properties of Zwitterionic Materials. *J. Am. Chem. Soc.* **2005,** *127* (41), 14473-14478.

30. Schlenoff, J. B., Zwitteration: Coating Surfaces with Zwitterionic Functionality to Reduce Nonspecific Adsorption. *Langmuir* **2014,** *30* (32), 9625-9636.

31. Liu, J., Interfacing Zwitterionic Liposomes with Inorganic Nanomaterials: Surface Forces, Membrane Integrity, and Applications. *Langmuir* **2016,** *32* (18), 4393-4404.

32. Wang, B.; Zhang, L.; Bae, S. C.; Granick, S., Nanoparticle-Induced Surface Reconstruction of Phospholipid Membranes. *Proc. Natl. acad. Sci. U.S.A.* **2008,** *105* (47), 18171-18175.

33. Vance, J. E.; Tasseva, G., Formation and Function of Phosphatidylserine and Phosphatidylethanolamine in Mammalian Cells. *Biochim. Biophys. Acta* **2013,** *1831* (3), 543-554.

34. Sendecki, A. M.; Poyton, M. F.; Baxter, A. J.; Yang, T.; Cremer, P. S., Supported Lipid Bilayers with Phosphatidylethanolamine as the Major Component. *Langmuir* **2017,** *33* (46), 13423-13429.

35. Hamai, C.; Yang, T.; Kataoka, S.; Cremer, P. S.; Musser, S. M., Effect of Average Phospholipid Curvature on Supported Bilayer Formation on Glass by Vesicle Fusion. *Biophys. J.* **2006,** *90* (4), 1241-1248.

36. Leventis, P. A.; Grinstein, S., The Distribution and Function of Phosphatidylserine in Cellular Membranes. *Annu. Rev. Biophys.* **2010,** *39*, 407-427.

37. Huang, B. X.; Akbar, M.; Kevala, K.; Kim, H.-Y., Phosphatidylserine is a Critical Modulator for Akt Activation. *J. Cell Biol.* **2011,** *192* (6), 979-992.

38. Lentz, B. R., Exposure of Platelet Membrane Phosphatidylserine Regulates Blood Coagulation. *Prog. Lipid Res.* **2003,** *42* (5), 423-438.

39. Yeung, T.; Gilbert, G. E.; Shi, J.; Silvius, J.; Kapus, A.; Grinstein, S., Membrane Phosphatidylserine Regulates Surface Charge and Protein Localization. *Science* **2008,** *319* (5860), 210-213.

40. Monson, C. F.; Cong, X.; Robison, A. D.; Pace, H. P.; Liu, C.; Poyton, M. F.; Cremer, P. S., Phosphatidylserine Reversibly Binds Cu^{2+} with Extremely High Affinity. *J. Am. Chem. Soc.* **2012,** *134* (18), 7773-7779.

41. Cong, X.; Poyton, M. F.; Baxter, A. J.; Pullanchery, S.; Cremer, P. S., Unquenchable Surface Potential Dramatically Enhances Cu^{2+} Binding to Phosphatidylserine Lipids. *J. Am. Chem. Soc.* **2015,** *137* (24), 7785-7792.

42. Wang, X.; Li, X.; Wang, H.; Zhang, X.; Zhang, L.; Wang, F.; Liu, J., Charge and Coordination Directed Liposome Fusion onto SiO_2 and TiO_2 Nanoparticles. *Langmuir* **2019,** *35* (5), 1672-1681.

43. Templeton, N. S.; Lasic, D. D.; Frederik, P. M.; Pavlakis, G. N., Improved DNA: Liposome Complexes for Increased Systemic Delivery and Gene Expression. *Nat. Biotechnol.* **1997,** *15*, 647-652.

44. Miller, A. D., Cationic Liposomes for Gene Therapy. *Angew. Chem. Int. Ed.* **1998,** *37* (13-14), 1768-1785.

45. Lonez, C.; Vandenbranden, M.; Ruysschaert, J.-M., Cationic Liposomal Lipids: from Gene Carriers to Cell Signaling. *Prog. Lipid. Res.* **2008,** *47* (5), 340-347.

46. Perttu, E. K.; Kohli, A. G.; Francis C. Szoka, J., Inverse-Phosphocholine Lipids: A Remix of a Common Phospholipid. *J. Am. Chem. Soc.* **2012,** *134* (10), 4485-4488.

47. Wang, F.; Liu, J., A Stable Lipid/TiO_2 Interface with Headgroup-Inversed Phosphocholine and a Comparison with SiO_2. *J. Am. Chem. Soc.* **2015,** *137* (36), 11736-11742.

48. Liu, Y.; Liu, J., Zn^{2+} Induced Irreversible Aggregation, Stacking, and Leakage of Choline Phosphate Liposomes. *Langmuir* **2017,** *33* (50), 14472-14479.

49. Wang, F.; Zhang, X.; Liu, Y.; Lin, Z. Y. W.; Liu, B.; Liu, J., Profiling Metal Oxides with Lipids: Magnetic Liposomal Nanoparticles Displaying DNA and Proteins. *Angew. Chem. Int. Ed.* **2016,** *55* (39), 12063-12067.

50. Liu, Y.; Wang, F.; Liu, J., Headgroup-Inversed Liposomes: Biointerfaces, Supported Bilayers and Applications. *Langmuir* **2018,** *34* (32), 9337-9348.

51. Li, S.; Wang, F.; Li, X.; Chen, J.; Zhang, X.; Wang, Y.; Liu, J., Dipole Orientation Matters: Longer-Circulating Choline Phosphate than Phosphocholine Liposomes for Enhanced Tumor Targeting. *ACS Appl. Mater. Interfaces* **2017,** *9* (21), 17736-17744.

52. Okur, H. I.; Tarun, O. B.; Roke, S., Chemistry of Lipid Membranes from Models to Living Systems: A Perspective of Hydration, Surface Potential, Curvature, Confinement and Heterogeneity. *J. Am. Chem. Soc.* **2019,** *141* (31), 12168-12181.

53. Castellana, E. T.; Cremer, P. S., Solid Supported Lipid Bilayers: From Biophysical Studies to Sensor Design. *Surf. Sci. Rep.* **2006,** *61* (10), 429-444.

54. Bangham, A. D.; Horne, R. W., Negative Staining of Phospholipids and their Structural Modificaion by Surface-Active Agents as Observed in the Electron Microscope. *J. Mol. Biol.* **1964,** *8* (5), 660-668.

55. Sessa, G.; Weissmann, G., Phospholipid Spherules (Liposomes) as A Model for Biological Membranes. *J. Lipid Res.* **1968,** *9*, 310-318.

56. Bangham, A. D.; Gier, J. D.; Greville, G. D., Osmotic Properties and Water Permeability of Phospholipid Liquid Crystals. *Chem. Phys. Lipids* **1967,** *1*, 225-246.

57. Pattni, B. S.; Chupin, V. V.; Torchilin, V. P., New Developments in Liposomal Drug Delivery. *Chem. Rev.* **2015,** *115* (19), 10938-10966.

58. Min, Y.; Caster, J. M.; Eblan, M. J.; Wang, A. Z., Clinical Translation of Nanomedicine. *Chem. Rev.* **2015,** *115* (19), 11147-11190.

59. Mazur, F.; Bally, M.; Städler, B.; Chandrawati, R., Liposomes and Lipid Bilayers in Biosensors. *Adv. Colloid. Interface Sci.* **2017,** *249*, 88-99.

60. Pick, H.; Alves, A. C.; Vogel, H., Single-Vesicle Assays Using Liposomes and Cell-Derived Vesicles: From Modeling Complex Membrane Processes to Synthetic Biology and Biomedical Applications. *Chem. Rev.* **2018,** *118* (18), 8598-8654.

61. Akbarzadeh, A.; Rezaei-Sadabady, R.; Davaran, S.; Joo, S. W.; Zarghami, N.; Hanifehpour, Y.; Samiei, M.; Kouhi, M.; Nejati-Koshki, K., Liposome: Classification, Preparation, and Applications. *Nanoscale Res. Lett.* **2013,** *8* (1), 102.

62. Lopez, A.; Liu, J., DNA Oligonucleotide-Functionalized Liposomes: Bioconjugate Chemistry, Biointerfaces, and Applications. *Langmuir* **2018,** *34* (49), 15000-15013.

63. Bigdeli, A.; Palchetti, S.; Pozzi, D.; Hormozi-Nezhad, M. R.; Bombelli, F. B.; Caracciolo, G.; Mahmoudi, M., Exploring Cellular Interactions of Liposomes Using Protein Corona Fingerprints and Physicochemical Properties. *ACS Nano* **2016,** *10* (3), 3723-3737.

64. Caracciolo, G., Liposome-Protein Corona in A Physiological Environment: Challenges and Opportunities for Targeted Delivery of Nanomedicines. *Nanomedicine* **2015,** *11* (3), 543-557.

65. Leroueil, P. R.; Berry, S. A.; Duthie, K.; Han, G.; Rotello, V. M.; McNerny, D. Q.; James R. Baker, J.; Orr, B. G.; Holl, M. M. B., Wide Varieties of Cationic Nanoparticles Induce Defects in Supported Lipid Bilayers. *Nano Lett.* **2008,** *8* (2), 420-424.

66. Kim, B.-E.; Nevitt, T.; Thiele, D. J., Mechanisms for Copper Acquisition, Distribution and Regulation. *Nat. Chem. Biol.* **2008,** *4* (3), 176-185.

67. Carter, K. P.; Young, A. M.; Palmer, A. E., Fluorescent Sensors for Measuring Metal Ions in Living Systems. *Chem. Rev.* **2014,** *114* (8), 4564-4601.

68. Knight, A. S.; Larsson, J.; Ren, J. M.; Zerdan, R. B.; Seguin, S.; Vrahas, R.; Liu, J.; Ren, G.; Hawker, C. J., Control of Amphiphile Self-Assembly via Bioinspired Metal Ion Coordination. *J. Am. Chem. Soc.* **2018,** *140* (4), 1409-1414.

69. Liu, Y.; Tang, Z., Nanoscale Biocoordination Polymers: Novel Materials from an Old Topic. *Chem. Eur. J.* **2012,** *18* (4), 1030-1037.

70. Holliday, B. J.; Mirkin, C. A., Strategies for the Construction of Supramolecular Compounds through Coordination Chemistry. *Angew. Chem. Int. Ed.* **2001,** *40* (11), 2922-2043.

71. Dong, H.; Du, S.-R.; Zheng, X.-Y.; Lyu, G.-M.; Sun, L.-D.; Li, L.-D.; Zhang, P.-Z.; Zhang, C.; Yan, C.-H., Lanthanide Nanoparticles: From Design toward Bioimaging and Therapy. *Chem. Rev.* **2015,** *115* (18), 10725-10815.

72. Li, R.; Ji, Z.; Chang, C. H.; Dunphy, D. R.; Cai, X.; Meng, H.; Zhang, H.; Sun, B.; Wang, X.; Dong, J.; Lin, S.; Wang, M.; Liao, Y.-P.; Brinker, J.; Nel, A.; Xia, T., Surface Interactions with Compartmentalized Cellular Phosphates Explain Rare Earth Oxide Nanoparticle Hazard and Provide Opportunities for Safer Design. *ACS Nano* **2014,** *8* (2), 1771-1783.

73. Huxford, R. C.; deKrafft, K. E.; Boyle, W. S.; Liu, D.; Lin, W., Lipid-Coated Nanoscale Coordination Polymers for Targeted Delivery of Antifolates to Cancer Cells. *Chem. Sci.* **2012,** *3* (1), 198-204.

74. Bishop, K. J. M.; Wilmer, C. E.; Soh, S.; Grzybowski, B. A., Nanoscale Forces and Their Uses in Self-Assembly. *Small* **2009,** *5* (14), 1600-1630.

75. Cosgrove, T., *Colloid Science: Principles, Methods and Applications, 2nd Edition*. John Wiley and Sons: **2010**.

76. Nel, A. E.; Mädler, L.; Velegol, D.; Xia, T.; Hoek, E. M. V.; Somasundaran, P.; Klaessig, F.; Castranova, V.; Thompson, M., Understanding Biophysicochemical Interactions at the Nano-Bio Interface. *Nat. Mater.* **2009,** *8* (7), 543-557.

77. Velegol, D., Assembling Colloidal Devices by Controlling Interparticle Forces. *J. Nanophotonics* **2009,** *1*, 012502.

78. Butt, H. J.; Graf, K.; Kappl, M., *Physics and Chemistry of Interfaces*. John Wiley and Sons: **2003**.

79. Chernomordik, L. V.; Kozlov, M. M., Mechanics of Membrane Fusion. *Nat. Struct. Mol. Biol.* **2008,** *15* (7), 675-683.

80. Kozlovsky, Y.; Efrat, A.; Siegel, D. A.; Kozlov, M. M., Stalk Phase Formation: Effects of Dehydration and Saddle Splay Modulus. *Biophys. J.* **2004,** *87* (4), 2508-2521.

81. Sinn, C. G.; Antonietti, M.; Dimova, R., Binding of Calcium to Phosphatidylcholine-Phophatidylserine Membranes. *Colloids Surf., A* **2006,** *282-283*, 410-419.

82. Binder, H.; Zschörnig, O., The Effect of Metal Cations on the Phase Behavior and Hydration Characteristics of Phospholipid Membranes. *Chem. Phys. Lipids* **2002,** *115* (1-2), 39-61.

83. Fortunelli, A.; Monti, S., Simulations of Lipid Adsorption on TiO_2 Surfaces in Solution. *Langmuir* **2008,** *24* (18), 10145-10154.

84. Jackman, J. A.; Zan, G. H.; Zhao, Z.; Cho, N.-J., Contribution of the Hydration Force to Vesicle Adhesion on Titanium Oxide. *Langmuir* **2014,** *30* (19), 5368-5372.

85. Garidel, P.; Blume, A., Interaction of Alkaline Earth Cations with the Negatively Charged Phospholipid 1,2-Dimyristoyl-*sn*-Glycero-3-Phosphoglycerol: A Differential Scanning and Isothermal Titrationn Calorimetric Study. *Langmuir* **1999,** *15* (17), 5526-5534.

86. Garidel, P.; Blume, A., 1,2-Dimyristoyl-*sn*-Glycero-3-Phosphoglycerol (DMPG) Monolayers: Influence of Temperature, pH, Ionic Strength and Binding of Alkaline Earth Cations. *Chem. Phys. Lipids* **2005,** *138* (1-2), 50-59.

87. Garidel, P.; Blume, A.; Hübner, W., A Fourier Transform Infrared Spectroscopic Study of the Interaction of Alkaline Earth Cations with the Negatively Charged Phospholipid 1,2-Dimyristoyl-*sn*-Glycero-3-Phosphoglycerol. *Biochim. Biophys. Acta* **2000,** *1466* (1-2), 245-259.

88. Papahadjopoulos, D.; Nir, S.; Düzgünes, N., Molecular Mechanisms of Calcium-Induced Membrane Fusion. *J. Bioenerg. Biomembr.* **1990,** *22* (2), 157-179.

89. Szule, J. A.; Jarvis, S. E.; Hibbert, J. E.; Spafford, J. D.; Braun, J. E. A.; Zamponi, G. W.; Wessel, G. M.; Coorssen, J. R., Calcium-Triggered Membrane Fusion Proceeds Independently of Specific Presynaptic Proteins. *J. Biol. Chem.* **2003,** *278* (27), 24251-24254.

90. Jahn, R.; Lang, T.; Südhof, T. C., Membrane Fusion. *Cell* **2003,** *112* (4), 519-533.

91. Pedersen, U. R.; Leidy, C.; Westh, P.; Peters, G. H., The Effect of Calcium on the Properties of Charged Phospholipid Bilayers. *Biochim. Biophys. Acta* **2006,** *1758* (5), 573-582.

92. Ohki, S.; Zschörnig, O., Ion-Induced Fusion of Phosphatidic Acid Vesicles and Correlation between Surface Hydrophobicity and Membrane Fusion. *Chem. Phys. Lipids* **1993,** *65* (3), 193-204.

93. Tsai, H.-H. G.; Lai, W.-X.; Lin, H.-D.; Lee, J.-B.; Juang, W.-F.; Tseng, W.-H., Molecular Dynamics Simulation of Cation-Phospholipid Clustering in Phospholipid Bilayers: Possible Role in Stalk Formation during Membrane Fusion. *Biochim. Biophys. Acta* **2012,** *1818* (11), 2742-2755.

94. Melcrová, A.; Pokorna, S.; Pullanchery, S.; Jurkiewicz, M. K. P.; Hof, M.; Jungwirth, P.; Cremer, P. S.; Cwiklik, L., The Complex Nature of Calcium Cation Interactions with Phospholipid Bilayers. *Sci. Rep.* **2016,** *6*, 38035.

95. Boettcher, J. M.; Davis-Harrison, R. L.; Clay, M. C.; Nieuwkoop, A. J.; Ohkubo, Y. Z.; Tajkhorshid, E.; Morrissey, J. H.; Rienstra, C. M., Atomic View of Calcium-Induced Clustering of Phosphatidylserine in Mixed Lipid Bilayers. *Biochemistry* **2011,** *50* (12), 2264-2273.

96. Bckmann, R. A.; Grubmüller, H., Multistep Binding of Divalent Cations to Phospholipid Bilayers: A Molecular Dynamics Study. *Angew. Chem. Int. Ed.* **2004,** *43* (8), 1021-1024.

97. Kučerka, N.; Dushanov, E.; Kholmurodov, K. T.; Katsaras, J.; Uhríková, D., Calcium and Zinc Differentially Affect the Structure of Lipid Membranes. *Langmuir* **2017,** *33* (12), 3134-3141.

98. Magarkar, A.; Róg, T.; Bunker, A., Molecular Dynamics Simulation of Inverse-Phosphocholine Lipids. *J. Phys. chem. C* **2014,** *118* (33), 19444-19449.

99. Poyton, M. F.; Sendecki, A. M.; Cong, X.; Cremer, P. S., Cu^{2+} Binds to Phosphatidylethanolamine and Increases Oxidation in Lipid Membranes. *J. Am. Chem. Soc.* **2016,** *138* (5), 1584-1590.

100. Limo, M. J.; Sola-Rabada, A.; Boix, E.; Thota, V.; Westcott, Z. C.; Puddu, V.; Perry, C. C., Interactions between Metal Oxides and Biomolecules: from Fundamental Understanding to Applications. *Chem. Rev.* **2018,** *118* (22), 11118-11193.

101. Richter, R. P.; Bérat, R.; Brisson, A. R., Formation of Solid-Supported Lipid Bilayers: An Integrated View. *Langmuir* **2006,** *22* (8), 3497-3505.

102. Richter, R.; Mukhopadhyay, A.; Brisson, A., Pathways of Lipid Vesicle Deposition on Solid Surfaces: A Combined QCM-D and AFM Study. *Biophys. J.* **2003,** *85* (5), 3035-3047.

103. Keller, C. A.; Glasmästar, K.; Zhdanov, V. P.; Kasemo, B., Formation of Supported Membranes from Vesicles. *Phys. Rev. Lett.* **2000,** *84* (23), 5443-5446.

104. Cremer, P. S.; Boxer, S. G., Formation and Spreading of Lipid Bilayers on Planar Glass Supports. *J. Phys. Chem. B* **1999,** *103* (13), 2554-2559.

105. Seantier, B.; Kasemo, B., Influence of Mono- and Divalent Ions on the Formation of Supported Phospholipid Bilayers via Vesicle Adsorption. *Langmuir* **2009,** *25* (10), 5767-5772.

106. Reviakine, I.; Rossetti, F. F.; Morozov, A. N.; Textor, M., Investigating the Properties of Supported Vesicular Layers on Titanium Dioxide by Quartz Crystal Microbalance with Dissipation Measurements. *J. Chem. Phys.* **2005,** *122* (20), 204711.

107. Reimhult, E.; Höök, F.; Kasemo, B., Intact Vesicle Adsorption and Supported Biomembrane Formation from Vesicles in Solution: Influence of Surface Chemistry, Vesicle Size, Temperature, and Osmotic Pressure. *Langmuir* **2003,** *19* (5), 1681-1691.

108. Cho, N.-J.; Frank, C. W., Fabrication of A Planar Zwitterionic Lipid Bilayer on Titanium Oxide. *Langmuir* **2010,** *26* (20), 15706-15710.

109. Cho, N.-J.; Jackman, J. A.; Liu, M.; Frank, C. W., pH-Driven Assembly of Various Supported Lipid Platforms: A Comparative Study on Silicon Oxide and Titanium Oxide. *Langmuir* **2011,** *27* (7), 3739-3748.

110. Rossetti, F. F.; Bally, M.; Michel, R.; Textor, M.; Reviakine, I., Interactions between Titanium Dioxide and Phosphatidyl Serine-Containing Liposomes: Formation and Patterning of Supported

Phospholipid Bilayers on the Surface of a Medically Relevant Material. *Langmuir* **2005,** *21* (14), 6443-6450.

111. Wang, F.; Liu, J., Liposome Supported Metal Oxide Nanoparticles: Interaction Mechanism, Light Controlled Content Release, and Intracellular Delivery. *Small* **2014,** *10* (19), 3927-3931.

112. Daniel, M.-C.; Astruc, D., Gold Nanoparticles: Assembly, Supramolecular Chemistry, Quantum-Size-Related Properties, and Applications toward Biology, Catalysis, and Nanotechnology. *Chem. Rev.* **2004,** *104* (1), 293-346.

113. Giljohann, D. A.; Seferos, D. S.; Daniel, W. L.; Massich, M. D.; Patel, P. C.; Mirkin, C. A., Gold Nanoparticles for Biology and Medicine. *Angew. Chem. Int. Ed.* **2010,** *49* (19), 3280-3294.

114. Wu, G.; Mikhailovsky, A.; Khant, H. A.; Fu, C.; Chiu, W.; Zasadzinski, J. A., Remontely Triggered Liposome Release by Near-Infrared Light Absorption via Hollow Gold Nanoshells. *J. Am. Chem. Soc.* **2008,** *130* (26), 8175-8177.

115. Pornpattananangkul, D.; Olson, S.; Aryal, S.; Sartor, M.; Huang, C.-M.; Vecchio, K.; Zhang, L., Stimuli-Responsive Liposome Fusion Mediated by Gold Nanoparticles. *ACS Nano* **2010,** *4* (4), 1935-1942.

116. Wang, F.; Liu, J., Self-Healable and Reversible Liposome Leakage by Citrate-Capped Gold Nanoparticles: Probing the Initial Adsorption/Desorption Induced Lipid Phase Transition. *Nanoscale* **2015,** *7* (38), 15599-15604.

117. Wang, F.; Curry, D. E.; Liu, J., Driving Adsorbed Gold Nanoparticle Assembly by Merging Lipid Gel/Fluid Interfaces. *Langmuir* **2015,** *31* (49), 13271-13274.

118. Liu, X.; Li, X.; Xu, W.; Zhang, X.; Huang, Z.; Wang, F.; Liu, J., Sub-Angstrom Gold Nanoparticle/Liposome Interfaces Controlled by Halides. *Langmuir* **2018,** *34* (22), 6628-6635.

119. Mammen, M.; Choi, S.-K.; Whitesides, G. M., Polyvalent Interactions in Biological Sysmtems: Implications for Design and Use of Multivalent Ligands and Inhibitors. *Angew. Chem. Int. Ed.* **1998,** *37* (20), 2754-2794.

120. Jayaraman, N., Multivalent Ligand Presentation as A Central Concept to Study Intricate Carbohydrate-Protein Interactions *Chem. Soc. Rev.* **2009,** *38* (12), 3463-3483.

121. Edidin, M., The State of Lipid Rafts: From Model Membranes to Cells. *Annu. Rev. Biophys. Biomol. Struct.* **2003,** *32*, 257-283.

122. Parikh, A. N.; Groves, J. T., Materials Science of Supported Lipid Membranes. *MRS Bull.* **2006,** *31* (7), 507-512.

123. Patolsky, F.; Lichtenstein, A.; Willner, I., Electrochemical Transduction of Liposome-Amplified DNA Sensing. *Angew. chem. Int. Ed.* **2000,** *39* (5), 940-943.

124. Edwards, K. A.; Baeumner, A. J., Optimization of DNA-Tagged Liposomes for Use in Microtiter Plate Analyses. *Anal. Bioanal. Chem.* **2006,** *386* (6), 1613-1623.

125. Cao, Z.; Tong, R.; Mishra, A.; Xu, W.; Wong, G. C. L.; Cheng, J.; Lu, Y., Reversible Cell-Specific Drug Delivery with Aptamer-Functionalized Liposomes. *Angew. Chem. Int. Ed.* **2009,** *48* (35), 6494-6498.

126. Chen, X.; Zhou, G.; Peng, X.; Yoon, J., Biosensors and Chemosensors Based on the Optical Responses of Polydiacetylenes. *Chem. Soc. Rev.* **2012,** *41* (13), 4610-4630.

127. Dave, N.; Liu, J., Biomimetic Sensing Based on Chemically Induced Assembly of a Signaling DNA Aptamer on a Fluid Bilayer Membrane. *Chem. Commun.* **2012,** *48* (31), 3718-3720.

128. Waggoner, T. A.; Last, J. A.; Kotula, P. G.; Sasaki, D. Y., Self-Assembled Columns of Stacked Lipid Bilayers Mediated by Metal Ion Recognition. *J. Am. Chem. Soc.* **2001,** *123* (3), 496-497.

129. Yigit, M. V.; Mishra, A.; Tong, R.; Cheng, J.; Wong, G. C. L.; Lu, Y., Inorganic Mercury Detection and Controlled Release of Chelating Agents from Ion-Responsive Liposomes. *Chem. Biol.* **2009,** *16* (9), 937-942.

130. Vos, C. H. R. D.; Schat, H.; Waal, M. A. M. D.; Vooijs, R.; Ernst, W. H. O., Increased Resistance to Copper-Induced Damage of the Root Cell Plasmalemma in Copper Tolerant Silene Cucubalus. *Physiol. Plant* **1991,** *82* (4), 523-528.

131. Chauhan, A.; Sheikh, A. M.; Chauhan, V., Increase Copper-Mediated Oxidation of Membrane Phosphatidylethanolamine in Autism. *Am. J. Biochem. Biotechnol.* **2008,** *4* (2), 95-100.

132. Hochstein, P.; Kumar, K. S.; Forman, S. J., Lipid Peroxidation and the Cytotoxicity of Copper. *Ann. N. Y. Acad. Sci.* **1980,** *355* (1), 240-248.

133. Kusler, K.; Odoh, S. O.; Silakov, A.; Poyton, M. F.; Pullanchery, S.; Cremer, P. S.; Gagliardi, L., What Is the Preferred Conformation of Phosphatidylserine-Copper(II) Complexes? A Combined Theoretical and Experimental Investigation. *J. Phys. Chem. B* **2016,** *120* (50), 12883-12889.

134. Sasaki, D. Y.; Shnek, D. R.; Pack, D. W.; Arnold, F. H., Metal-Induced Dispersion of Lipid Aggergates: A Simple, Selective, and Sensitive Fluorescent Metal Ion Sensor. *Angew. Chem. Int. Ed.* **1995,** *34* (8), 905-907.

135. Sasaki, D. Y.; Padilla, B. E., Dithioamide Metal Ion Receptors on Fluorescent Lipid Bilayers for the Selective Optical Detection of Mercuric Ion. *chem. Comm.* **1998**, 1581-1582.

136. Maity, P.; Saha, B.; Kumar, G. S.; Karmakar, S., Binding of Monovalent Alkali Metal Ions with Negatively Charged Phospholipid Membranes. *Biochim. Biophys. Acta* **2016,** *1858* (4), 706-714.

137. Klasczyk, B.; Knecht, V.; Lipowsky, R.; Dimova, R., Interactions of Alkali Metal Chlorides with Phosphatidylcholine Vesicles. *Langmuir* **2010,** *26* (24), 18951-18958.

138. Molenbroek, E.; Straathof, N.; Dück, S.; Rashid, Z.; Lenthe, J. H. v.; Lutz, M.; Gandubert, A.; Gebbink, R. J. M. K.; Cola, L. D.; Bonnet, S., Zinc Coordination to the bapbpy Ligand in Homogeneous Solutions and at Liposomes: Zinc Detection via Fluorescence Enhancement. *Dalton Trans.* **2013,** *42* (8), 2973-2984.

139. Jose, D. A.; König, B., Polydiacetylene Vesicles Functionalized with N-Heterocyclic Ligands for Metal Cation Binding. *Org. Biomol. Chem.* **2010,** *8* (3), 655-662.

140. Bürgel, S. C.; Guillaume-Gentil, O.; Zheng, L.; Vörös, J.; Bally, M., Zirconium Ion Mediated Formation of Liposome Multilayers. *Langmuir* **2010,** *26* (13), 10995-11002.

141. Caël, V.; Heyden, A. V. d.; Champmartin, D.; Barzyk, W.; Rubini, P.; Rogalska, E., Interfacial Approach to Aluminum Toxicity: Interactions of Al(III) and Pr(III) with Model Phospholipid Bilayer and Monolayer Membranes. *Langmuir* **2003,** *19* (21), 8697-8708.

142. Minami, H.; Inoue, T., Aggregation of Dipalmitoylphosphatidylcholine Vesicles Induced by Some Metal Ions with High Activity for Hydrolysis. *Langmuir* **1999,** *15* (20), 6643-6651.

143. Chen, X.; Chen, T.; Lin, Z.; Li, X. e.; Wu, W.; Li, J., Choline Phosphate Functionalized Surface: Protein-Resistant but Cell-Adhesive Zwitterionic Surface Potential for Tissue Engineering. *Chem. Commun.* **2015,** *51* (3), 487-490.

144. Wang, S.; McGuirk, C. M.; Ross, M. B.; Wang, S.; Chen, P.; Xing, H.; Liu, Y.; Mirkin, C. A., General and Direct Method for Preparing Oligonucleotide-Functionalized Metal-Organic Framework Nanoparticles. *J. Am. Chem. Soc.* **2017,** *139* (29), 9827-9830.

145. Maret, W., Analyzing Free Zinc(II) Ion Concentrations in Cell Biology with Fluorescent Chelating Molecules. *Metallomics* **2015,** *7* (2), 202-211.

146. Zago, M. P.; Oteiza, P. I., The Antioxidant Properties of Zinc: Interactions with Iron and Antioxidants. *Free Radical Biol. Med.* **2001,** *31* (2), 266-274.

147. Ojida, A.; Nonaka, H.; Miyahara, Y.; Tamaru, S.-i.; Sada, K.; Hamachi, I., Bis(Dpa-Zn(II)) Appended Xanthone: Excitation Ratiometric Chemosensor for Phosphate Anions. *Angew. Chem. Int. Ed.* **2006,** *45* (33), 5518-5521.

148. Langlais, M.; Tajmir-Riahi, H. A.; Savoie, R., Raman Spectroscopic Study of the Effects of Ca^{2+}, Mg^{2+}, Zn^{2+}, and Cd^{2+} Ions on Calf Thymus DNA: Binding Sites and Conformational Changes. *Biopolymers* **1990,** *30* (7-8), 743-752.

149. Ma, L.; Liu, B.; Huang, P.-J. J.; Zhang, X.; Liu, J., DNA Adsorption by ZnO Nanoparticles near Its Solubility Limit: Implications for DNA Fluorescence Quenching and DNAzyme Activity Assays. *Langmuir* **2016,** *32* (22), 5672-5680.

150. Liu, Y.; Liu, J., Adsorption of Nanoceria by Phosphocholine Liposomes. *Langmuir* **2016,** *32* (49), 13276-13283.

151. Gao, W.; Hu, C.-M. J.; Fang, R. H.; Zhang, L., Liposome-Like Nanostructures for Drug Delivery. *J. Mater. Chem. B* **2013,** *1* (48), 6569-6585.

152. Tan, S.; Li, X.; Guo, Y.; Zhang, Z., Lipid-Enveloped Hybrid Nanoparticles for Drug Delivery. *Nanoscale* **2013,** *5* (3), 860-872.

153. Perttu, E. K.; Jr., F. C. S., Zwitterionic Sulfobetaine Lipids that Form Vesicles with Salt-Dependent Thermotropic Properties. *Chem. Commun.* **2011,** *47* (47), 12613-12615.

154. Hassanin, M.; Kerek, E.; Chiu, M.; Anikovskiy, M.; Prenner, E. J., Binding Affinity of Inorganic Mercury and Cadmium to Biomimetic Erythrocyte Membranes. *J. Phys. Chem. B* **2016,** *120* (50), 12872-12882.

155. Lu, Y.; Yeung, N.; Sieracki, N.; Marshall, N. M., Design of Functional Metalloproteins. *Nature* **2009,** *460* (7257), 855-862.

156. Zeng, L.; Miller, E. W.; Pralle, A.; Isacoff, E. Y.; Chang, C. J., A Selective Turn-On Fluorescent Sensor for Imaging Copper in Living Cells. *J. Am. Chem. Soc.* **2006,** *128* (1), 10-11.

157. Segawa, K.; Nagata, S., An Apoptotic 'Eat Me' Signal: Phosphatidylserine Exposure. *Trends Cell Biol.* **2015,** *25* (11), 639-650.

158. Huang, C.; Mason, J. T., Geometric Packing Constraints in Egg Phosphatidylcholine Vesicles. *Proc. Natl. acad. Sci. U.S.A.* **1978,** *75* (1), 308-310.

159. Friedrich, H.; Frederik, P. M.; With, G. d.; Sommerdijk, N. A. J. M., Imaging of Self-Assembled Structures: Interpretation of TEM and Cryo-TEM images. *Angew. Chem. Int. Ed.* **2010,** *49* (43), 7850-7858.

160. Ip, A. C.-F.; Liu, B.; Huang, P.-J. J.; Liu, J., Oxidation Level-Dependent Zwitterionic Liposome Adsorption and Rupture by Graphene-based Materials and Light-Induced Content Release. *Small* **2013,** *9* (7), 1030-1035.

161. Ogle, B. M.; Cascalho, M.; Platt, J. L., Biological Implications of Cell Fusion. *Nat. Rev. Mol. Cell Biol.* **2005,** *6* (7), 567-575.

162. Liang, H.; Lin, F.; Zhang, Z.; Liu, B.; Jiang, S.; Yuan, Q.; Liu, J., Multicopper Laccase Mimicking Nanozymes with Nucleotides as Ligands. *ACS Appl. Mater. Interfaces* **2017,** *9* (2), 1352-1360.

163. Kerek, E.; Hassanin, M.; Prenner, E. J., Inorganic Mercury and Cadmium Induce Rigidity in Eukaryotic Lipid Extracts While Mercury also Ruptures Red Blood Cells. *Biochim. Biophys. Acta, Biomembr.* **2018,** *1860* (3), 710-717.

164. Payliss, B. J.; Hassanin, M.; Prenner, E. J., The Structural and Functional Effects of Hg(II) and Cd(II) on Lipid Model Systems and Human Erythrocytes: A Review. *Chem. Phys. Lipids* **2015,** *193*, 36-51.

165. Sabín, J.; Prieto, G.; Sennato, S.; Ruso, J. M.; Angelini, R.; Bordi, F.; Sarmiento, F., Effect of Gd^{3+} on the Colloidal Stability of Liposomes. *Phys. Rev. E* **2006,** *74*, 031913.

166. Bentz, J.; Alford, D.; Cohen, J.; Düzgünes, N., La^{3+}-Induced Fusion of Phosphatidylserine Liposomes. Close Approach, Intermembrane Intermediates, and the Electrostatic Surface Potential. *Biophys. J.* **1988,** *53*, 593-607.

167. Sercombe, L.; Veerati, T.; Moheimani, F.; Wu, S. Y.; Sood, A. K.; Hua, S., Advances and Challenges of Liposome Assisted Drug Delivery. *Front. Pharmacol.* **2015,** *6*, 286.

168. Liu, J.; Stace-Naughton, A.; Jiang, X.; Brinker, C. J., Porous Nanoparticle Supported Lipid Bilayers (Protocells) as Delivery Vehicles. *J. Am. Chem. Soc.* **2009,** *131* (4), 1354-1355.

169. Mornet, S.; Lambert, O.; Duguet, E.; Brisson, A., The Formation of Supported Lipid Bilayers on Silica Nanoparticles Revealed by Cryoelectron Microscopy. *Nano Lett.* **2005,** *5* (2), 281-285.

170. Zhang, Z.; Liu, Y.; Zhang, X.; Liu, J., A Cell-Mimicking Structure Converting Analog Volume Changes to Digital Colorimetric Output with Molecular Selectivity. *Nano Lett.* **2017,** *17* (12), 7926-7931.

171. Temprana, C. F.; Prieto, M. J.; Igartúa, D. E.; Femia, A. L.; Amor, S.; Alonso, S. d. V., Diacetylenic Lipids in the Design of Stable Lipopolymers Able to Complex and Protect Plasmid DNA. *PLoS One* **2017,** *12* (10), e0186194.

172. Zong, W.; Hu, Y.; Su, Y.; Luo, N.; Zhang, X.; Li, Q.; Han, X., Polydopamine-Coated Liposomes as pH-Sensitive Anticancer Drug Carriers. *J. Microencapsulation* **2016,** *33* (3), 257-262.

173. Zhang, L.; Granick, S., How to Stabilize Phospholipid Liposomes (Using Nanoparticles). *Nano Lett.* **2006,** *6* (4), 694-698.

174. Jin, Y.; Gao, X., Spectrally Tunable Leakage-Free Gold Nanocontainers. *J. Am. Chem. Soc.* **2009,** *131* (49), 17774-17776.

175. Mohanraj, V. J.; Barnes, T. J.; Prestidge, C. A., Silica Nanoparticle Coated Liposomes: A New Type of Hybrid Nanocapsule. *Int. J. Pharm.* **2010,** *392* (1-2), 285-293.

176. Li, C.; Zhang, Y.; Su, T.; Long, Y.; Chen, Z., Silica-Coated Flexible Liposomes as A Nanohybrid Delivery System for Enhanced Oral Bioavailability of Curcumin. *Int. J. Nanomed.* **2012,** *7*, 5995-6002.

177. Song, Y.; Garcia, R. M.; Dorin, R. M.; Wang, H.; Qiu, Y.; Shelnutt, J. A., Synthesis of Platinum Nanocages by Using Liposomes Containing Photocatalyst Molecules. *Angew. Chem. Int. Ed.* **2006,** *45* (48), 8126-8130.

178. Schmidt, H. T.; Ostafin, A. E., Liposome Directed Growth of Calcium Phosphate Nanoshells. *Adv. Mater.* **2002,** *14* (7), 532-535.

179. Wang, F.; Liu, B.; Huang, P.-J. J.; Liu, J., Rationally Designed Nucleobase and Nucleotide Coordinated Nanoparticles for Selective DNA Adsorption and Detection. *Anal. Chem.* **2013,** *85* (24), 12144-12151.

180. Wei, H.; Li, B.; Du, Y.; Dong, S.; Wang, E., Nucleobase-Metal Hybrid Materials: Preparation of Submicrometer-Scale, Spherical Colloidal Particles of Adenine-Gold(III) via a Supramolecular Hierarchical Self-Assembly Approach. *Chem. Mater.* **2007,** *19* (12), 2987-2993.

181. Nishiyabu, R.; Hashimoto, N.; Cho, T.; Watanabe, K.; Yasunaga, T.; Endo, A.; Kaneko, K.; Niidome, T.; Murata, M.; Adachi, C.; Katayama, Y.; Hashizume, M.; Kimizuka, N., Nanoparticles of Adaptive Supramolecular Networks Self-Assembled from Nucleotides and Lanthanide Ions. *J. Am. Chem. Soc.* **2009,** *131* (6), 2151-2158.

182. Lopez, A.; Liu, J., Self-Assembly of Nucleobase, Nucleoside and Nucleotide Coordination Polymers: From Synthesis to Applications. *ChemNanoMat* **2017,** *3* (10), 670-684.

183. Liang, H.; Liu, B.; Yuan, Q.; Liu, J., Magnetic Iron Oxide Nanoparticle Seeded Growth of Nucleotide Coordinated Polymers. *ACS Appl. Mater. Interfaces* **2016,** *8* (24), 15615-15622.

184. He, Y.; Lopez, A.; Zhang, Z.; Chen, D.; Yang, R.; Liu, J., Nucleotide and DNA Coordinated Lanthanides: From Fundamentals to Applications. *Coord. Chem. Rev.* **2019,** *387*, 235-248.

185. Zhou, P.; Shi, R.; Yao, J.-f.; Sheng, C.-f.; Li, H., Supramolecular Self-Assembly of Nucleotide–Metal Coordination Complexes: From Simple Molecules to Nanomaterials. *Coord. Chem. Rev.* **2015,** *292*, 107-143.

186. Liu, Y.; Liu, J., Cu^{2+}-Directed Liposome Membrane Fusion, Positive-Stain Electron Microscopy, and Oxidation. *Langmuir* **2018,** *34* (25), 7545-7553.

187. Das, A.; Adhikari, C.; Chakraborty, A., Interaction of Different Divalent Metal Ions with Lipid Bilayer: Impact on the Encapsulation of Doxorubicin by Lipid Bilayer and Lipoplex Mediated Deintercalation. *J. Phys. Chem. B* **2017,** *121* (8), 1854-1865.

188. Kotyńska, J.; Dobrzyńska, I.; Figaszewski, Z. A., Association of Alkali Metal Cations with Phosphatidylcholine Liposomal Membrane Surface. *Eur. Biophys. J.* **2017,** *46* (2), 149-155.

189. Kotyńska, J.; Figaszewski, Z. A., Binding of Trivalent Metal Ions (Al^{3+}, In^{3+}, La^{3+}) with Phosphatidylcholine Liposomal Membranes Investigated by Microelectrophoresis. *Eur. Phys. J. E* **2018,** *41* (5), 70.

190. Yamasaki, S.; Shirai, O.; Kano, K.; Kozai, N.; Sakamoto, F.; Ohnuki, T., Adsorption Behavior of Lanthanide Ions on Nonbiological Phospholipid Membranes: A Model Study Using Liposome. *Chem. Lett.* **2013,** *42* (8), 819-821.

191. Smith, C. E.; Kong, H., Cross-Linkable Liposomes Stabilize a Magnetic Resonance Contrast-Enhancing Polymeric Fastener. *Langmuir* **2014,** *30* (13), 3697-3704.

192. Jones, M. N.; Hammond, K.; Reboiras, M. D.; Acerete, C.; Jackson, S. M.; Nogueira, M.; Nicholas, A. R., The Interaction of Lanthanum Ions with Dipalmitoylphosphatidylcholine-Phosphatidylinositol Vesicles. *Colloids Surf.* **1986,** *18*, 75-91.

193. Tanaka, T.; Yamazaki, M., Membrane Fusioin of Giant Unilamellar Vesicles of Neutral Phospholipid Membranes Induced by La^{3+}. *Langmuir* **2004,** *20* (13), 5160-5164.

194. Ermakov, Y. A.; Kamaraju, K.; Sengupta, K.; Sukharev, S., Gadolinium Ions Block Mechanosensitive Channels by Altering the Packing and Lateral Pressure of Anionic Lipids. *Biophys. J.* **2010,** *98* (6), 1018-1027.

195. Wheelwright, E. J.; Spedding, F. H.; Schwarzenbach, G., The Stability of the Rare Earth Complexes with Ethylenediaminetetraacetic Acid. *J. Am. Chem. Soc.* **1953,** *75* (17), 4196-4201.

196. Zhang, Z.; Morishita, K.; Lin, W. T. D.; Huang, P.-J. J.; Liu, J., Nucleotide Coordination with 14 Lanthanides Studied by Isothermal Titration Calorimetry. *Chin. Chem. Lett.* **2018,** *29* (1), 151-156.

197. Montini, T.; Melchionna, M.; Monai, M.; Fornasiero, P., Fundamentals and Catalytic Applications of CeO_2-Based Materials. *Chem. Rev.* **2016,** *116* (10), 5987-6041.

198. Qu, C. X. a. X., Cerium Oxide Nanoparticle: A Remarkably Versatile Rare Earth Nanomaterial for Biological Applications. *NPG Asia Mater.* **2014,** *6* (3), e90.

199. Ujjain, S. K.; Das, A.; Srivastava, G.; Ahuja, P.; Roy, M.; Arya, A.; Bhargava, K.; Sethy, N.; Singh, S. K.; Sharma, R. K.; Das, M., Nanoceria Based Electrochemical Sensor for Hydrogen Peroxide Detection. *Biointerphases* **2014,** *9* (3), 031011.

200. Celardo, I.; Pedersen, J. Z.; Traversa, E.; Ghibelli, L., Pharmacological Potential of Cerium Oxide Nanoparticles. *Nanoscale* **2011,** *3* (4), 1411-1420.

201. Korsvik, C.; Patil, S.; Seal, S.; Self, W. T., Superoxide Dismutase Mimetic Properties Exhibited by Vacancy Engineered Ceria Nanoparticles. *Chem. Commun.* **2007,** (10), 1056-1058.

202. Dowding, J. M.; Das, S.; Kumar, A.; Dosani, T.; McCormack, R.; Gupta, A.; Sayle, T. X. T.; Sayle, D. C.; Kalm, L. v.; Seal, S.; Self, W. T., Cellular Interaction and Toxicity Depend on

Physicochemical Properties and Surface Modification of Redox-Active Nanomaterials. *ACS Nano* **2013,** *7* (6), 4855-4858.

203. Chen, J.; Patil, S.; Seal, S.; McGinnis, J. F., Rare Earth Nanoparticles Prevent Retinal Degeneration Induced by Intracellular Peroxides. *Nat. Nanotechnol.* **2006,** *1* (2), 142-150.

204. Lin, Y.; Ren, J.; Qu, X., Catalytically Active Nanomaterials: A Promising Candidate for Artificial Enzymes. *Acc. Chem. Res.* **2014,** *47* (4), 1097-1105.

205. Walkey, C.; Das, S.; Seal, S.; Erlichman, J.; Heckman, K.; Ghibelli, L.; Traversa, E.; McGinnis, J. F.; Self, W. T., Catalytic Properties and Biomedical Applications of Cerium Oxide Nanoparticles. *Environ. Sci. Nano* **2015,** *2* (1), 33-53.

206. Xia, T.; Kovochich, M.; Liong, M.; Mädler, L.; Gilbert, B.; Shi, H.; Yeh, J. I.; Zink, J. I.; Nel, A. E., Comparison of the Mechanism of Toxicity of Zinc Oxide and Cerium Oxide Nanoparticles Based on Dissolution and Oxidative Stress Properties. *ACS Nano* **2008,** *2* (10), 2121-2134.

207. Hirst, S. M.; Karakoti, A. S.; Tyler, R. D.; Sriranganathan, N.; Seal, S.; Reilly, C. M., Anti-Inflammatory Properties of Cerium Oxide Nanoparticles. *Small* **2009,** *5* (24), 2848-2856.

208. Lyu, G.-M.; Wang, Y.-J.; Huang, X.; Zhang, H.-Y.; Sun, L.-D.; Liu, Y.-J.; Yana, C.-H., Hydrophilic CeO_2 Nanocubes Protect Pancreatic β-Cell Line INS-1 from H_2O_2-Induced Oxidative Stress. *Nanoscale* **2016,** *8* (15), 7923-7932.

209. Celardo, I.; Nicola, M. D.; Mandoli, C.; Pedersen, J. Z.; Traversa, E.; Ghibelli, L., Ce^{3+} Ions Determine Redox-Dependent Anti-Apoptotic Effect of Cerium Oxide Nanoparticles. *ACS Nano* **2011,** *5* (6), 4537-4549.

210. Perez, J. M.; Asati, A.; Nath, S.; Kaittanis, C., Synthesis of Biocompatible Dextran-Coated Nanoceria with pH-Dependent Antioxidant Properties. *Small* **2008,** *4* (5), 552-556.

211. Tarnuzzer, R. W.; Colon, J.; Patil, S.; Seal, S., Vacancy Engineered Ceria Nanostructures for Proteciton from Radiation-Induced Cellular Damage. *Nano Lett.* **2005,** *5* (2), 2573-2577.

212. Ji, Z.; Wang, X.; Zhang, H.; Lin, S.; Meng, H.; Sun, B.; George, S.; Xia, T.; Nel, A. E.; Zink, J. I., Designed Synthesis fo CeO_2 Nanorods and Nanowires for Studying Toxicological Effects of High Aspect Ratio Nanomaterials. *ACS Nano* **2012,** *6* (6), 5366-5380.

213. Kim, C. K.; Kim, T.; Choi, I.-Y.; Soh, M.; Kim, D.; Kim, Y.-J.; Jang, H.; Yang, H.-S.; Kim, J. Y.; Park, H.-K.; Park, S. P.; Park, S.; Yu, T.; Yoon, B.-W.; Lee, S.-H.; Hyeon, T., Ceria Nanoparticles that can Protect against Ischemic Stroke. *Angew. Chem. Int. Ed.* **2012,** *51* (44), 11039-11043.

214. Kumar, A.; Das, S.; Munusamy, P.; Self, W.; Baer, D. R.; Sayle, D. C.; Seal, S., Behavior of Nanoceria in Biologically-Relevant Environments. *Environ. Sci.: Nano* **2014,** *1* (6), 516-532.

215. Verma, A.; Stellacci, F., Effect of Surface Properties on Nanoparticle-Cell Interactions. *Small* **2010,** *6* (1), 12-21.

216. Michel, R.; Kesselman, E.; Plostica, T.; Danino, D.; Gradzielski, M., Internalization of Silica Nanoparticles into Fluid Liposomes: Formation of Interesting Hybrid Colloids. *Angew. Chem. Int. Ed.* **2014,** *53* (46), 12441-12445.

217. Sehgal, A.; Lalatonne, Y.; Berret, J.-F.; Morvan, M., Precipitation-Redispersion of Cerium Oxide Nanoparticles with Poly(acrylic acid): Toward Stable Dispersions. *Langmuir* **2005,** *21* (20), 9359-9364.

218. Qi, L.; Sehgal, A.; Castaing, J.-C.; Chapel, J.-P.; Fresnais, J.; Berret, J.-F.; Cousin, F., Redispersible Hybrid Nanopowders: Cerium Oxide Nanoparticle Complexes with Phosphonated-PEG Oligomers. *ACS Nano* **2008,** *2* (5), 879-888.

219. Asati, A.; Santra, S.; Kaittanis, C.; Nath, S.; Perez, J. M., Oxidase-Like Activity of Polymer-Coated Cerium Oxide Nanoparticles. *Angew. Chem. Int. Ed.* **2009,** *48* (13), 2308-2312.

220. Pautler, R.; Kelly, E. Y.; Huang, P.-J. J.; Cao, J.; Liu, B.; Liu, J., Attaching DNA to Nanoceria: Regulating Oxidase Activity and Fluorescence Quenching. *ACS Appl. Mater. Interfaces* **2013,** *5* (15), 6820-6825.

221. Mousseau, F.; Borgne, R. L.; Seyrek, E.; Berret, J.-F., Biophysicochemical Interaction of a Clinical Pulmonary Surfactant with Nanoalumina. *Langmuir* **2015,** *31* (26), 7346-7354.

222. McCormack, R. N.; Mendez, P.; Barkam, S.; Neal, C. J.; Das, S.; Seal, S., Inhibition of Nanoceria's Catalytic Activity due to Ce^{3+} Site-Specific Interaction with Phosphate Ions. *J. Phys. Chem. C* **2014,** *118* (33), 18992-19006.

223. Liu, B.; Sun, Z.; Huang, P.-J. J.; Liu, J., Hydrogen Peroxide Displacing DNA from Nanoceria: Mechanism and Detection of Glucose in Serum. *J. Am. Chem. Soc.* **2015,** *137* (3), 1290-1295.

224. Verma, A.; Uzun, O.; Hu, Y.; Hu, Y.; Han, H.-S.; Watson, N.; Chen, S.; Irvine, D. J.; Stellacci, F., Surface-Structure-Regulated Cell-Membrane Penetration by Monolayer-Protected Nanoparticles. *Nat. Mater.* **2008,** *7* (7), 588-595.

225. De, M.; Ghosh, P. S.; Rotello, V. M., Applications of Nanoparticles in Biology. *Adv. Mater.* **2008,** *20* (22), 4225-4241.

226. Yao, C.; Wang, P.; Li, X.; Hu, X.; Hou, J.; Wang, L.; Zhang, F., Near-Infrared-Triggered Azobenzene-Liposome/Upconversion Nanoparticle Hybrid Vesicles for Remotely Controlled Drug Delivery to Overcome Cancer Multidrug Resistance. *Adv. Mater.* **2016,** *28* (42), 9341-9348.

227. Luo, D.; Li, N.; Carter, K. A.; Lin, C.; Geng, J.; Shao, S.; Huang, W.-C.; Qin, Y.; Atilla-Gokcumen, G. E.; Lovell, J. F., Rapid Light-Triggered Drug Release in Liposomes Containing Small Amounts of Unsaturated and Porphyrin-Phospholipids. *Small* **2016,** *12* (22), 3039-3047.

228. Li, X.; Che, Z.; Mazhar, K.; Price, T. J.; Qin, Z., Ultrafast Near-Infrared Light-triggered Intracellular Uncaging to Probe Cell Signaling. *Adv. Funct. Mater.* **2017,** *27* (11), 1605778.

229. Pornpattananangkul, D.; Zhang, L.; Olson, S.; Aryal, S.; Obonyo, M.; Vecchio, K.; Huang, C.-M.; Zhang, L., Bacterial Toxin-Triggered Drug Release From Gold Nanoparticle-Stabilized Liposomes for the Treatment of Bacterial Infection. *J. Am. Chem. Soc.* **2011,** *133* (11), 4132-4139.

230. Mirshafiee, V.; Sun, B.; Chang, C. H.; Liao, Y.-P.; Jiang, W.; Jiang, J.; Liu, X.; Wang, X.; Xia, T.; Nel, A. E., Toxicological Profiling of Metal Oxide Nanoparticles in Liver Context Reveals Pyroptosis in Kupffer Cells and Macrophages versus Apoptosis in Hepatocytes. *ACS Nano* **2018,** *12* (4), 3836-3852.

231. Cho, E. C.; Xie, J.; Wurm, P. A.; Xia, Y., Understanding the Role of Surface Charges in Cellular Adsorption versus Internalization by Selectively Removing Gold Nanoparticles on the Cell Surface with a I_2/KI Etchant. *Nano Lett.* **2009,** *9* (3), 1080-1084.

232. Arvizo, R. R.; Miranda, O. R.; Thompson, M. A.; Pabelick, C. M.; Bhattacharya, R.; Robertson, J. D.; Rotello, V. M.; Prakash, Y. S.; Mukherjee, P., Effect of Nanoparticle Surface Charge at the Plasma Membrane and Beyond. *Nano Lett.* **2010,** *10* (7), 2543-2548.

233. Cheng, L.-C.; Jiang, X.; Wang, J.; Chen, C.; Liu, R.-S., Nano-Bio Effects: Interaction of Nanomaterials with Cells. *Nanoscale* **2013,** *5* (9), 3547-3569.

234. Magrez, A.; Kasas, S.; Salicio, V. r.; Pasquier, N.; Seo, J. W.; Celio, M.; Catsicas, S.; Schwaller, B.; Forró, L., Cellular Toxicity of Carbon-Based Nanomaterials. *Nano Lett.* **2006,** *6* (6), 1121-1125.

235. Wang, X.; Wang, X.; Bai, X.; Hu, G.; Gu, Z.; Miao, Q.; Chen, C.; Yan, L.; Liu, T.; Wang, M.; Song, Y., Nanoparticle Ligand Exchange and Its Effects at the Nanoparticle-Cell Membrane Interface. *Nano Lett.* **2019,** *19* (1), 8-18.

236. London, E.; Brown, D. A., Insolubility of Lipids in Triton X-100: Physical Origin and Relationship to Sphingolipid/Cholesterol Membrane Domains (Rafts). *Biochim. Biophys. Acta* **2000,** *1608*, 182-195.

237. Hong, S.; Bielinska, A. U.; Mecke, A.; Keszler, B.; Beals, J. L.; Shi, X.; Balogh, L.; Orr, B. G.; James R. Baker, J.; Holl, M. M. B., Interaction of Poly(amidoamine) Dendrimers with Supported Lipid Bilayers and Cells: Hole Formation and the Relation to Transport. *Bioconjugate Chem.* **2004,** *15* (4), 774-782.

238. Mecke, A.; Majoros, I. J.; Patri, A. K.; James R. Baker, J.; Holl, M. M. B.; Orr, B. G., Lipid Bilayer Disruption by Polycationic Polymers: The Role of Size and Chemical Functional Group. *Langmuir* **2005,** *21* (23), 10348-10354.

239. Mecke, A.; Lee, D.-K.; Ramamoorthy, A.; Orr, B. G.; Holl, M. M. B., Synthetic and Natural Polycationic Polymer Nanoparticles Interact Selectivley with Fluid-Phase Domains of DMPC Lipid Bilayers. *Langmuir* **2005,** *21* (19), 8588-8590.

240. Hong, S.; Leroueil, P. R.; Janus, E. K.; Peters, J. L.; Kober, M.-M.; Islam, M. T.; Orr, B. G.; James R. Baker, J.; Holl, M. M. B., Interaction of Polycationic Polymers with Supported Lipid Bilayers and Cells: Nanoscale Hole Formation and Enhanced Membrane Permeability. *Bioconjugate Chem.* **2006,** *17* (3), 728-734.

241. Leroueil, P. R.; Hong, S.; Mecke, A.; James R. Baker, J.; Orr, B. G.; Holl, M. M. B., Nanoparticle Interaction with Biological Membranes: Does Nanotechnology Present a Janus Face? *Acc. Chem. Res.* **2007,** *40* (5), 335-342.

242. Ginzburg, V. V.; Balijepalli, S., Modeling the Thermodynamics of the Interaction of Nanoparticles with Cell Membranes. *Nano Lett.* **2007,** *7* (12), 3716-3722.

243. Moghadam, B. Y.; Hou, W.-C.; Corredor, C.; Westerhoff, P.; Posner, J. D., Role of Nanoparticle Surface Functionality in the Disruption of Model Cell Membranes. *Langmuir* **2012,** *28* (47), 16318-16326.

244. Lai, L.; Li, S.-J.; Feng, J.; Mei, P.; Ren, Z.-H.; Chang, Y.-L.; Liu, Y., Effects of Surface Charges on the Bactericide Activity of CdTe/ZnS Quantum Dots: A Cell Membrane Disruption Perspective. *Langmuir* **2017,** *33* (9), 2378-2386.

245. Karoonuthaisiri, N.; Titiyevskiy, K.; Thomas, J. L., Destabilization of Fatty Acid-Containing Liposomes by Polyamidoamine Dendrimers. *Colloids Surf., B* **2003,** *27* (4), 365-375.

246. Zhang, L.; Hong, L.; Yu, Y.; Bae, S. C.; Granick, S., Nanoparticle-Assisted Surface Immobilization of Phospholipid Liposomes. *J. Am. Chem. Soc.* **2006,** *128* (28), 9026-9027.

247. Yu, Y.; Anthony, S. M.; Zhang, L.; Bae, S. C.; Granick, S., Cationic Nanoparticles Stabilize Zwitterionic Liposomes Better than Anionic Ones. *J. Phys. Chem. C* **2007,** *111* (23), 8233-8236.

248. Lee, K.; Zhang, L.; Yi, Y.; Wang, X.; Yu, Y., Rupture of Lipid Membranes Induced by Amphiphilic Janus Nanoparticles. *ACS Nano* **2018,** *12* (4), 3646-3657.

249. Alder, G. M.; Arnold, W. M.; Bashford, C. L.; Drake, A. F.; Pasternak, C. A.; Zimmermann, U., Divalent Cation-Sensitive Pores Formed by Natural and Synthetic Mellittin and by Triton X-100. *Biochim. Biophys. Acta* **1991,** *1061* (1), 111-120.

250. Lee, H.; Larson, R. G., Molecular Dynamics Simulations of PAMAM Dendrimer-Induced Pore Formation in DPPC Bilayers with a Coarse-Grained Model. *J. Phys. Chem. B* **2006,** *110* (37), 18204-18211.

251. Zhang, L.; Jiang, Y.; Ding, Y.; Povey, M.; York, D., Investigation into the Antibacterial Behaviour of Suspensions of ZnO Nanoparticles (ZnO Nanofluids). *J. Nanopart. Res.* **2007,** *9* (3), 479-489.

252. Liu, B.; Ma, L.; Huang, Z.; Hu, H.; Wu, P.; Liu, J., Janus DNA Orthogonal Adsorption of Graphene Oxide and Metal Oxide Nanoparticles Enabling Stable Sensing in Serum. *Mater. Horiz.* **2018,** *5* (1), 65-69.

253. Huang, P.-J. J.; Vazin, M.; Matuszek, Ż.; Liu, J., A New Heavy Lanthanide-Dependent DNAzyme Displaying Strong Metal Cooperativity and Unrescuable Phosphorothioate Effect. *Nucleic Acids Res.* **2015,** *43* (1), 461-469.

254. Hu, S.; Huang, P.-J. J.; Wang, J.; Liu, J., Phosphorothioate DNA Mediated Sequence-Insensitive Etching and Ripening of Silver Nanoparticles. *Front. Chem.* **2019,** *7*, 198.

255. Liu, Y.; Liu, J., Leakage and Rupture of Lipid Membranes by Charged Polymers and Nanoparticles. *Langmuir* **2020,** *36* (3), 810-818.

256. Wei, H.; Wang, E., Nanomaterials with Enzyme-Like Characteristics (Nanozymes): Next-Generation Artificial Enzymes. *Chem. Soc. Rev.* **2013,** *42* (14), 6060-6093.

257. Kurapati, R.; Kostarelos, K.; Prato, M.; Bianco, A., Biomedical Uses for 2D Materials Beyond Graphene: Current Advances and Challenges Ahead. *Adv. Mater.* **2016,** *28* (29), 6052-6074.

258. Wu, M.-X.; Yang, Y.-W., Metal-Organic Framework (MOF)-Based Drug/Cargo Delivery and Cancer Therapy. *Adv. Mater.* **2017,** *29* (23), 1606134.

259. Chen, G.; Qiu, H.; Prasad, P. N.; Chen, X., Upconversion Nanoparticles: Design, Nanochemistry, and Applications in Theranostics. *Chem. Rev.* **2014,** *114* (10), 5161–5214.